



**Calhoun: The NPS Institutional Archive**  
**DSpace Repository**

---

Theses and Dissertations

1. Thesis and Dissertation Collection, all items

---

1975-12

# Thermal studies of a heated cylinder placed near a plane surface

Köseman, Ender

Monterey, California. Naval Postgraduate School

---

<http://hdl.handle.net/10945/21090>

---

Copyright is reserved by the copyright owner

*Downloaded from NPS Archive: Calhoun*



Calhoun is the Naval Postgraduate School's public access digital repository for research materials and institutional publications created by the NPS community. Calhoun is named for Professor of Mathematics Guy K. Calhoun, NPS's first appointed -- and published -- scholarly author.

**Dudley Knox Library / Naval Postgraduate School**  
**411 Dyer Road / 1 University Circle**  
**Monterey, California USA 93943**

<http://www.nps.edu/library>

THERMAL STUDIES OF A HEATED  
CYLINDER PLACED NEAR A  
PLANE SURFACE

Ender Köseman

DUDLEY KNOX LIBRARY  
NAVAL POSTGRADUATE SCHOOL  
MONTEREY, CALIFORNIA 93940

# NAVAL POSTGRADUATE SCHOOL

## Monterey, California



# THESIS

THERMAL STUDIES OF A HEATED CYLINDER  
PLACED NEAR A PLANE SURFACE

by

Ender Kösemen

December 1975

Thesis Advisor:

Thomas E. Cooper

Approved for public release; distribution unlimited.

T170801



REPORT DOCUMENTATION PAGE		READ INSTRUCTIONS BEFORE COMPLETING FORM
1. REPORT NUMBER	2. GOVT ACCESSION NO.	3. RECIPIENT'S CATALOG NUMBER
4. TITLE (and Subtitle) Thermal Studies of a Heated Cylinder Placed Near a Plane Surface		5. TYPE OF REPORT & PERIOD COVERED Master's Thesis; December 1975
7. AUTHOR(s) Ender Kösemen		6. PERFORMING ORG. REPORT NUMBER
9. PERFORMING ORGANIZATION NAME AND ADDRESS Naval Postgraduate School Monterey, California 93940		8. CONTRACT OR GRANT NUMBER(s)
11. CONTROLLING OFFICE NAME AND ADDRESS Naval Postgraduate School Monterey, California 93940		10. PROGRAM ELEMENT, PROJECT, TASK AREA & WORK UNIT NUMBERS
14. MONITORING AGENCY NAME & ADDRESS (if different from Controlling Office) Naval Postgraduate School Monterey, California 93940		12. REPORT DATE December 1975
		13. NUMBER OF PAGES 111
		15. SECURITY CLASS. (of this report) Unclassified
		15a. DECLASSIFICATION/DOWNGRADING SCHEDULE
16. DISTRIBUTION STATEMENT (of this Report)  ** Approved for public release; distribution unlimited.		
17. DISTRIBUTION STATEMENT (of the abstract entered in Block 20, if different from Report)		
18. SUPPLEMENTARY NOTES		
19. KEY WORDS (Continue on reverse side if necessary and identify by block number)		
20. ABSTRACT (Continue on reverse side if necessary and identify by block number) Local and average Nusselt numbers have been experimentally determined around the circumference of a uniformly heated right circular cylinder placed near a plane surface in a cross flow of air. Experiments were carried out for Reynolds numbers ranging from 16,000 to 153,000, three plate lengths and varying cylinder to plate spacings. The variation of the average Nusselt number as a function of gap spacing was found to exhibit an interesting		



SECURITY CLASSIFICATION OF THIS PAGE(When Data Entered)

and unexpected trend. The average Nusselt number exhibited a minimum value when the cylinder was resting on the plate and attained a maximum value at a gap spacing of approximately one to two cylinder radii. Flow visualization studies together with measurements of the vortex shedding frequency in the cylinder wake indicate that when the plate is within approximately one cylinder radius of the cylinder, it inhibits the formation of the regular vortex pattern that forms in the wake of a free cylinder. This has a strong influence on the base Nusselt number which, in turn, exerts a controlling influence on the magnitude of the average Nusselt number.



Thermal Studies of a Heated Cylinder  
Placed Near a Plane Surface

by

Ender Kösemen  
Lieutenant, Turkish Navy  
B.S.M.E., Naval Postgraduate School, 1975

Submitted in partial fulfillment of the  
requirements for the degree of

MASTER OF SCIENCE IN MECHANICAL ENGINEERING

from the

NAVAL POSTGRADUATE SCHOOL  
December 1975

c.1

## ABSTRACT

Local and average Nusselt numbers have been experimentally determined around the circumference of a uniformly heated right circular cylinder placed near a plane surface in a cross flow of air. Experiments were carried out for Reynolds numbers ranging from 16,000 to 153,000, three plate lengths and varying cylinder to plate spacings. The variations of the average Nusselt number as a function of gap spacing was found to exhibit an interesting and unexpected trend. The average Nusselt number exhibited a minimum value when the cylinder was resting on the plate and attained a maximum value at a gap spacing of approximately one to two cylinder radii. Flow visualization studies together with measurements of the vortex shedding frequency in the cylinder wake indicate that when the plate is within approximately one cylinder radius of the cylinder, it inhibits the formation of the regular vortex pattern that forms in the wake of a free cylinder. This has a strong influence on the base Nusselt number which, in turn, exerts a controlling influence on the magnitude of the average Nusselt number.



## TABLE OF CONTENTS

I.	INTRODUCTION -----	12
II.	BACKGROUND -----	16
III.	EXPERIMENTAL APPARATUS -----	18
	1. Wind Tunnel -----	18
	2. Liquid Crystals -----	20
	3. Temsheet -----	20
	4. Cylinder -----	21
	5. Plates -----	23
IV.	EXPERIMENTAL PROCEDURE -----	25
V.	RESULTS -----	28
VI.	DISCUSSION -----	42
VII.	SUMMARY -----	51
	APPENDIX A Heat Transfer Data Reduction -----	53
	APPENDIX B Uncertainty Analysis -----	58
	APPENDIX C Wind Tunnel Velocity Profiles -----	66
	APPENDIX D Polar Plots of local Nusselt Number versus Angular Location As a Function of Gap Spacings -----	74
	LIST OF REFERENCES -----	110
	INITIAL DISTRIBUTION LIST -----	111



## LIST OF ILLUSTRATIONS

1.	Cylinder-plate configuration -----	13
2.	Schematic diagram of the wind tunnel -----	19
3.	Photograph of the Tensheet cylinder -----	22
4.	Photograph of the plate and cylinder assembly -----	24
5.	Local Nusselt number and pressure coefficient on the surface of a cylinder placed near a plane surface for $Re = 153,000$ , $L/D = 4$ , $d/r = 0$ -----	30
6.	Local Nusselt number and pressure coefficient on the surface of a cylinder placed near a plane surface for $Re = 153,000$ , $L/D = 4$ , $d/r = 0.25$ -----	31
7.	Local Nusselt number and pressure coefficient on the surface of a cylinder placed near a plane surface for $Re = 153,000$ , $L/D = 4$ , $d/r = 0.5$ -----	32
8.	Local Nusselt number and pressure coefficient on the surface of a cylinder placed near a plane surface for $Re = 153,000$ , $L/D = 4$ , $d/r = 1.0$ -----	33
9.	Local Nusselt number and pressure coefficient on the surface of a cylinder placed near a plane surface for $Re = 153,000$ , $L/D = 4$ , $d/r = 2.0$ -----	34
10.	Local Nusselt number and pressure coefficient on the surface of a cylinder placed near a plane surface for $Re = 153,000$ , $L/D = 4$ , $d/r = 3.0$ -----	35
11.	Local Nusselt number and pressure coefficient on the surface of a cylinder placed near a plane surface for $Re = 153,000$ , $L/D = 4$ , $d/r = 4.0$ -----	36
12.	Local Nusselt number and pressure coefficient on the surface of a cylinder placed near a plane surface for $Re = 153,000$ , $L/D = 4$ , $d/r = 5.33$ -----	37



13.	Average Nusselt number variation as a function of gap size and Reynolds number for $L/D = 4$ ---	38
14.	Average Nusselt number variation as a function of plate length and gap size for a Reynolds number of 153,000 -----	39
15.	Variation of normalized drag coefficient, Strouhal number and average Nusselt number as a function of gap size for $Re = 153,000$ and $L/D = 4$ -----	40
16.	Variation of normalized Strouhal number and base Nusselt number as a function of gap size for $Re = 153,000$ and $L/D = 4$ -----	41
17.	Shift of the laminar separation points and the stagnation point as a function of $d/r$ -----	45
18.	Velocity profile at the top of the cylinder for $d/r = 0.0$ -----	68
19.	Velocity profiles at the top and bottom of the cylinder for $d/r = 5.33$ -----	69
20.	Velocity profile at the top of the cylinder for $d/r = 0.0$ -----	70
21.	Velocity profiles at the top and bottom of the cylinder for $d/r = 5.33$ -----	71
22.	Velocity profile at the top of the cylinder for $d/r = 0.0$ -----	72
23.	Velocity profiles at the top and bottom of the cylinder for $d/r = 5.33$ -----	73
24.	Local Nusselt number on the surface of a cylinder placed near a plane surface for $Re = 16,000$ , $L/D = 4$ , $d/r = 0$ -----	75
25.	Local Nusselt number on the surface of a cylinder placed near a plane surface for $Re = 16,000$ , $L/D = 4$ , $d/r = 0.25$ -----	76
26.	Local Nusselt number on the surface of a cylinder placed near a plane surface for $Re = 16,000$ , $L/D = 4$ , $d/r = 0.5$ -----	77
27.	Local Nusselt number on the surface of a cylinder placed near a plane surface for $Re = 16,000$ , $L/D = 4$ , $d/r = 1.0$ -----	78



28.	Local Nusselt number on the surface of a cylinder placed near a plane surface for $Re = 16,000$ , $L/D = 4$ , $d/r = 2.0$ -----	79
29.	Local Nusselt number on the surface of a cylinder placed near a plane surface for $Re = 16,000$ , $L/D = 4$ , $d/r = 3.0$ -----	80
30.	Local Nusselt number on the surface of a cylinder placed near a plane surface for $Re = 16,000$ , $L/D = 4$ , $d/r = 4.0$ -----	81
31.	Local Nusselt number on the surface of a cylinder placed near a plane surface for $Re = 16,000$ , $L/D = 4$ , $d/r = 5.33$ -----	82
32.	Local Nusselt number and pressure coefficient on the surface of a cylinder placed near a plane surface for $Re = 90,000$ , $L/D = 4$ , $d/r = 0.0$ ----	83
33.	Local Nusselt number and pressure coefficient on the surface of a cylinder placed near a plane surface for $Re = 90,000$ , $L/D = 4$ , $d/r = 0.25$ ---	84
34.	Local Nusselt number and pressure coefficient on the surface of a cylinder placed near a plane surface for $Re = 90,000$ , $L/D = 4$ , $d/r = 0.5$ ----	85
35.	Local Nusselt number and pressure coefficient on the surface of a cylinder placed near a plane surface for $Re = 90,000$ , $L/D = 4$ , $d/r = 1.0$ ----	86
36.	Local Nusselt number and pressure coefficient on the surface of a cylinder placed near a plane surface for $Re = 90,000$ , $L/D = 4$ , $d/r = 2.0$ ----	87
37.	Local Nusselt number and pressure coefficient on the surface of a cylinder placed near a plane surface for $Re = 90,000$ , $L/D = 4$ , $d/r = 3.0$ ----	88
38.	Local Nusselt number and pressure coefficient on the surface of a cylinder placed near a plane surface for $Re = 90,000$ , $L/D = 4$ , $d/r = 4.0$ ----	89
39.	Local Nusselt number and pressure coefficient on the surface of a cylinder placed near a plane surface for $Re = 90,000$ , $L/D = 4$ , $d/r = 5.33$ ---	90
40.	Local Nusselt number and pressure coefficient on the surface of a cylinder placed near a plane surface for $Re = 153,000$ , $L/D = 2$ , $d/r = 0$ -----	91



41.	Local Nusselt number and pressure coefficient on the surface of a cylinder placed near a plane surface for $Re = 153,000$ , $L/D = 2$ , $d/r = 0.25$ --	92
42.	Local Nusselt number and pressure coefficient on the surface of a cylinder placed near a plane surface for $Re = 153,000$ , $L/D = 2$ , $d/r = 0.5$ ---	93
43.	Local Nusselt number and pressure coefficient on the surface of a cylinder placed near a plane surface for $Re = 153,000$ , $L/D = 2$ , $d/r = 1.0$ ---	94
44.	Local Nusselt number and pressure coefficient on the surface of a cylinder placed near a plane surface for $Re = 153,000$ , $L/D = 2$ , $d/r = 2.0$ ---	95
45.	Local Nusselt number and pressure coefficient on the surface of a cylinder placed near a plane surface for $Re = 153,000$ , $L/D = 2$ , $d/r = 3.0$ ---	96
46.	Local Nusselt number and pressure coefficient on the surface of a cylinder placed near a plane surface for $Re = 153,000$ , $L/D = 2$ , $d/r = 4.0$ ---	97
47.	Local Nusselt number and pressure coefficient on the surface of a cylinder placed near a plane surface for $Re = 153,000$ , $L/D = 2$ , $d/r = 5.33$ --	98
48.	Local Nusselt number and pressure coefficient on the surface of a cylinder placed near a plane surface for $Re = 153,000$ , $L/D = 8$ , $d/r = 0$ -----	99
49.	Local Nusselt number and pressure coefficient on the surface of a cylinder placed near a plane surface for $Re = 153,000$ , $L/D = 8$ , $d/r = 0.25$ --	100
50.	Local Nusselt number and pressure coefficient on the surface of a cylinder placed near a plane surface for $Re = 153,000$ , $L/D = 8$ , $d/r = 0.5$ ---	101
51.	Local Nusselt number and pressure coefficient on the surface of a cylinder placed near a plane surface for $Re = 153,000$ , $L/D = 8$ , $d/r = 1.0$ ---	102
52.	Local Nusselt number and pressure coefficient on the surface of a cylinder placed near a plane surface for $Re = 153,000$ , $L/D = 8$ , $d/r = 2.0$ ---	103
53.	Local Nusselt number and pressure coefficient on the surface of a cylinder placed near a plane surface for $Re = 153,000$ , $L/D = 8$ , $d/r = 3.0$ ---	104



54.	Local Nusselt number and pressure coefficient on the surface of a cylinder placed near a plane surface for $Re = 153,000$ , $L/D = 8$ , $d/r = 4.0$ ---	105
55.	Local Nusselt number and pressure coefficient on the surface of a cylinder placed near a plane surface for $Re = 153,000$ , $L/D = 8$ , $d/r = 5.33$ --	106
56.	Local Nusselt number on the surface of a free cylinder for $Re = 16,000$ -----	107
57.	Local Nusselt number and pressure coefficient on the surface of a free cylinder for $Re = 90,000$ -----	108
58.	Local Nusselt number and pressure coefficient on the surface of a free cylinder for $Re = 153,000$ -----	109



## ACKNOWLEDGEMENT

I would like to thank Mr. Thomas Christian for his contribution in conducting the experimental phase.

I would like to express my special appreciation to Professor Matthew Kelleher for his helpful suggestions and assistance.

I would also like especially to thank my advisor, Professor Thomas E. Cooper, for the knowledge, encouragement, guidance and inspirations he provided to me throughout this study.



## I. INTRODUCTION

An experimental investigation was carried out to examine the influence of wall proximity effects on the heat transfer characteristics of a uniformly heated cylinder placed in a cross-flow of air. Recently, McComas [1] initiated an investigation of the heat transfer characteristics of a uniformly heated cylinder attached to a plate and Gnerlich [2] continued the same study varying the cylinder to plate spacings. The present work is an extensive follow-on study of the work of McComas and Gnerlich differing in that a range of Reynolds numbers has been investigated as well as three different plate lengths. The present experimental work was conducted in the Mechanical Engineering Department wind tunnel (described in detail in Section III) in Building 500 at the Naval Postgraduate School.

Local Nusselt numbers were obtained around the circumference of the cylinder at Reynolds numbers of 16,000, 90,000 and 153,000 without a plate as well as with a plate. In the case with a plate, the cylinder to plate spacings were varied from  $d/r = 0$  to  $d/r = 5.33$  with  $L/D = 4$  where  $d$  = gap width,  $r$  = cylinder radius,  $D$  = cylinder diameter and  $L$  = length of plate from the centerline of the cylinder to the leading edge of the plate (Figure 1). Experiments were also conducted at a Reynolds number of 153,000 with  $L/D = 2$  and 8 in order to see the effect of the length of the plate's leading edge on the heat transfer results.



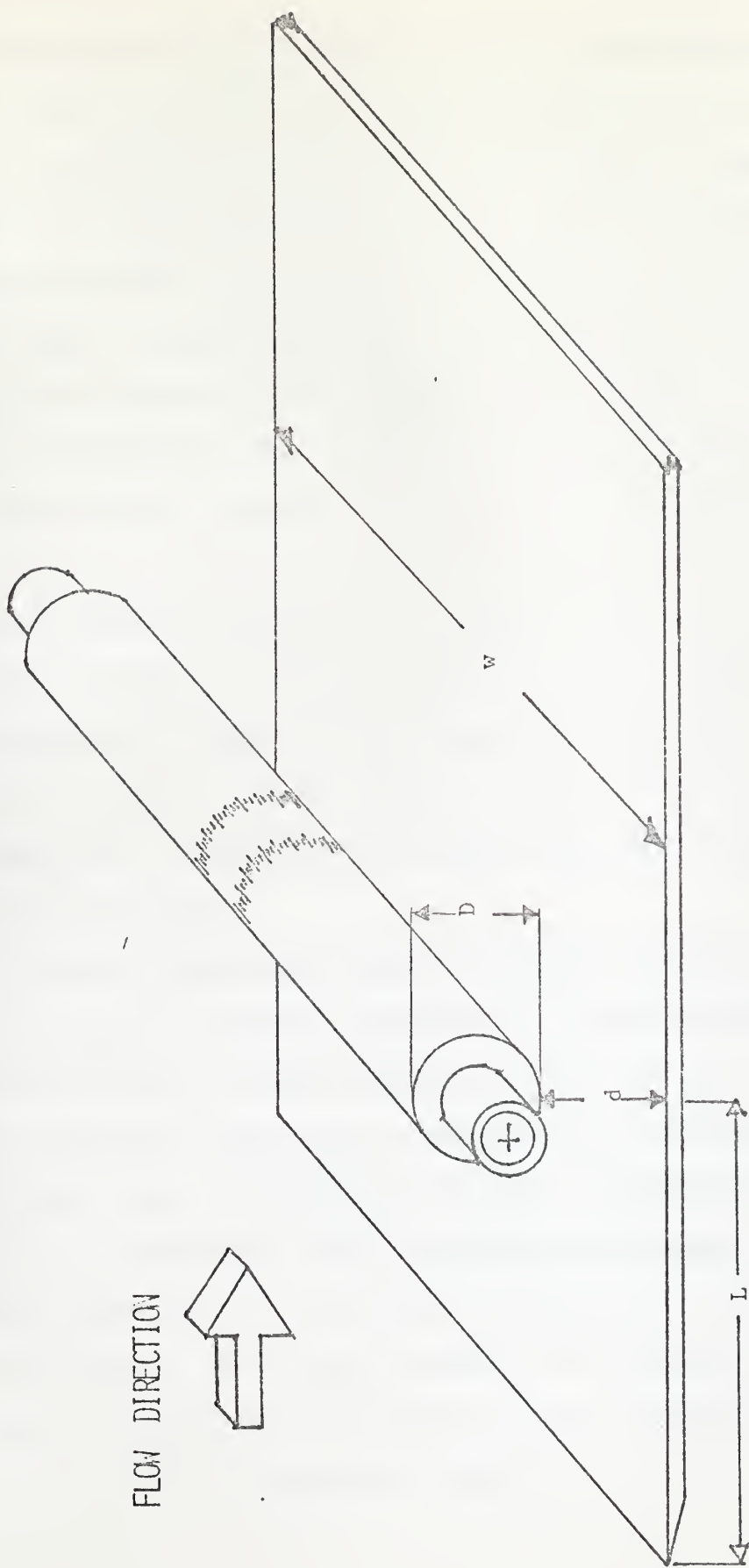


Figure 1. Cylinder-plate configuration.



Before proceeding further, a brief qualitative description of flow past a cylinder will help to explain and interpret the results obtained from this experimental study. Since the present experiments examined Reynolds numbers ranging from 16,000 to 153,000, only the subcritical and critical flow regimes will be described here. See Achenbach [3] for a complete discussion of the various flow regimes.

In subcritical flow, a laminar hydrodynamic boundary layer grows from a minimum thickness at the forward stagnation point on the cylinder to a maximum thickness at an angular location of approximately 80-85 degrees. At this location, the kinetic energy of the moving fluid is no longer sufficient to overcome the adverse pressure gradient present on the cylinder's surface and the laminar boundary layer separates. Upon separation a turbulent wake then develops on the rear side of the cylinder.

In critical flow, the laminar boundary layer again grows from the forward stagnation point to the laminar separation point which occurs at approximately 80-85 degrees. In contrast to the subcritical flow case, a transition occurs from laminar to turbulent flow. A turbulent boundary layer then reattaches itself to the cylinder. This reattached turbulent layer eventually separates at a position downstream of the laminar separation point. The region between the laminar separation point and the point of reattachment of the turbulent boundary layer is known as a "separation bubble."



The results of the experiments with the cylinder attached to the flat plate indicate a critical flow pattern exists on the top half of the cylinder for all Reynolds numbers investigated. This flow pattern changed from critical to subcritical over the top as the cylinder to plate spacing was increased to approximately  $d/r = 0.1$  to  $0.2$ . The flow over the bottom half of the cylinder revealed critical flow immediately after a space existed. Flow over the bottom turned from critical to subcritical in the interval of  $0.8 \leq d/r \leq 1.2$ .

Plots of the average Nusselt number versus gap spacing have shown that the minimum average Nusselt number occurs when the plate is attached to the cylinder and the maximum average Nusselt number occurs at  $d/r = 2.0$ .

Qualitative studies [4], using a flow visualization technique in the water tunnel together with measurements of the vortex shedding frequency in the wind tunnel, have contributed a plausible explanation about the trends of average Nusselt number curves.

It is theorized that trends in the average Nusselt number curves are a direct consequence of the strength and frequency of the vortex pattern which forms in the wake of the cylinder.



## II. BACKGROUND

The present investigation of the heat transfer characteristics of a uniformly heated cylinder placed in close proximity to a plane surface in an air stream was conducted concurrently with an investigation by Göktun [4] of the flow characteristics of a cylinder placed near a plane surface. Information obtained from the survey of the heat transfer experiments proved useful in explaining the nature of the flow field observed by Göktun. In the same manner, Göktun's observations made significant contributions to a better understanding of the heat transfer characteristics of the cylinder.

Although extensive investigations have been directed at obtaining a better understanding of the heat transfer and flow characteristics of "free" cylinders (for extensive references on this subject see Cooper, Field and Meyer [5]), data relating to the heat transfer and flow characteristics of the cylinder-plate geometry under investigation were not available in the literature. Such information would be of obvious value in the design of heated piping systems placed near walls and in the design of heat exchangers.

As previously mentioned, the present investigation is a follow-on study of an investigation initiated by McComas [1] and continued by Gnerlich [2]. Although McComas experimentally determined local and average heat transfer



coefficients around a uniformly heated cylinder attached to a wall and Gnerlich did likewise for various cylinder to plate spacings, both of these investigators found no references to theoretical work on this subject.

Convective heat transfer is significantly affected by the fluid flow characteristics occurring adjacent to a solid boundary. Since forced-convection heat transfer is a result of the movement of fluids and the mixing of fluid particles, the mechanism of fluid flow must be understood in order to understand the mechanism of heat transfer and to explain the phenomena occurring during the heat transfer process. Because of this, this project was conducted concurrently with Göktun's [4] study of the flow field near the cylinder-plate geometry. In explaining the heat transfer results obtained in this work, frequent reference will be made to Göktun's concurrent flow investigation.



### III. EXPERIMENTAL APPARATUS

#### 1. Wind Tunnel

An open circuit, subsonic wind tunnel was used for the experiments. The tunnel was specially designed by Kenney Engineering Corp., of Monrovia, California for research quality work. The entire exterior dimensions are given in Figure 2. The tunnel has a test section which is 20 inches wide, 28 inches high at the entrance and expands to 31 inches at the exit to provide for boundary layer growth. It is powered by a 75 HP, 1750 RPM variable speed controlled D.C. motor which provides a belt drive to an adjustable pitch vaneaxial fan. The fan is 45 inches in diameter and is capable of supplying air at 10,000 to 70,000 cfm, producing wind velocities ranging from 10 mph (14.7 ft/sec) to 175 mph (256.7 ft/sec). The tunnel is equipped with six graded mesh screens to control turbulence. A 24 inch water manometer connected in to the stilling chamber and test section may be used to measure velocity. Utilizing a hot wire anemometer, a turbulence intensity level of 0.2% was found in the wind tunnel at a free stream velocity of 98.1 ft/sec. A mercury thermometer was installed in the stilling chamber to measure the free stream temperature.



SCALE: 1" = 5'

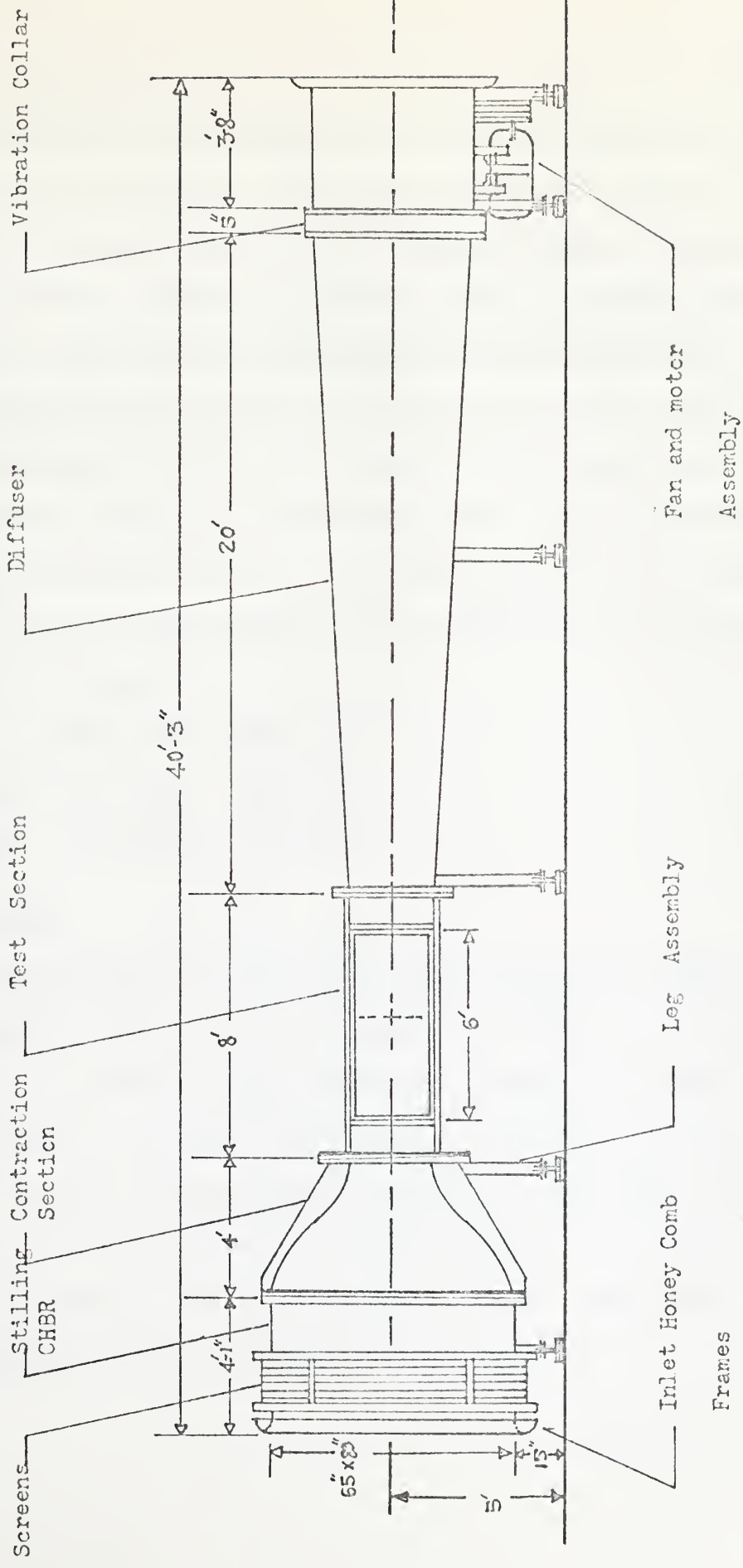


Figure 2. Schematic diagram of the wind tunnel.



## 2. Liquid Crystals

Microencapsulated cholesteric liquid crystals were used to obtain both qualitative and quantitative heat transfer and fluid flow information on the uniformly heated cylinder. The liquid crystals provide a visual display of temperature over discrete, reproducible temperature ranges (called the "event" temperature range) by means of a change of color (see Cooper, Field and Meyer [57]). The visible color spectrum, which falls within a certain temperature band, has an accuracy of 0.2°F. All experiments in this investigation were conducted using a liquid crystal designated as NCR S-43 having an event temperature range of

Red : 109.8°F (43.2°C)

Green: 111.0°F (43.9°C)

Blue : 112.3°F (44.6°C)

## 3. Tensheet

An electrically resistive carbon impregnated paper known as "Tensheet" was used as the heating element in these studies. Tensheet is a thin, highly flexible, fibrous material containing no wires or ribbons and therefore is free of localized hot spots, burnout, and breakage problems. The nominal thickness is 0.1 cm and the electrical resistivity is about 2.5 ohm-cm. Using the Tensheet it is possible to heat large areas within less than 2% deviation from point to point.



#### 4. Cylinder

The test cylinder utilized in obtaining the heat transfer data was the one used by Gnerlich [27]. It was made of three cylinders attached end to end (see Figure 3) having a total length of 20 inches, corresponding to the test section width, and a diameter of 3 inches. The two end sections were hollow wood cylinders connected by a wooden brace, curved to match the cylinder contour. The central cylinder, henceforth designated as the test section, was formed from a sheet of Temsheet. It was tightly packed with glass wool which served the dual purpose of providing insulation against possible internal heat losses due to conduction and free convection and also provided the paper cylinder with added resistance to deformation. The circumference of the Temsheet cylinder was marked at five degree angular intervals in two locations 2 inches apart for accurate location of the liquid crystal isotherms during the experiment. Aluminum foil conducting tape served as electrodes. The aluminum tape was circumferentially attached on the inner surface of the Temsheet. Silver conducting paint was applied to the interface between the tape and Temsheet to insure good electrical contact was maintained between the two surfaces. Two lead wires were connected to the aluminum foil through one end of the cylinder. The lead wires were attached to a regulated DC power supply (model: LAMBDA LK 345A FM). The resistance of the Temsheet was measured by a digital multimeter (model: FLUKE 8100A).



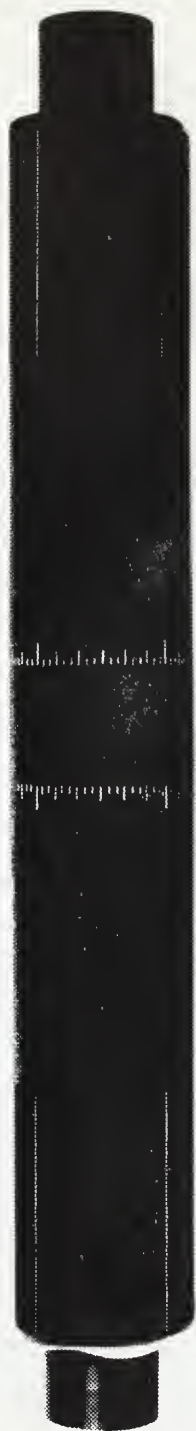


Figure 3 Photograph of the Tensheet cylinder.



## 5. Plates

The plates used in the experiments were constructed of plexiglass and were 0.5 inch thick, 20 inches wide and had total lengths of 40, 46 and 58 inches, respectively. The plates were installed horizontally in the wind tunnel in such a way that the leading edge of the plates extended 2, 4 and 8 cylinder diameters (i.e. 6, 12 and 24 inches, respectively) ahead of the cylinder centerline. The plates were beveled on the under side of the leading edge with an angle of 12 degrees. The plates were capable of being located at any position relative to the cylinder (Figure 4), from attached to a maximum distance of 8 inches away (i.e.  $d/r = 5.33$ ). The plates were moved vertically by means of a threaded rod extending through the tunnel floor, and a rear brace which locked in position by means of a split nut.



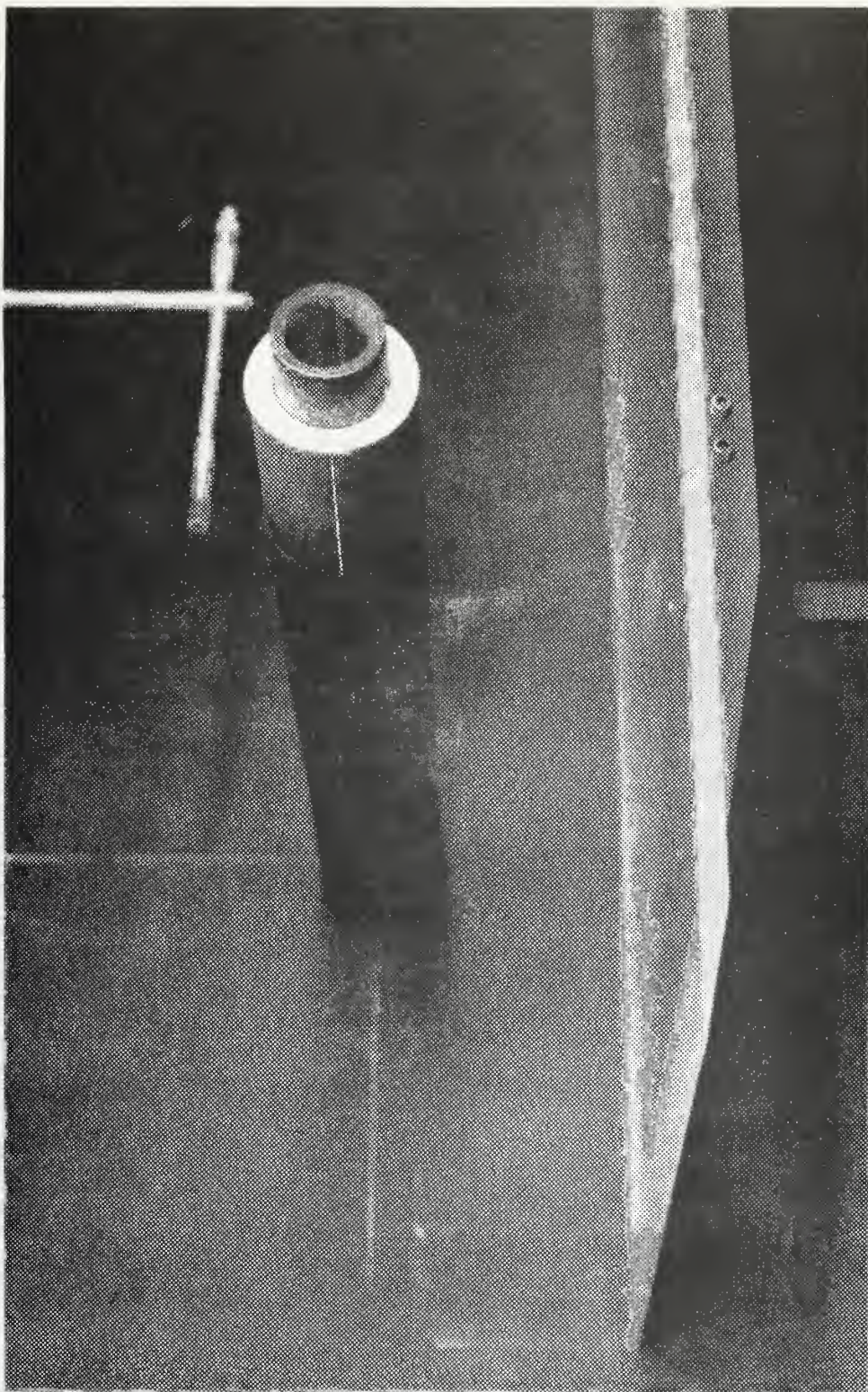


Figure 4 Photograph of the plate and cylinder assembly.



#### IV. EXPERIMENTAL PROCEDURE

The present investigation was conducted using the same test facilities as employed by Gnerlich [2]. Gnerlich, however, performed experiments only for a Reynolds number of 153,000 (based on the cylinder diameter) and a plate leading edge of 12 inches. In the present work, experiments were conducted at Reynolds numbers of 16,000, 90,000 as well as 153,000 and the plate leading edge was varied from 6 to 24 inches.

To initiate the experiment, a sufficient voltage (from 12 to 15 volts) was applied to the cylinder to insure that the liquid crystals reached their event temperature and changed color over the entire surface of the cylinder. This was done to check for hot and cold spots which would indicate improper packing of the glass wool inside the cylinder. The wind tunnel was then started and set to a predetermined velocity at which it was maintained throughout the run. The applied voltage was adjusted until the first faint red color trace was observed. The power supply was then turned off and the multimeter was switched from DC voltmeter to ohmmeter. The same procedure was also followed at the end of the experiment. In this manner, an accurate value of the paper resistance, which was taken to be the arithmetic mean of initial and final resistance values, was determined. The multimeter was then switched back to the DC voltmeter and power was re-applied



to the test section. A steady state condition was usually attained in from five to ten minutes depending upon the wind velocity. Generally, at least 40 minutes were spent to take the first data point in order to be extremely certain about steady state conditions.

The first color band observed on the cylinder was at the location of the value of the lowest local Nusselt number. The voltage was then increased such that the liquid crystal color bands would appear at various angular positions around the circumference of the cylinder. The temperature obtained in this manner could be compared to the air stream temperature which was obtained from a thermometer mounted in the stilling chamber. Using this temperature difference and power dissipation, the local Nusselt number based on the cylinder diameter could be obtained around the cylinder (see Appendix A).

Due to the method of construction, there was a seam along the length of the test cylinder. Measurements within 30 degrees of a sector of the seam were considered unreliable. The majority of Nusselt number data were collected with the seam located at 180 degrees. The Nusselt number data in the vicinity of 180 degrees were taken by turning the cylinder such that the seam was facing forward at 0 degrees. Several other seam positions were also checked but it was ultimately decided that the 0 and 180 degrees locations were the best for the seam position. In all experiments, the location of the liquid crystal color transition points were easily



distinguishable around the circumference of cylinder except in the region of 0 to 45 degrees and 160 to 200 degrees. Especially in the forward stagnation region the temperature gradient was very shallow and the whole region appeared isothermal. In the vicinity of the rear stagnation point, the temperature gradient was indistinct due to the turbulent behavior of the flow in the cylinder wake.



## V. RESULTS

The results shown in this section were obtained from the heat transfer experiments discussed in Section VI. The results are classified in two groups:

### A. LOCAL NUSSELT NUMBERS, $Nu$

a. Typical data and a sample calculation for the heat transfer coefficient and the local Nusselt number are shown in Appendix A.

b. Figures 5 through 12 show the variation of the local Nusselt number with gap size at a Reynolds number of 153,000 and a plate leading length of 12 inches ( $L/D = 4$ ). These plots also show the variation of the pressure coefficient as a function of gap size. All pressure data were taken from Gökten's [4] results and are informative in that they show the relationship between surface pressure and heat transfer characteristics.

c. Additional plots of the Nusselt number versus gap size for Reynolds numbers of 16,000, 90,000 (with  $L/D = 4$ ) and 153,000 (with  $L/D = 2$  and 8) can be found in Appendix D, Figures 24 through 55. Local Nusselt number distributions on the surface of a free cylinder are also contained in Appendix D, Figures 56 through 58.

### B. AVERAGE NUSSELT NUMBERS, $\overline{Nu}$

a. A graph of  $\overline{Nu}$  versus  $d/r$  (the cylinder to plate spacings) for Reynolds numbers of 16,000, 90,000 and 153,000



and  $L/D = 4.0$  is shown in Figure 13. A comparison is made with Gnerlich's [2] results on the same graph.

b. A graph of  $\overline{Nu}$  versus  $d/r$  for Reynolds number of 153,000 and  $L/D = 2, 4$  and 8 is shown in Figure 14.

c. A graph of normalized drag coefficient ( $C_d/C_{d\infty}$ ), Strouhal number ( $S/S_\infty$ ) and average Nusselt number ( $\overline{Nu}/\overline{Nu}_\infty$ ) versus  $d/r$  is shown in Figure 15. The " $\infty$ " subscript refers to values obtained with no plate in the tunnel.

d. A graph of normalized Strouhal number and local base Nusselt number ( $Nu_{base}/Nu_{\infty base}$ ) versus  $d/r$  is shown in Figure 16.



Nu .

Cp x

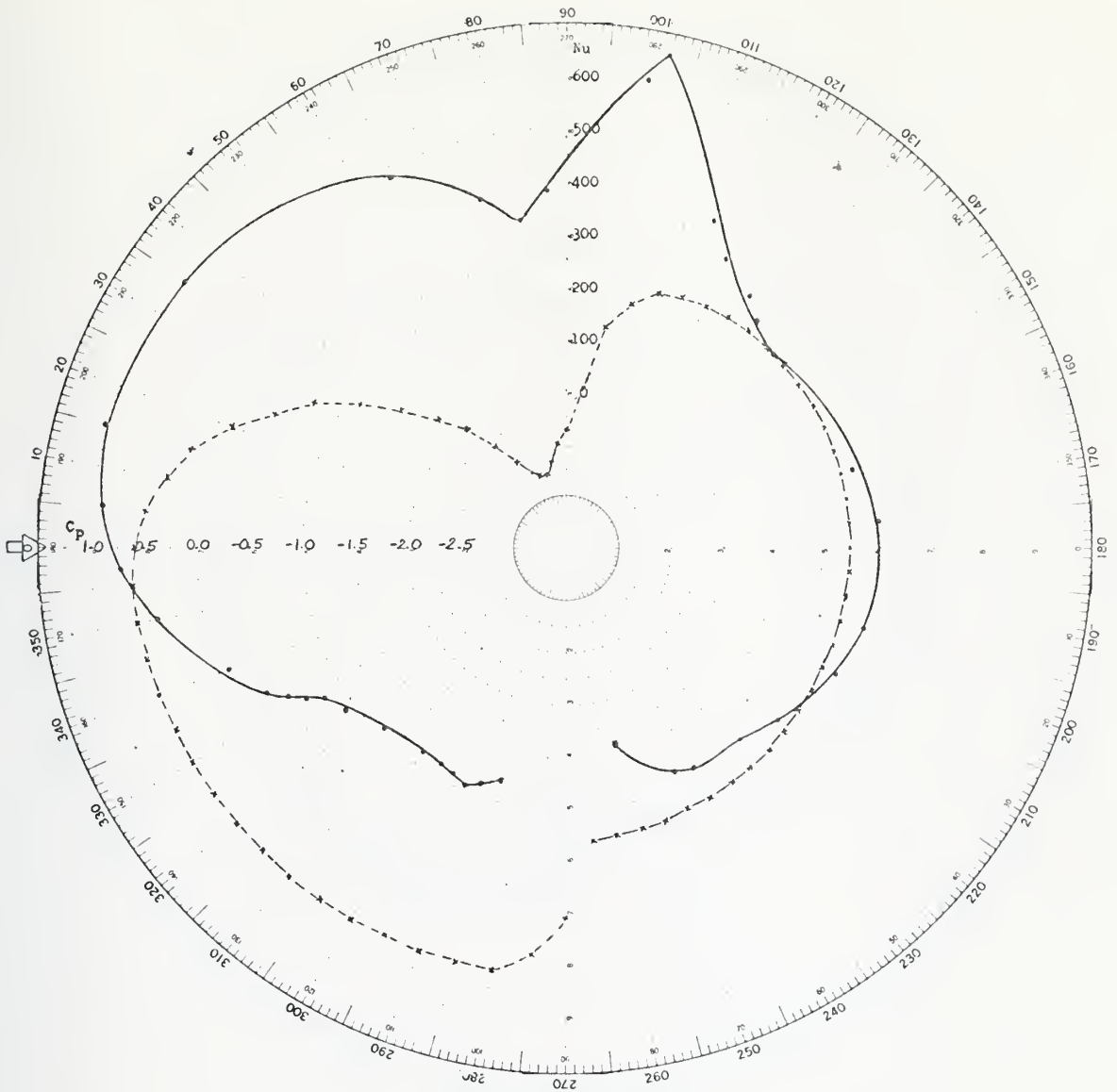


Figure 5. Local Nusselt number and pressure coefficient on the surface of a cylinder placed near a plane surface for  $Re = 153,000$ ,  $L/D = 4$ ,  $d/r = 0.0$ .



Nu .

Cp x

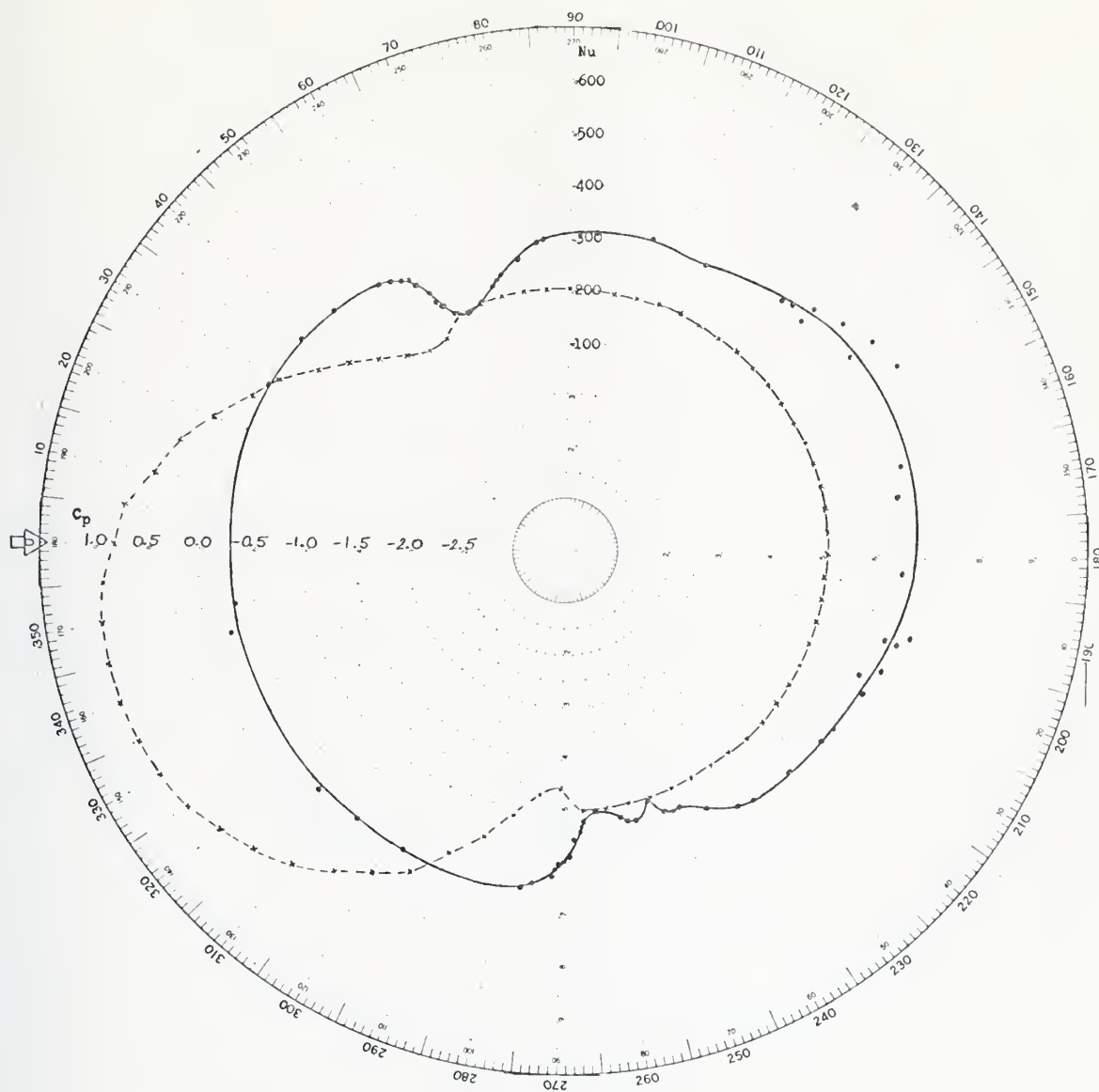


Figure 6. Local Nusselt number and pressure coefficient on the surface of a cylinder placed near a plane surface for

$Re = 15000$ ,  $L/D = 4$ ,  $d/r = 0.25$ .



Nu

$C_p$  x

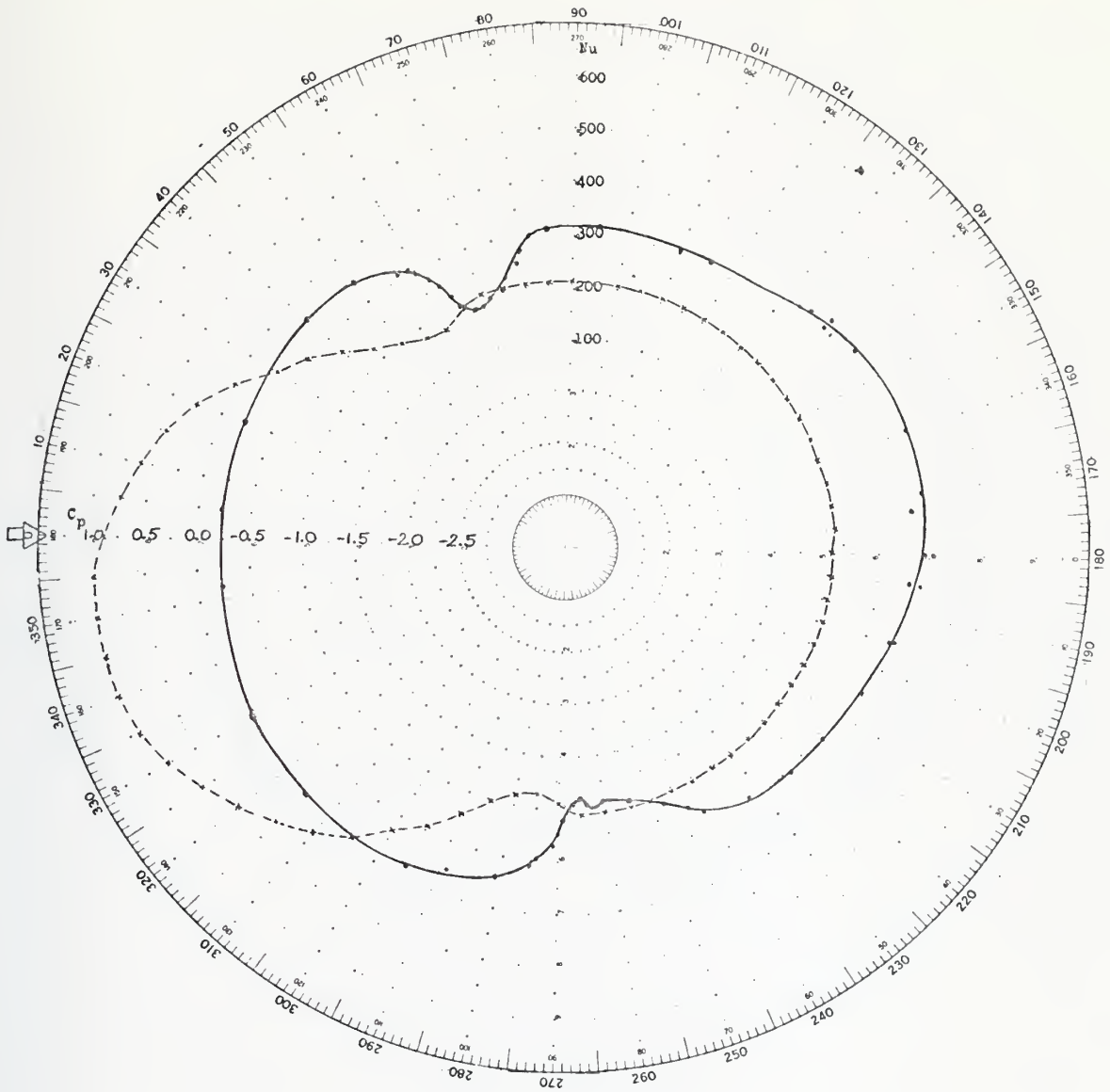


Figure 7. Local Nusselt number and pressure coefficient on the surface of a cylinder placed near a plane surface for  $Re = 153,000$ ,  $L/D = 4$ ,  $d/r = 0.5$ .



$Nu$  .

$C_p$  x

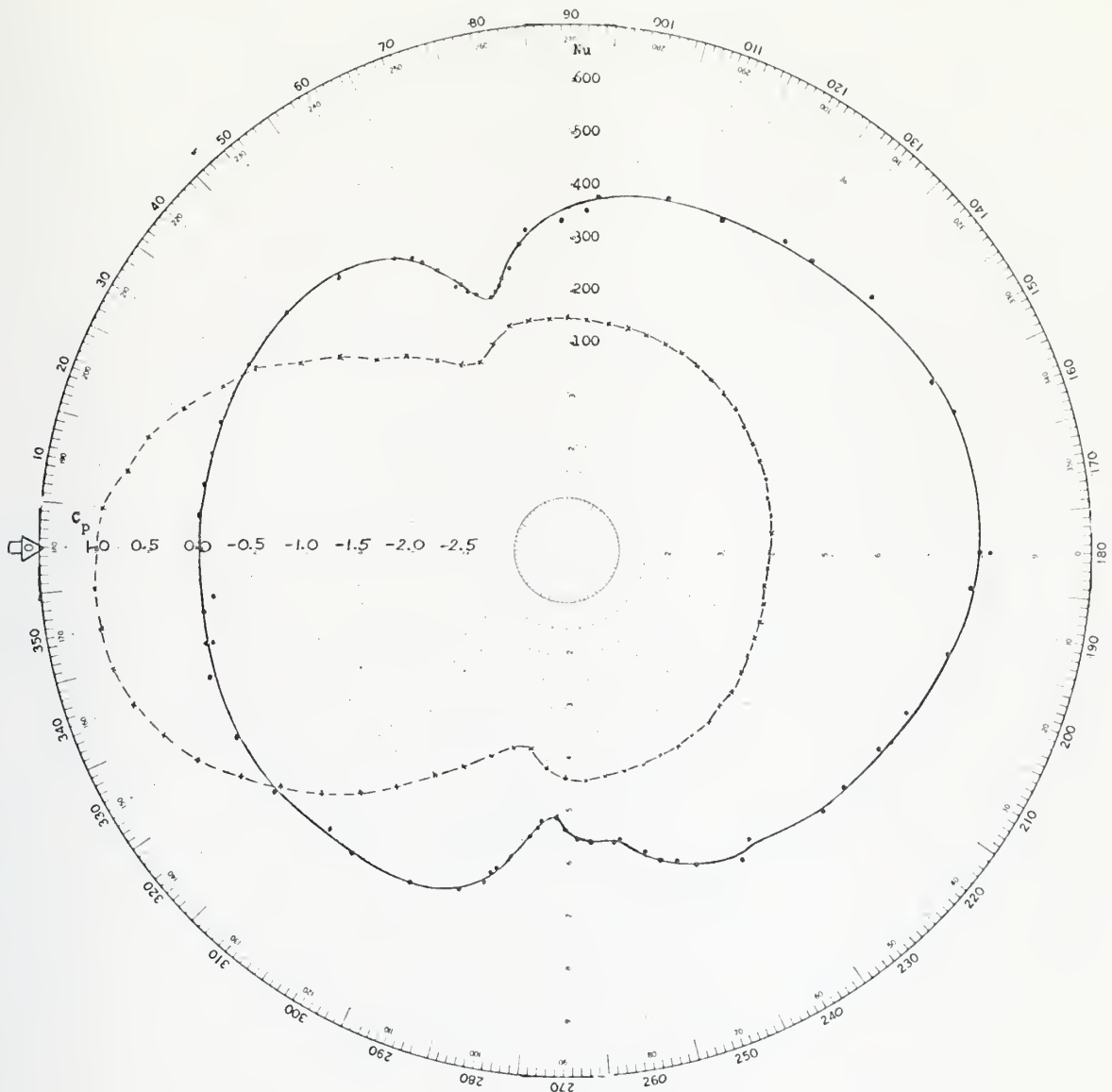


Figure 8. Local Nusselt number and pressure coefficient on the surface of a cylinder placed near a plane surface for  $Re = 153,000$ ,  $L/D = 4$ ,  $d/r = 1.0$ .



$Nu$  .

$C_p$  x

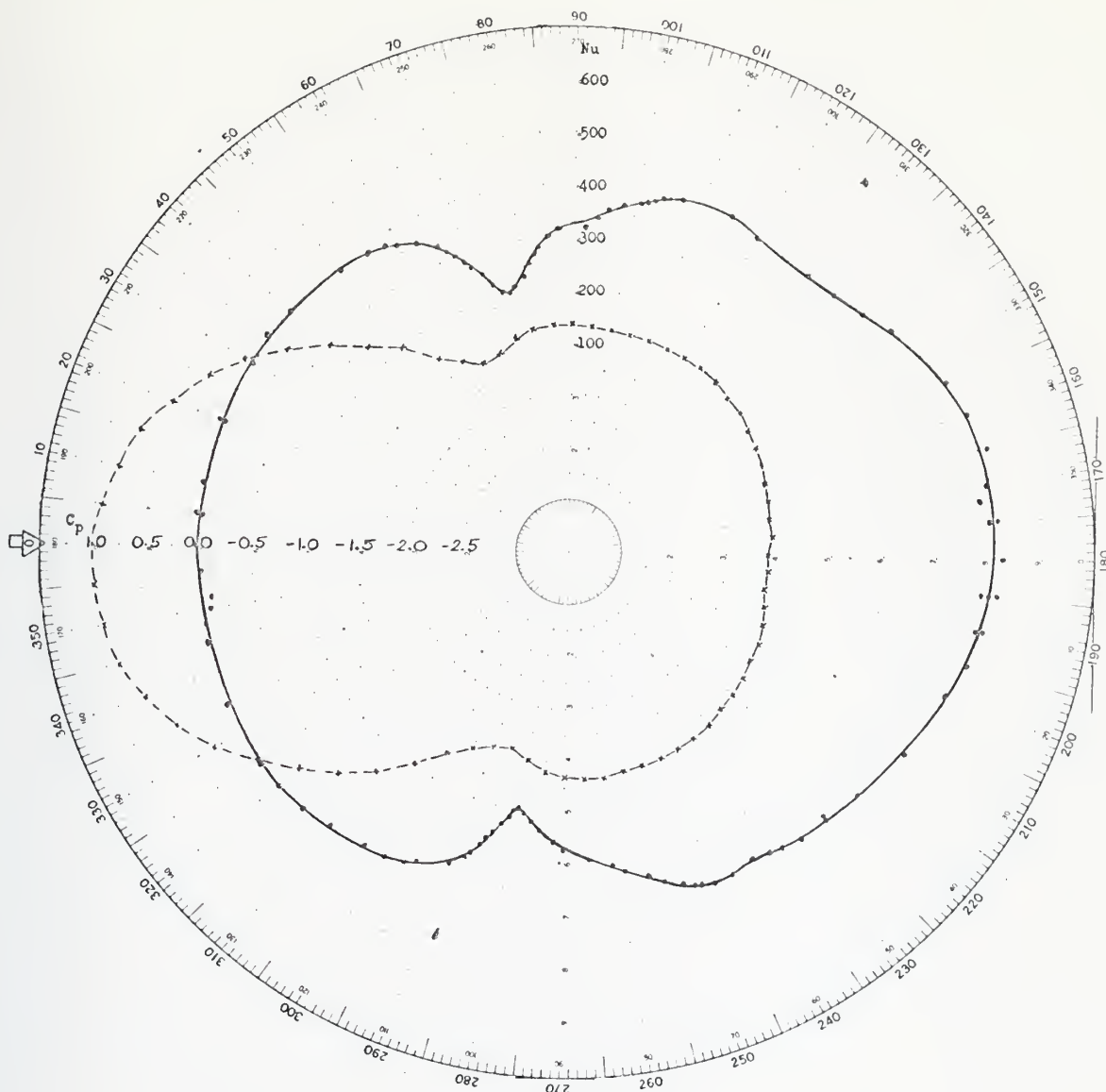


Figure 9. Local Nusselt number and pressure coefficient on the surface of a cylinder placed near a plane surface for  $Re = 153,000$ ,  $L/D = 4$ ,  $d/r = 2.0$ .



Nu    .

Cp   x

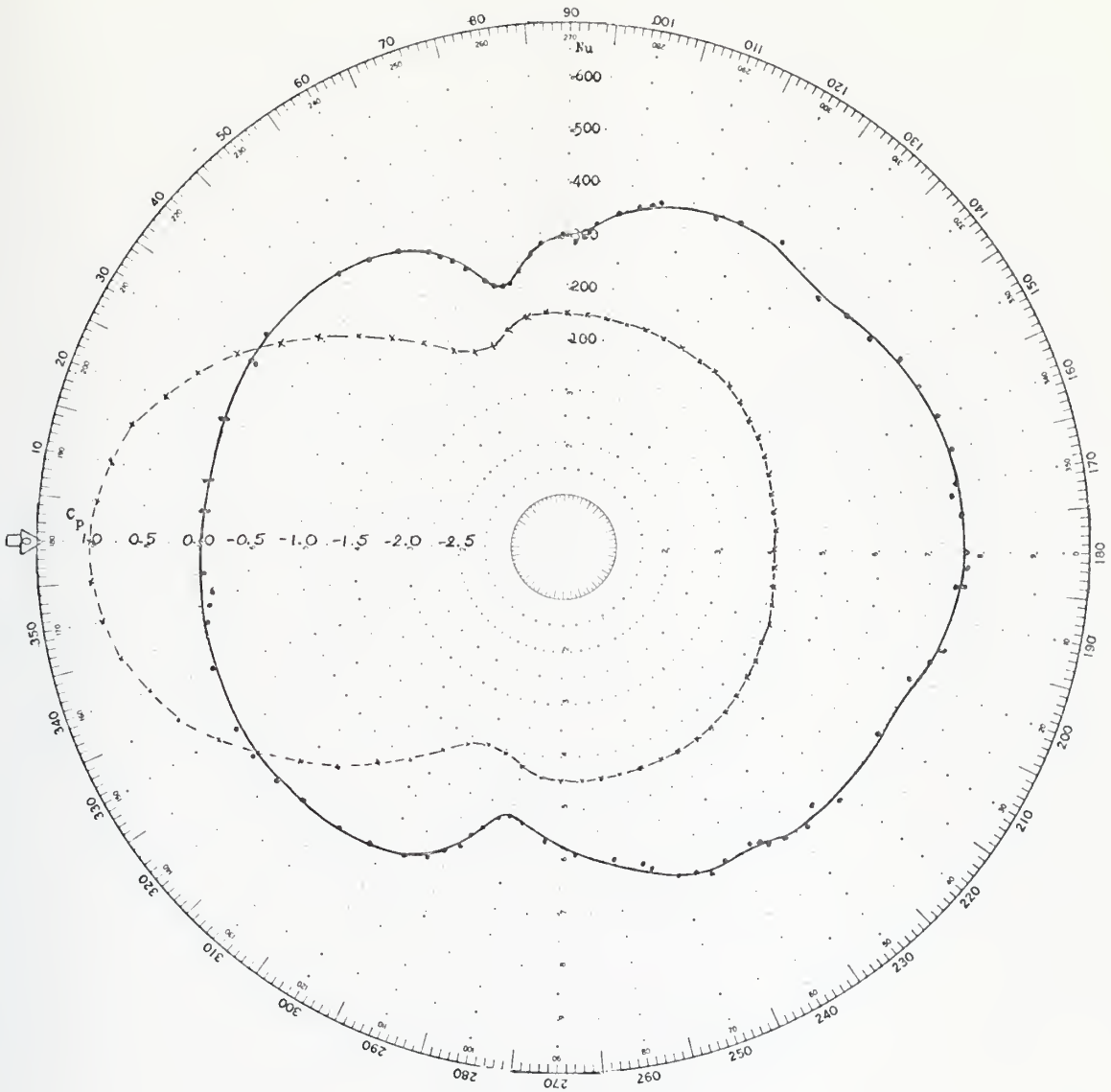


Figure 10. Local Nusselt number and pressure coefficient on the surface of a cylinder placed near a plane surface for  $Re = 153,000$ ,  $L/D = 4$ ,  $d/r = 3.0$ .



Nu

$C_p$  x

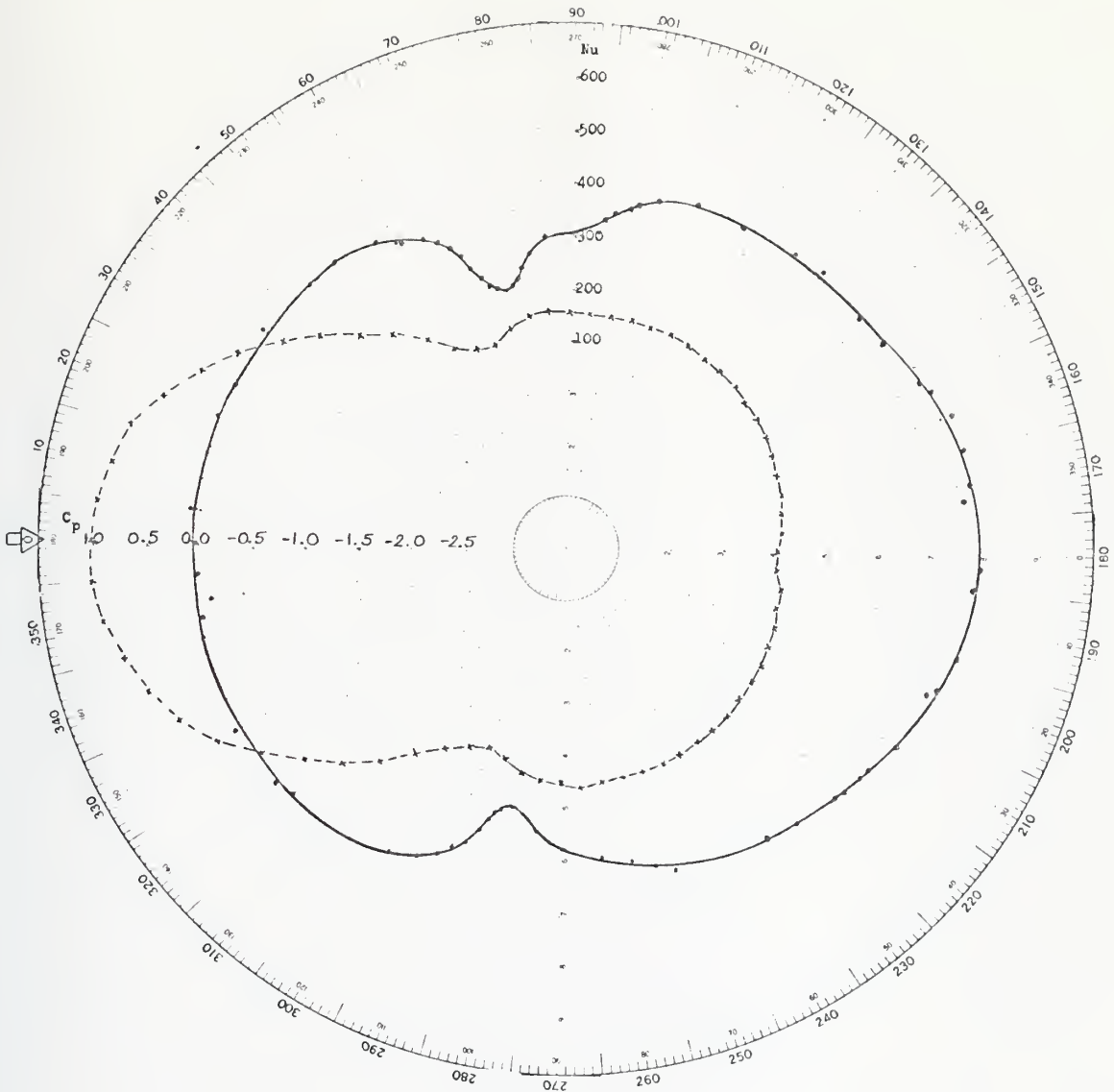


Figure 11. Local Nusselt number and pressure coefficient on the surface of a cylinder placed near a plane surface for  $Re = 153,000$ ,  $L/D = 4$ ,  $d/r = 4.0$ .



Nu

Cp x

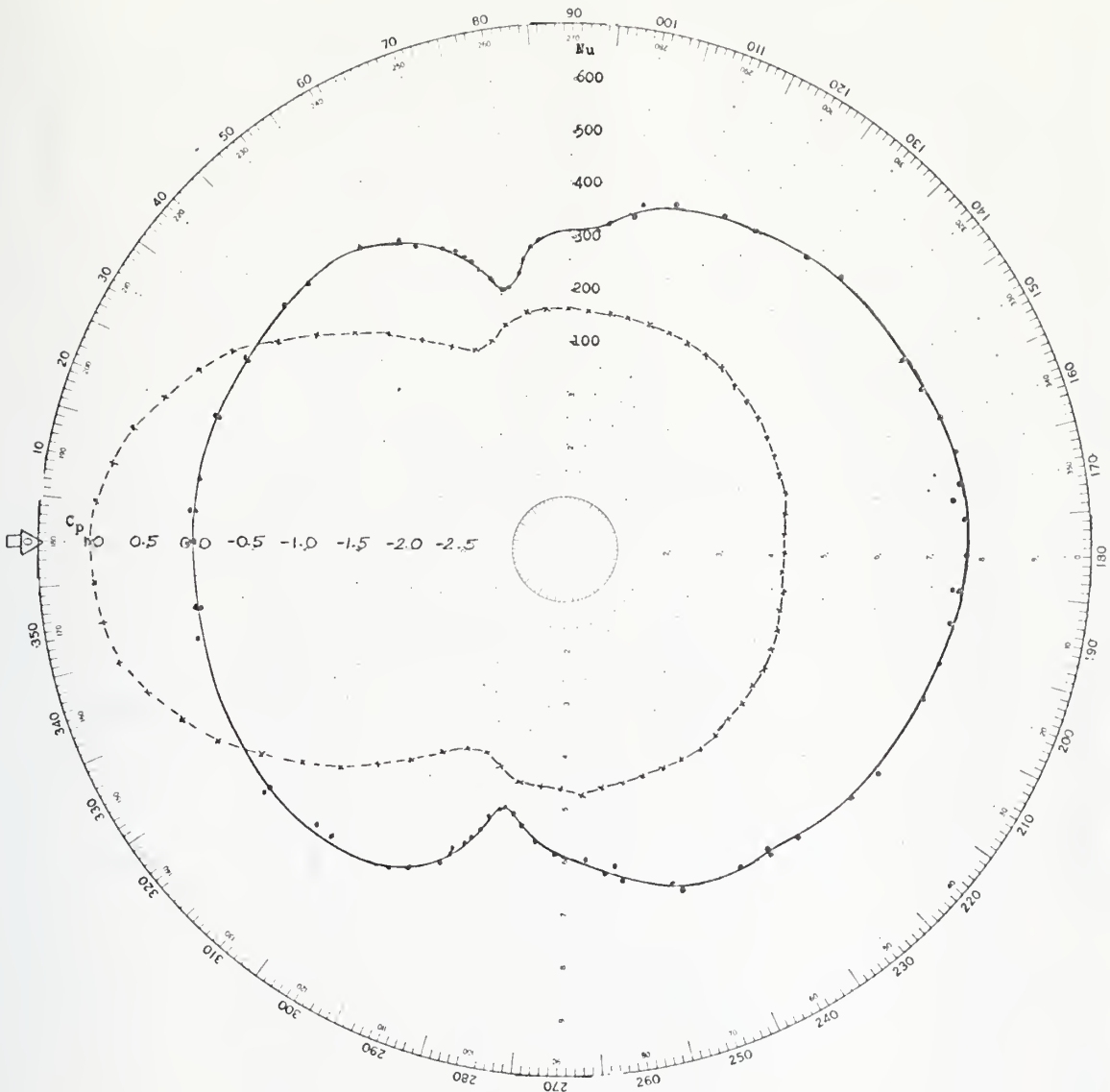


Figure 12. Local Nusselt number and pressure coefficient on the surface of a cylinder placed near a plane surface for  $Re = 153,000$ ,  $L/D = 4$ ,  $d/r = 5.33$ .



• Kösemen

○ Gnerlich [2]

I Uncertainty

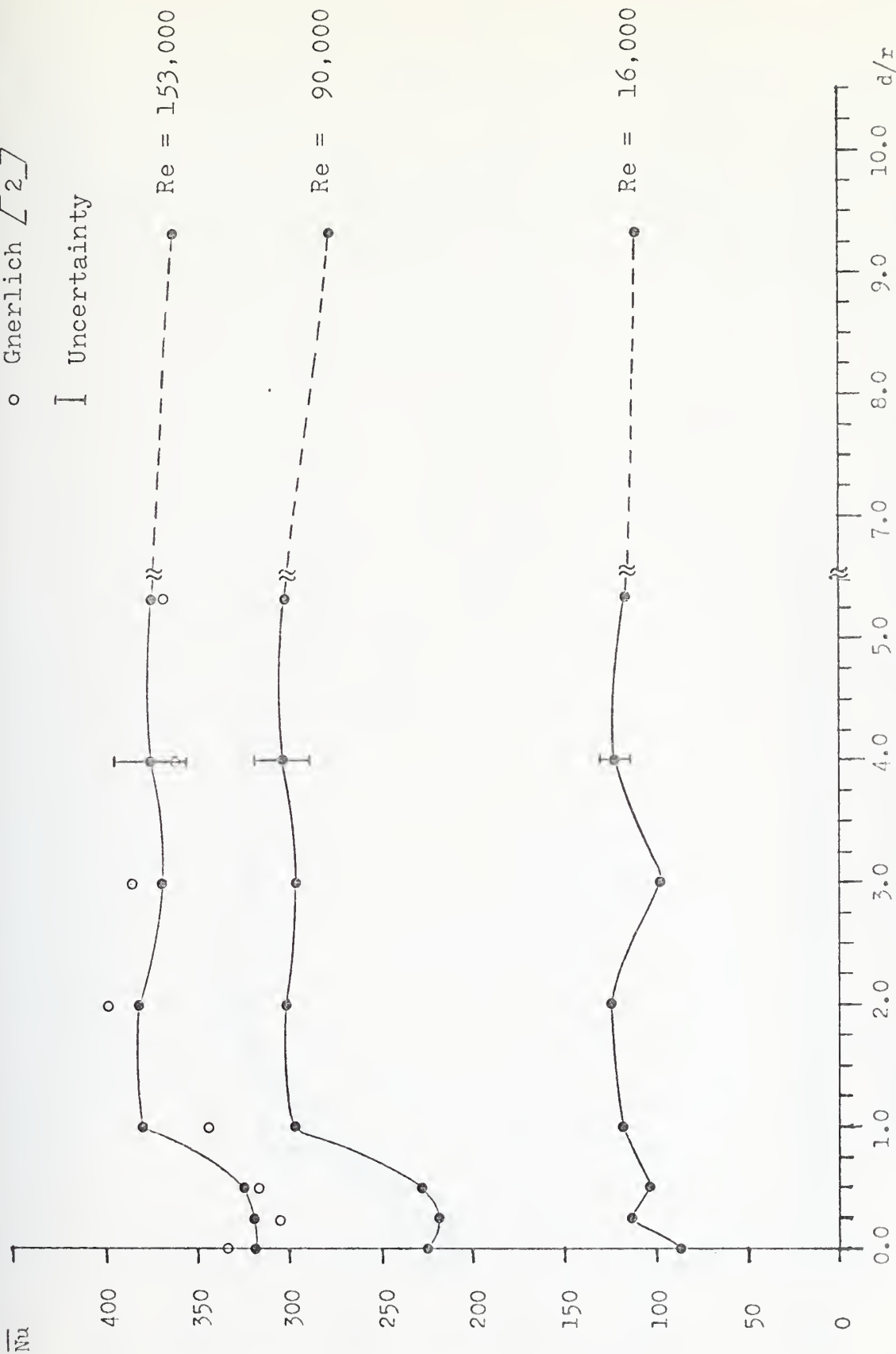


Figure 13. Average Nusselt number variation as a function gap size and Reynolds number for  $L/D = 4$ .



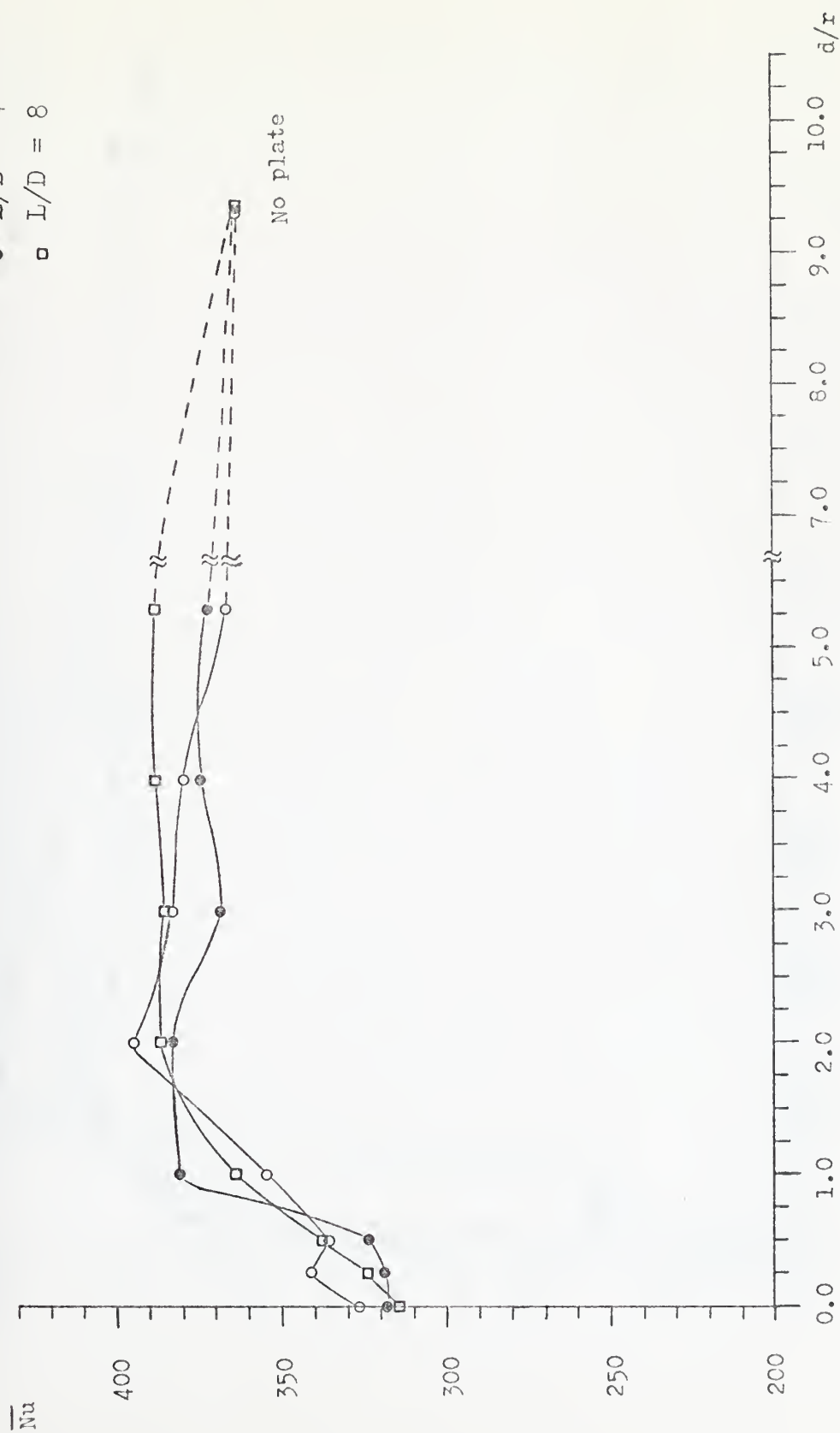


Figure 14. Average Nusselt number variation as a function of plate length and gap size for a Reynolds number of 153,000.



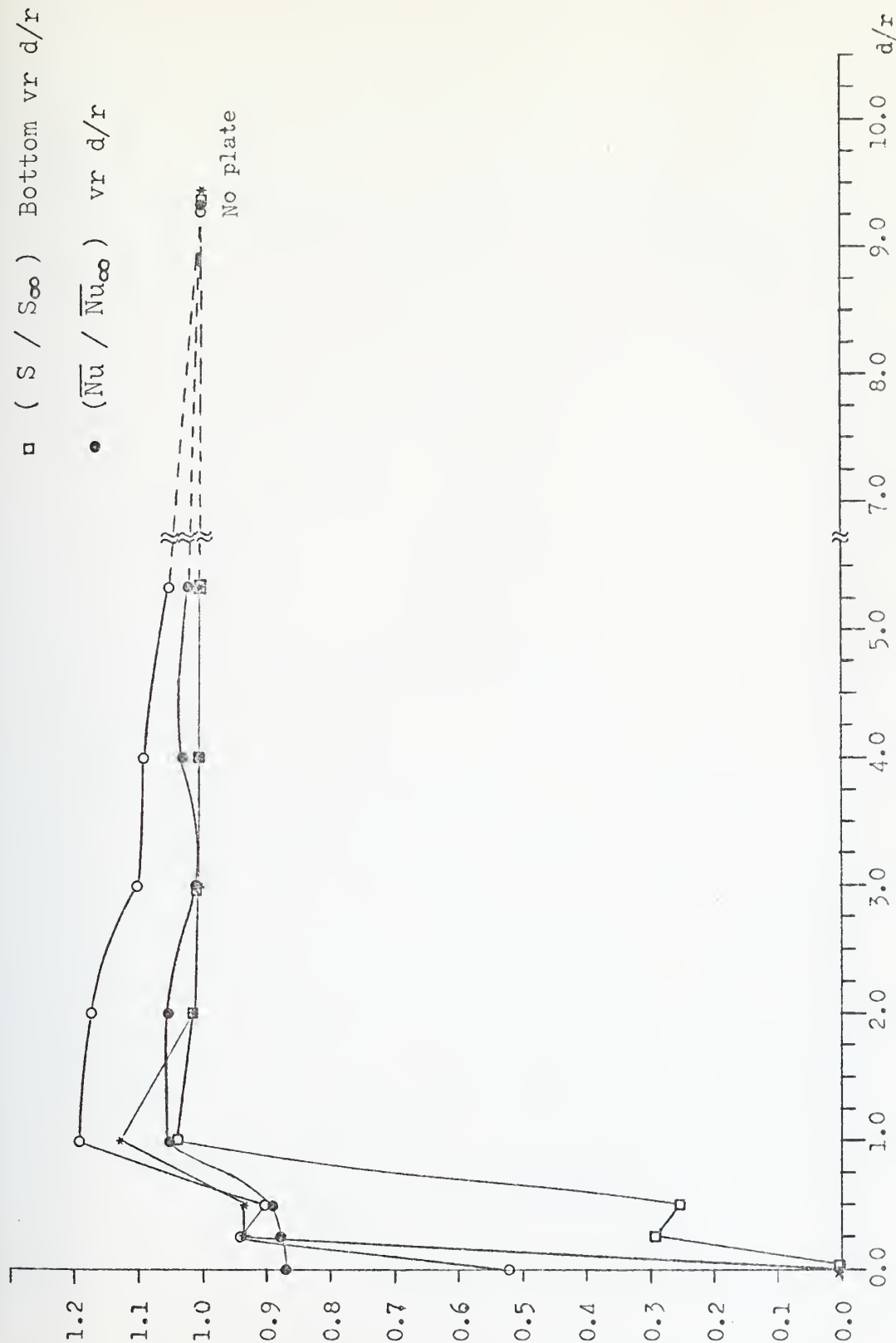


Figure 15. Variation of normalized drag coefficient ( $C_d/C_{d\infty}$ ), Strouhal number ( $S/S_{\infty}$ ) and average Nusselt number ( $\overline{Nu}/\overline{Nu}_{\infty}$ ) as a function of gap size for  $Re = 153,000$  and  $L/D = 4$ .



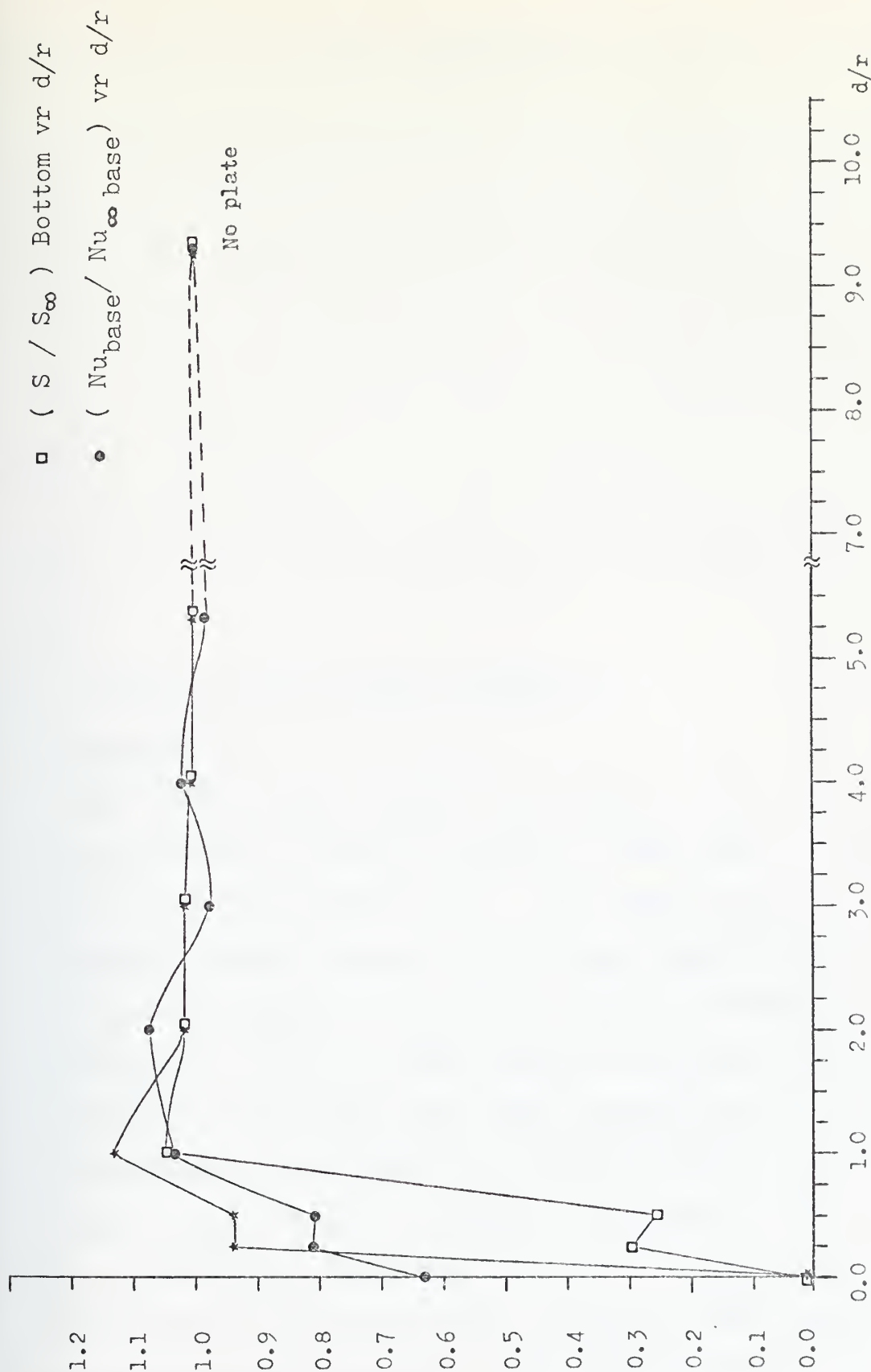


Figure 16. Variation of normalized Strouhal number ( $S / S_{\infty}$ ) and base Nusselt number ( $Nu_{base} / Nu_{\infty base}$ ) as function of gap size for  $Re = 153,000$  and  $L/D = 4$ .



## VI. DISCUSSION

Because of the relationship between the flow characteristics (i.e. pressure distribution around the cylinder, pressure drag and vortex dynamics) and the heat transfer characteristics of the cylinder, the parallel flow study of Göktun [4] will be referred to in some parts of the following discussion. Göktun obtained his results using an unheated aluminum cylinder placed in proximity to the plane surface.

The general nature and trends of the results obtained from the present investigation can be discussed in two groups:

### A. TRENDS IN LOCAL NUSSELT NUMBERS, $Nu$

At  $d/r = 0$

The initial heat transfer measurements were made with the uniformly heated cylinder attached to the plate at a Reynolds number of 153,000 with  $L/D = 4$ . The data obtained in this arrangement agreed within the estimated experimental uncertainty of  $\pm 5\%$  (See Appendix B) with the results of McComas [1] and Gnerlich [2]. A local maximum and minimum value of the Nusselt number were once again observed near the point of attachment of the plate and cylinder and are indicative of a large trapped vortex as proposed by McComas [1]. In the flow visualization experiment, at  $d/r = 0$ , Göktun [4] also observed that a series of small, circular, three dimensional vortices were also present in the upstream cavity as well as



a large turbulent vortex. The large turbulent vortex occurs within the separated region where the flow separates from the flat plate and reattaches to the cylinder. The point of flow reattachment occurs at approximately 140 to 170 degrees from the point of attachment of the plate and cylinder. The existence of this large turbulent vortex produces the observed local maximum and minimum values in the Nusselt number curve.

The existence of a separation bubble on the top of the cylinder was the obvious mark of critical flow. A laminar boundary layer started to grow on the forward half of the cylinder and separated between 80-85 degrees and a subsequent transition to turbulent flow occurred resulting in the reattachment of a turbulent boundary layer at about  $100^{\circ}$ - $105^{\circ}$ . The reattached turbulent layer ultimately separated at approximately 130-135 degrees.

The decrease in the local Nusselt number (see Figure 5) at the aft end of the cylinder was unexpected. The flow visualization studies clearly showed, however, that when the cylinder is resting on the plate a large wake with very little fluid motion develops on the downstream side of the cylinder. The absence of fluid motion therefore explains the decrease in Nusselt number on the back of the cylinder.

At  $d/r = 0.25$  to  $d/r = 5.33$

Further experimental results at a Reynolds number of 153,000 were obtained with the plate as far removed from the cylinder as possible,  $d/r = 5.33$ .



Examination of the polar plots in Figure 6 to 12 for significant trends or unusual nature show two items of interest:

1. A shift in the location of the forward stagnation point, rear stagnation point and the laminar separation points (see Figure 17).

Starting from  $d/r = 0.25$  and moving the plate to  $d/r = 2.0$ , it appears as though an imaginary axis initially passing through 340 and 160 degrees is pivoted about the origin. As this axis turns clockwise through 20 degrees of arc to 360 degrees, the angular position of the stagnation and separation points changed correspondingly up to  $d/r = 2$ , and then reached a constant behaviour (see Figure 6 to 9).

This observed shifting of stagnation points was definitely not affected by the variation of the length of the plate's leading edge and/or the Reynolds number as shown in Appendix D, in Figures 40 to 55.

2. The transition from critical to subcritical flow.

The transition from critical to subcritical flow was investigated in order to find the  $d/r$  ratio associated with the transition on the top and bottom of the cylinder. At a Reynold's number of 153,000 and  $L/D = 4$ , the flow was critical over the top of the cylinder with the plate attached and was subcritical over the top at  $d/r = 0.25$ . By alternately varying the plate to cylinder spacing, carefully adjusting the voltage and noting the liquid crystal display, the transition point from critical to subcritical flow was precisely found at  $d/r = 0.1$ .



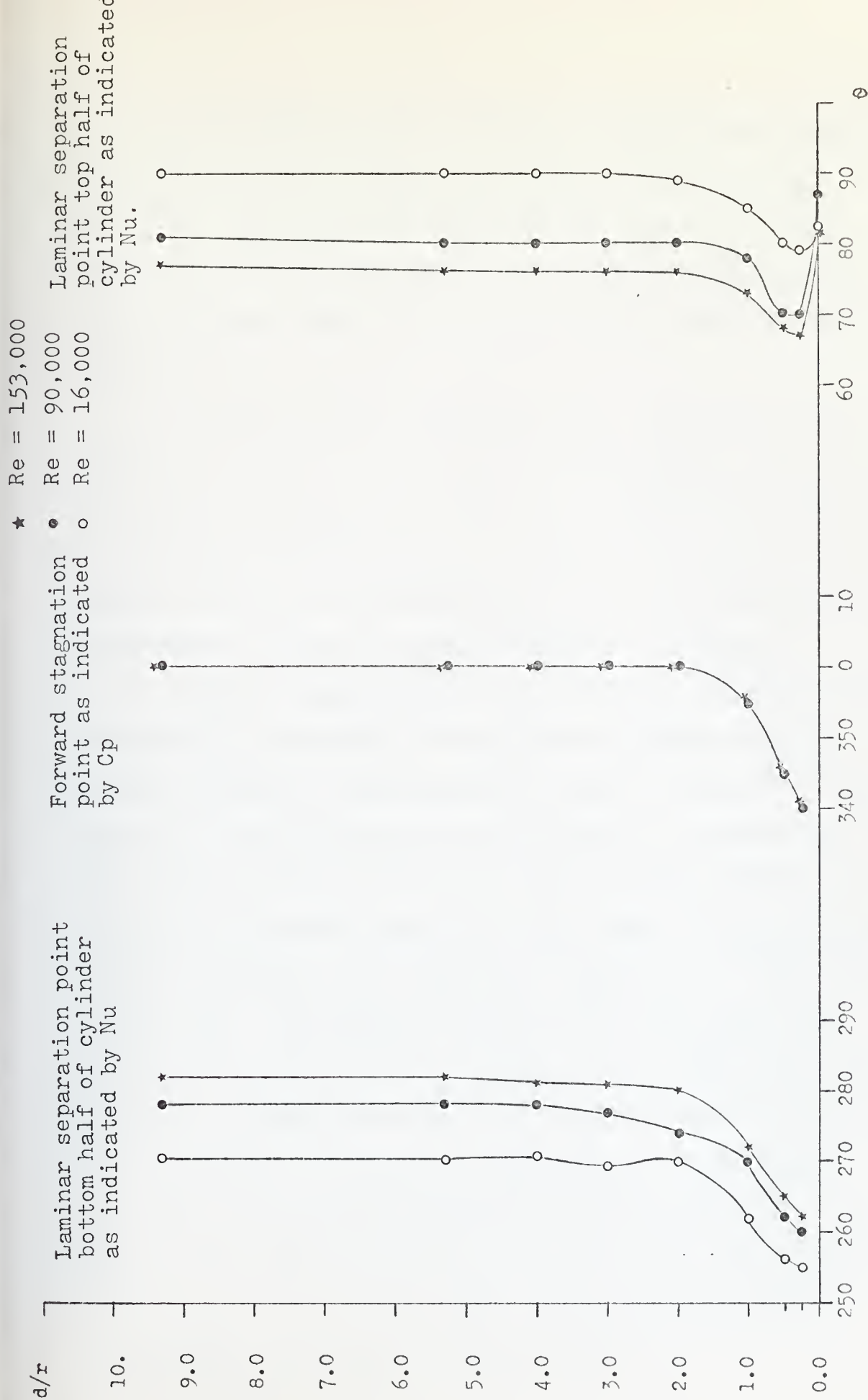


Figure 17. Shift of the Laminar separation points and the stagnation point as a function of  $d/r$ .



A transition from critical to subcritical flow over the bottom of the cylinder was found at approximately  $d/r = 1.2$ . In this case, although the pattern of the separation bubble displayed by the liquid crystal band was less pronounced than over the top, it was clearly observed as far as  $d/r = 1.2$ .

As also noted by Gnerlich [2], flow over both the top and bottom of the cylinder are definitely critical for the stated  $d/r$  ranges but there is a significant difference in the degree of criticality on the top and bottom of the cylinder as far as the magnitudes of the local Nusselt numbers are concerned. This is seen in Figures 5 through 8.

Further study was also conducted in order to see the influence of the length of the plate's leading edge and Reynolds numbers. The results are shown in Table 1. Table 1 shows the transition points from critical to subcritical flow that occurred over the top and bottom of the cylinder as a function of Reynolds number and  $L/D$  ratios. It is worthwhile to note all points fell within the range of  $0.1 \leq d/r \leq 0.2$  for the top. The transition points for the bottom were found in the interval of  $0.8 \leq d/r \leq 1.2$ . Also to be noted in Table 1 is that the transition from critical to subcritical flow at various  $d/r$  ratios is apparently independent of  $L/D$  ratios but is mildly dependent on Reynolds number. As the Reynolds number increased, the  $d/r$  ratios for transition on the top of cylinder decrease slightly; on the bottom of the cylinder the behaviour was reversed.



Re	L/D = 2		L/D = 4		L/D = 8	
	Top at "d/r"	Bottom at "d/r"	Top at "d/r"	Bottom at "d/r"	Top at "d/r"	Bottom at "d/r"
16000	0.20	1.0	0.20	0.9	0.2	0.8
90000	0.15	0.90	0.15	0.9	0.15	0.8
153000	0.15	1.2	0.10	1.2	0.1	1.2

Table 1. Transition from critical to subcritical flow as a function of Reynolds number, d/r and L/D ratios.

#### B. TRENDS IN AVERAGE NUSSELT NUMBER, $\overline{Nu}$

In order to gain further information about the cylinder heat transfer characteristics, the average Nusselt number,  $\overline{Nu}$  was computed from the formula

$$\overline{Nu} = \frac{1}{2\pi} \int_0^{2\pi} Nu \cdot d\theta$$

The integration was carried out on an IBM-360 computer using Simpson's Rule of Quadrature with a step size of 5 degrees.

Figure 13 shows the variation of the average Nusselt number as a function of gap spacing for three Reynolds number and L/D = 4.

A comparison of the results obtained at Re = 153,000 and L/D = 4, with those obtained by Gnerlich indicates that the trends are essentially the same. The decrease in  $\overline{Nu}$  at d/r = 0.5 in Gnerlich's results was not observed in the



present experiments but, considering the magnitude of the decrease and the 5% experimental uncertainty involved in both experiments, it is not felt to be significant. The maximum  $\overline{Nu}$  was observed at  $d/r = 2.0$  and it is readily apparent that the presence of the plate radically altered the magnitude of  $\overline{Nu}$  in the range  $0 \leq d/r \leq 2$ . Beyond a  $d/r$  of 2.0,  $\overline{Nu}$  approached a nearly constant value.

It is important to emphasize that the trends of the  $\overline{Nu}$  versus  $d/r$  curves are nearly the same for all Reynolds numbers.

In order to see the effect of the length of the plate's leading edge, results were obtained for a Reynolds number of 153,000 for  $L/D$  ratios of 2, 4 and 8. The results, which are shown in Figure 14, clearly indicated that there is no significant effect on the trends in the  $\overline{Nu}$  curve due to changing the  $L/D$  ratios. Göktun [4] also noted that changing the  $L/D$  ratio had no significant influence on the drag and lift characteristics of the cylinder.

For the sake of simplicity, the flow characteristics (pressure drag and vortex shedding frequency) and the heat transfer characteristics (average and base local Nusselt number) are combined and plotted in normalized form in Figures 15 and 16.

Göktun's qualitative flow visualization study [4] in the water tunnel together with the vortex shedding frequency measurements in the wind tunnel indicated that vortex dynamics control the drag on the cylinder. Figure 15 clearly indicates



the interrelation between the drag and heat transfer. It is seen that as the drag coefficient increases, the average heat transfer coefficient also increases. It is therefore concluded that the vortex dynamics are responsible for the trends observed in both the drag and average Nusselt number curves.

In the range  $0 < d/r < 1$ , Göktun found that the natural or regular vortex pattern formed in the wake of a free cylinder is inhibited by the presence of the plate. The plate significantly reduces the vortex shedding frequency. This in turn has an effect on the base pressure (see Figures 5 through 8) and base Nusselt number (Figure 16). The more stagnant the wake, the higher the base pressure and the lower the base Nusselt number. Therefore, the stagnant wake results in poor heat transfer. This trend, in turn, influences the drag and average Nusselt number (Figure 15).

Göktun [4] observed that strong and violent vortices were formed behind the cylinder when  $d/r$  was approximately 1.0 to 2.0. These vortices transfer high-momentum cool fluid from outside the boundary layer in toward the rear surface of the cylinder. The cool fluid in the vortex which impacts on the hot cylinder surface has a large capacity to remove energy. The "scrubbing" motion of these vortices building up behind the cylinder and breaking away to be carried downstream in the wake, results in high rates of heat transfer and this results in a large base Nusselt number. This trend, in turn, influences both the drag coefficient and the average Nusselt number.



As the plate is moved further from the cylinder, the drag and Nusselt number approach their "free" cylinder values.



## VII. SUMMARY

This experimental investigation was carried out to gain an understanding of the heat transfer behavior of a uniformly heated right circular cylinder placed near a plane surface. A concurrent study by Göktun [4] was also carried out to study the lift and drag characteristics of a cylinder in the same configuration. Local Nusselt numbers were measured around the cylinder circumference for various plate to cylinder spacings, plate lengths and Reynolds numbers. The average Nusselt numbers were obtained from the local Nusselt number distributions by numerical integration.

An unusual trend which was observed in the plots of both the average Nusselt number and overall drag versus cylinder to plate separation curves lead to a flow visualization experiment and hotwire anemometer measurements of the vortex shedding frequency in the cylinder wake. Based on these observations and measurements, it was concluded that the structure of vortex pattern that develops in the wake of the cylinder exerts a controlling influence on the shape of the average Nusselt number and drag curves. In the range of a plate to cylinder spacing of one cylinder radius, it was found that the presence of the plate inhibits the formation of the regular vortex pattern that forms in the wake of a free cylinder. This significantly affected both the cylinder



base pressure and local Nusselt number distribution which, in turn, influenced the drag and average Nusselt number curves.



## APPENDIX A

### HEAT TRANSFER DATA REDUCTION

The procedure followed in reducing the heat transfer data is shown below. In this manner the local Nusselt numbers at various locations were obtained for the case of a uniformly heated (constant heat flux) cylinder.

#### HEAT FLUX

The heat flux produced by Joulean heating is given by;

$$\dot{q}_w = \frac{E^2}{A \cdot R}$$

where: E = Voltage applied to the test section, [volts]  
R = Total resistance of Tensheet, [ohms]  
A = Total heated area of Tensheet ( =0.315) [ft<sup>2</sup>]  
 $\dot{q}_w$  = Rate of total heat transfer,  $\frac{V^2}{\Omega - ft^2}$

$$\text{Conversion: } 1 \frac{V^2}{\Omega - ft^2} = 3.413 \frac{BTU}{hr-ft^2}$$

$$\text{Hence, } \dot{q}_w = \frac{3.413}{0.315} \frac{E^2}{R} = 10.842 \frac{E^2}{R} \frac{BTU}{hr-ft^2}$$



## HEAT TRANSFER COEFFICIENT

The total heat transfer coefficient is determined by dividing the heat flux by the measured local temperature difference  $(T - T_{\infty})$ :

$$h_t = \frac{\dot{q}_w}{T - T_{\infty}} = \frac{\dot{q}_w}{\Delta T}$$

$$h_t = h_c + h_r$$

$$h_c = \frac{\dot{q}_w}{\Delta T} - h_r$$

$$h_r = \sigma \cdot \mathcal{F}_{1-2} \cdot (T + T_{\infty}) (T^2 + T_{\infty}^2)$$

where:

$$h_t = \text{total heat transfer coefficient, } \frac{\text{BTU}}{\text{hr-ft}^2 - ^{\circ}\text{F}}$$

$T$  = cylinder surface temperature at angular location  $\theta$ , as determined by liquid crystals,  $^{\circ}\text{F}$

$T_{\infty}$  = air stream temperature,  $^{\circ}\text{F}$

$$h_c = \text{convective heat transfer coefficient, } \frac{\text{BTU}}{\text{hr - ft}^2 - ^{\circ}\text{F}}$$

$$h_r = \text{radiation heat transfer coefficient, } \frac{\text{BTU}}{\text{hr - ft}^2 - ^{\circ}\text{F}}$$

$$\sigma = \text{Stefan-Boltzman constant} = 0.1714 \times 10^{-8} \frac{\text{BTU}}{\text{hr - ft}^2 - ^{\circ}\text{R}^4}$$

$\mathcal{F}_{1-2}$  = radiation exchange factor between cylinder and surroundings = 0.9



## NUSSELT NUMBER

$$Nu = \frac{h_c \cdot D}{k_f}$$

where:  $D$  = cylinder diameter =  $\frac{1}{4}$  ft

$k_f$  = thermal conductivity of air evaluated at  
film temperature  $T_f = \frac{T + T_\infty}{2}$  ,  $\frac{\text{BTU}}{\text{hr} - \text{ft} - ^\circ\text{F}}$

### NUMERICAL EXAMPLE:

A sample calculation of the local Nusselt number is shown below using the data (see page 57 ) obtained at a Reynolds number of 153,000,  $d/r = 4.0$ ,  $L/D = 8$  and angular location of  $\theta = 63$  degrees.

$$V = 31 \text{ volts}$$

$$R = 13.3$$

$$T = 111^\circ\text{F} = 571^\circ\text{R}$$

$$T_\infty = 70^\circ\text{F} = 530^\circ\text{R}$$

$$\Delta T = T - T_\infty = 41^\circ\text{F}$$

$$\sigma_{1-2} = 0.9$$

$$\sigma = 0.1714 \times 10^{-8} \frac{\text{BTU}}{\text{hr} - \text{ft}^2 - ^\circ\text{R}^4}$$

$$D = 3'' = \frac{1}{4}'$$

$$\dot{q}_w = 10.842 \frac{V^2}{R} = 10.842 \frac{(31)^2}{13.3} = 783.39 \frac{\text{BTU}}{\text{hr} - \text{ft}^2}$$

$$h_t = \frac{\dot{q}_w}{\Delta T} = \frac{783.39}{41} = 19.1 \frac{\text{BTU}}{\text{hr} - \text{ft}^2 - ^\circ\text{F}}$$



$$\begin{aligned}
 h_r &= \sigma \cdot F_{1-2} (T + T_\infty)(T^2 + T_\infty^2) \\
 &= (0.1714 \times 10^{-8}) (0.9) (571 + 530) (571^2 + 530^2) \\
 &= 1 \frac{\text{BTU}}{\text{hr} - \text{ft}^2 - ^\circ\text{F}}
 \end{aligned}$$

$$h_c = h_t - h_r = 19.1 - 1 = 18.1 \frac{\text{BTU}}{\text{hr} - \text{ft}^2 - ^\circ\text{F}}$$

$$T_f = \frac{T + T_\infty}{2} = \frac{111 + 70}{2} = 90.5^\circ\text{F}$$

$$k_f = 0.0154 \frac{\text{BTU}}{\text{hr} - \text{ft} - ^\circ\text{F}} \text{ (evaluated at film temperature of } 90.5^\circ\text{F)}$$

$$\text{Nu} = \frac{h_c \cdot D}{k_f} = \frac{(18.1) \left(\frac{1}{4}\right)}{0.0154}$$

$$\text{Nu} = 294 \text{ at } \theta = 63 \text{ degrees.}$$



$L/D = 8.0$ 

DATA

DATE: 23 / Sept. / 1975

$$U_{\infty} = 98.1 \text{ ft/sec}$$
$$= 2.2 \text{ in-H}_2\text{O}$$
$$R_G = 153,000$$
$$R_T = 13.3 \text{ Ohm.}$$
[illegible]



## APPENDIX B

### UNCERTAINTY ANALYSIS

Since there are uncertainties in the measured quantities, an uncertainty analysis was performed to ascertain the degree of uncertainty in the experimental results at three ranges of Reynolds numbers of 153,000, 90,000 and 16,000. The method of Kline and McClintock [6] was used.

Being conservative, the following uncertainties were estimated in the measured variables:

voltage, $V \pm 0.1$ volts	(20:1)
resistance, $R \pm 0.4$ ohms	(20:1)
temperature, $T \pm 1.0$ °F	(20:1)
area, $A \pm 0.001$ ft <sup>2</sup>	(20:1)
diameter, $D \pm 0.001$ ft	(20:1)
wall manometer, $H \pm 0.05$ in - H <sub>2</sub> O	(20:1)
radiation exchange factor $\bar{F}_r \pm 0.05$	(20:1)

The uncertainties associated with the properties of air were considered to be negligible.

The uncertainty analysis is performed for the data obtained at Reynolds numbers of 153,000, 90,000 and 16,000 as follows;

1. Illustration of procedure of uncertainty analysis for  
Re = 153,000 :



Total Heat Transfer Coefficient,  $h_t$  :

As shown previously in Appendix A, the total heat transfer coefficient was calculated from the equation:

$$h_t = \frac{V^2}{R \cdot A \cdot (T - T_\infty)} = \frac{V^2}{R \cdot A \cdot \Delta T}$$

The uncertainty in the heat transfer coefficient is then expressed as:

$$\frac{\omega_{h_t}}{h_t} = \sqrt{\left(\frac{2\omega_V}{V}\right)^2 + \left(\frac{\omega_R}{R}\right)^2 + \left(\frac{\omega_A}{A}\right)^2 + \left(\frac{\omega_{\Delta T}}{\Delta T}\right)^2}$$

For the run at a Reynolds number of 153,000,  $L/D = 8$ ,  $d/r = 4$  and an angular location of 63 degrees:

$$V = 31 \pm 0.1 \text{ volts}$$

$$R = 13.3 \pm 0.4 \text{ ohms}$$

$$\Delta T = 41 \pm 1.0 \text{ } ^\circ\text{F} \text{ ( } T = 111^\circ\text{F} = 571^\circ\text{R, } T_\infty = 70^\circ\text{F} = 530^\circ\text{R)}$$

$$A = 0.314 \pm 0.001 \text{ ft}^2$$

$$H = 2.20 \pm 0.05 \text{ in} - \text{H}_2\text{O}$$

$$\omega_{h_t} = 19.1 \frac{\text{BTU}}{\text{hr} - \text{ft}^2 - ^\circ\text{F}}$$

$$\frac{\omega_{h_t}}{h_t} = 0.04 \text{ or } \omega_{h_t} = \pm 0.8 \frac{\text{BTU}}{\text{hr} - \text{ft}^2 - ^\circ\text{F}}$$

This result does not take into consideration the uncertainty in the angular location of the liquid crystal band. This uncertainty is estimated to be  $\pm 3$  degrees.



The uncertainty in the total heat transfer coefficient remained relatively constant around the circumference of the cylinder. However, the uncertainty in the angular location of the liquid crystal band varied. An estimated maximum uncertainty of  $\pm 5$  degrees occurred in the forward and rear stagnation regions and a minimum of  $\pm 1$  degree occurred in the regions near the separation and reattachment points.

Radiation Heat Transfer Coefficient,  $h_r$  :

The equation used to calculate  $h_r$  was:

$$h_r = \sigma \cdot \mathcal{F}_{1-2} \cdot (T + T_\infty)(T^2 + T_\infty^2)$$

defining  $T_m = \frac{1}{2} (T + T_\infty)$

$$h_r \cong 4 \cdot \sigma \cdot \mathcal{F}_{1-2} \cdot T_m^3$$

Since  $\sigma$  is constant, it is not considered in the uncertainty analysis. The uncertainty in  $h_r$  is then expressed as:

$$\frac{\omega_{h_r}}{h_r} = \sqrt{\left(\frac{\omega_{\mathcal{F}_{1-2}}}{\mathcal{F}_{1-2}}\right)^2 + \left(\frac{3\omega_{T_m}}{T_m}\right)^2}$$

$$\frac{\omega_{h_r}}{h_r} = 0.06 \quad \text{or} \quad \omega_{h_r} = 0.06 \frac{\text{BTU}}{\text{hr} - \text{ft}^2 - ^\circ\text{F}}$$

$$h_r = 1.00 \pm 0.06 \frac{\text{BTU}}{\text{hr} - \text{ft}^2 - ^\circ\text{F}}$$



Local Nusselt number, Nu:

The local Nusselt number was calculated from the equation:

$$Nu = \frac{h_c \cdot D}{k_f}$$

Therefore,

$$\frac{\omega_{Nu}}{Nu} = \sqrt{\left(\frac{\omega_{h_c}}{h_c}\right)^2 + \left(\frac{\omega_D}{D}\right)^2 + \left(\frac{\omega_{k_f}}{k_f}\right)^2}$$

Note that;  $h_c = h_t - h_r$

$$\frac{\omega_{h_c}}{h_c} = \sqrt{\left(\frac{\omega_{h_t}}{h_c}\right)^2 + \left(\frac{\omega_{h_r}}{h_c}\right)^2}$$

Since the uncertainties in the properties of air are considered to be negligible and the uncertainty in the cylinder diameter is negligibly small;

$$\frac{\omega_{Nu}}{Nu} = \sqrt{\left(\frac{\omega_{h_t}}{h_c}\right)^2 + \left(\frac{\omega_{h_r}}{h_c}\right)^2}$$

$$\frac{\omega_{Nu}}{Nu} = 0.044 \quad \text{or} \quad \omega_{Nu} = 13$$

$$Nu = 294 \pm 13$$



Reynolds Number, Re :

The equation used to calculate Reynolds number was:

$$Re = \frac{U_{\infty} \cdot D}{\nu}$$

Therefore

$$\frac{\omega_{Re}}{Re} = \sqrt{\left(\frac{\omega_{U_{\infty}}}{U_{\infty}}\right)^2 + \left(\frac{\omega_D}{D}\right)^2 + \left(\frac{\omega_{\nu}}{\nu}\right)^2}$$

Since the uncertainty in the kinematic viscosity and in the cylinder diameter are negligible:

$$\frac{\omega_{Re}}{Re} = \frac{\omega_{U_{\infty}}}{U_{\infty}}$$

The quantity  $U_{\infty}$  is proportional to the square root of the wall manometer reading, hence:

$$\frac{\omega_{Re}}{Re} = \frac{1}{2} \frac{\omega_H}{H}$$

$$\frac{\omega_{Re}}{Re} = 0.011 \quad \text{or} \quad \omega_{Re} = 2000$$

$$Re = 153,000 \pm 2000$$

2. The uncertainty analysis for the run at  $Re = 90,000$ :

For the data obtained at a Reynolds number of 90,000,

$L/D = 4$ ,  $d/r = 2.0$  and  $\theta = 67$  degrees:



$$V = 28.0 \pm 0.1 \text{ volts}$$

$$R = 13.0 \pm 0.4 \text{ ohms}$$

$$\Delta T = 38.6 \pm 1 \text{ } ^\circ\text{F} \quad (T = 111^\circ\text{F} = 571^\circ\text{R}, T_\infty = 72.4^\circ\text{F} = 532.4^\circ\text{R})$$

$$A = 0.314 \pm 0.001 \text{ ft}^2$$

$$H = 0.76 \pm 0.05 \text{ in} - \text{H}_2\text{O}$$

Similarly, the uncertainties calculated in following variables were:

$$\frac{\omega_{h_t}}{h_t} = 0.04 \quad \text{or} \quad \omega_{h_t} = \pm 0.7 \quad \frac{\text{BTU}}{\text{hr} - \text{ft}^2 - ^\circ\text{F}}$$

$$h_t = 16.9 \pm 0.7 \quad \frac{\text{BTU}}{\text{hr} - \text{ft}^2 - ^\circ\text{F}}$$

$$\frac{\omega_{h_r}}{h_r} = 0.06 \quad \text{or} \quad \omega_{h_r} = 0.06 \quad \frac{\text{BTU}}{\text{hr} - \text{ft}^2 - ^\circ\text{F}}$$

$$h_r = 1.00 \pm 0.06 \quad \frac{\text{BTU}}{\text{hr} - \text{ft}^2 - ^\circ\text{F}}$$

$$\frac{\omega_{\text{Nu}}}{\text{Nu}} = 0.044 \quad \text{or} \quad \omega_{\text{Nu}} = 11$$

$$\text{Nu} = 259 \pm 11$$

$$\frac{\omega_{\text{Re}}}{\text{Re}} = .032 \quad \omega_{\text{Re}} \cong 3000$$

$$\text{Re} = 90,000 \pm 3000$$



3. The uncertainty analysis for the run at  $Re = 16,000$  :

For the data obtained at a Reynolds number of 16,000  
 $L/D = 4$ ,  $d/r = 2.0$  and  $\theta = 65$  degrees:

$$V = 21.1 \pm 0.1 \text{ volts}$$

$$R = 13.4 \pm 0.4 \text{ ohms}$$

$$\Delta T = 43 \pm 1 \text{ } ^\circ\text{F} \text{ ( } T = 111^\circ\text{F} = 571^\circ\text{R, } T_\infty = 68^\circ\text{F} = 528^\circ\text{R)}$$

$$A = 0.314 \pm 0.001 \text{ ft}^2$$

The following uncertainties were calculated:

$$\frac{\omega_{h_t}}{h_t} = 0.039 \text{ or } \omega_{h_t} = \pm 0.3 \frac{\text{BTU}}{\text{hr} - \text{ft}^2 - ^\circ\text{F}}$$

$$h_t = 8.3 \pm 0.3 \frac{\text{BTU}}{\text{hr} - \text{ft}^2 - ^\circ\text{F}}$$

$$\frac{\omega_{h_r}}{h_r} = 0.06 \text{ or } \omega_{h_r} = \pm 0.06 \frac{\text{BTU}}{\text{hr} - \text{ft}^2 - ^\circ\text{F}}$$

$$h_r = 1.00 \pm 0.06 \frac{\text{BTU}}{\text{hr} - \text{ft}^2 - ^\circ\text{F}}$$

$$\frac{\omega_{Nu}}{Nu} = 0.04 \text{ or } \omega_{Nu} = \pm 5$$

$$Nu = 120 \pm 5$$

For this particular Reynolds number it was impossible to measure the free stream velocity using the wall manometer. The hot wire anemometer was therefore used to measure the velocity. Thus, the uncertainty estimated in  $U_\infty$  was:



$$U_{\infty} \pm 2 \text{ ft/sec}$$

$$(20:1)$$

$$\frac{\omega_{Re}}{Re} = \frac{\omega U_{\infty}}{U_{\infty}} = \frac{2}{10} = 0.2 \quad \text{or} \quad \omega_{Re} \cong 3000$$

$$Re = 16,000 \pm 3000$$

The high uncertainty in  $U_{\infty}$  and consequently in the Reynolds number was primarily due to the unstable operation of the fan motor at its lowest operating point.



## APPENDIX C

### WIND TUNNEL VELOCITY PROFILES

For the three ranges of Reynolds numbers of 16,000, 90,000 and 153,000 and with  $L/D = 4$ , velocity profiles were obtained in the tunnel test section (see Figure 18 through 23). Data were collected at  $d/r = 0$  and  $d/r = 5.33$  (see next page for data).

The hot wire anemometer was used to probe the test section at various positive and negative  $Y$  - locations at 90 degrees and 270 degrees, measured from the forward stagnation point on the cylinder. The velocity profile at the test section entrance was also measured at various locations and it was found to be fairly uniform.

The turbulence intensity in the test section was obtained for a Reynolds number of 153,000 and was found to be approximately 0.2%.



DATA for the velocity profiles

X=0, Z=0 ,  Re= 153,000  U <sub>∞</sub> = 98.1 (ft/se.)	d/r = 5.33						d/r = 0.0		
	+ Y <sub>(in)</sub>	u <sub>(ft/s)</sub>	u/U <sub>∞</sub>	- Y <sub>(in)</sub>	u <sub>(ft/s)</sub>	u/U <sub>∞</sub>	+ Y <sub>(in)</sub>	u <sub>(ft/s)</sub>	u/U <sub>∞</sub>
	1.7	134.56	1.37	- 1.7	132.25	1.34	1.7	166.4	1.69
	2.0	122.22	1.31	- 2.0	127.7	1.30	2.0	156.2	1.53
	3.0	118.7	1.21	- 3.0	116.7	1.19	3.0	139.2	1.41
	4.0	113.42	1.15	- 4.0	114.5	1.167	4.0	132.2	1.34
	5.0	110.75	1.12	- 5.0	111.3	1.13	5.0	127.7	1.30
	6.0	105.14	1.10	- 6.0	109.2	1.11	6.0	126.5	1.29
	7.0	107.12	1.09	- 7.0	107.1	1.10	7.0	124.3	1.26
	8.0	106.03	1.089				8.0	123.2	1.25
	9.0	105.7	1.077				9.0	122.1	1.24
	10.0	105.4	1.07				10.0	121	1.23
	11.0	104.44	1.064				11.0	121	1.23
	12.0	104	1.06				12.0	121	1.23

Re= 90,000  U <sub>∞</sub> = 57.76 (ft/se.)	1.7	26.47	1.49	- 1.7	83.17	1.44	1.7	106.09	1.87
	2.0	82.81	1.43	- 2.0	79.21	1.37	2.0	100	1.73
	3.0	74.22	1.29	- 3.0	70.56	1.22	3.0	75.56	1.48
	4.0	68.7	1.2	- 4.0	67.25	1.16	4.0	70.1	1.31
	5.0	62	1.17	- 5.0	65.61	1.13	5.0	77.44	1.34
	6.0	65.9	1.13	- 6.0	64	1.1	6.0	75.64	1.31
	7.0	65.61	1.13	- 7.0	64	1.1	7.0	74.82	1.29
	8.0	65.61	1.13				8.0	73.86	1.28
	9.0	65.61	1.13				9.0	73.1	1.26
	10.0	64	1.1				10.0	72.25	1.25
	11.0	64	1.1				11.0	72.25	1.25
	12.0	64	1.1				12.0	72.25	1.25

Re= 16,000  U <sub>∞</sub> = 10 (ft/se.)	1.7	16.0	1.6	- 1.8	16.81	1.68	1.8	15.4	1.56
	2.0	14.8	1.48	- 2.0	15.6	1.56	2.0	15.2	1.50
	3.0	13.32	1.33	- 3.0	12.96	1.29	3.0	14.96	1.43
	4.0	12.25	1.22	- 4.0	11.9	1.19	4.0	14.7	1.37
	5.0	11.9	1.19	- 5.0	11.9	1.19	5.0	12.96	1.29
	6.0	11.9	1.19	- 6.0	11.9	1.19	6.0	12.96	1.29
	7.0	11.9	1.19	- 7.0	11.5	1.15	7.0	12.96	1.29
	8.0	11.56	1.15				8.0	12.2	1.22
	9.0	11.56	1.15				9.0	12.2	1.22
	10.0	11.22	1.12				10.0	12.2	1.22
	11.0	10.54	1.08				11	11.5	1.15
	12.0	10.55	1.07				12	10.5	1.08



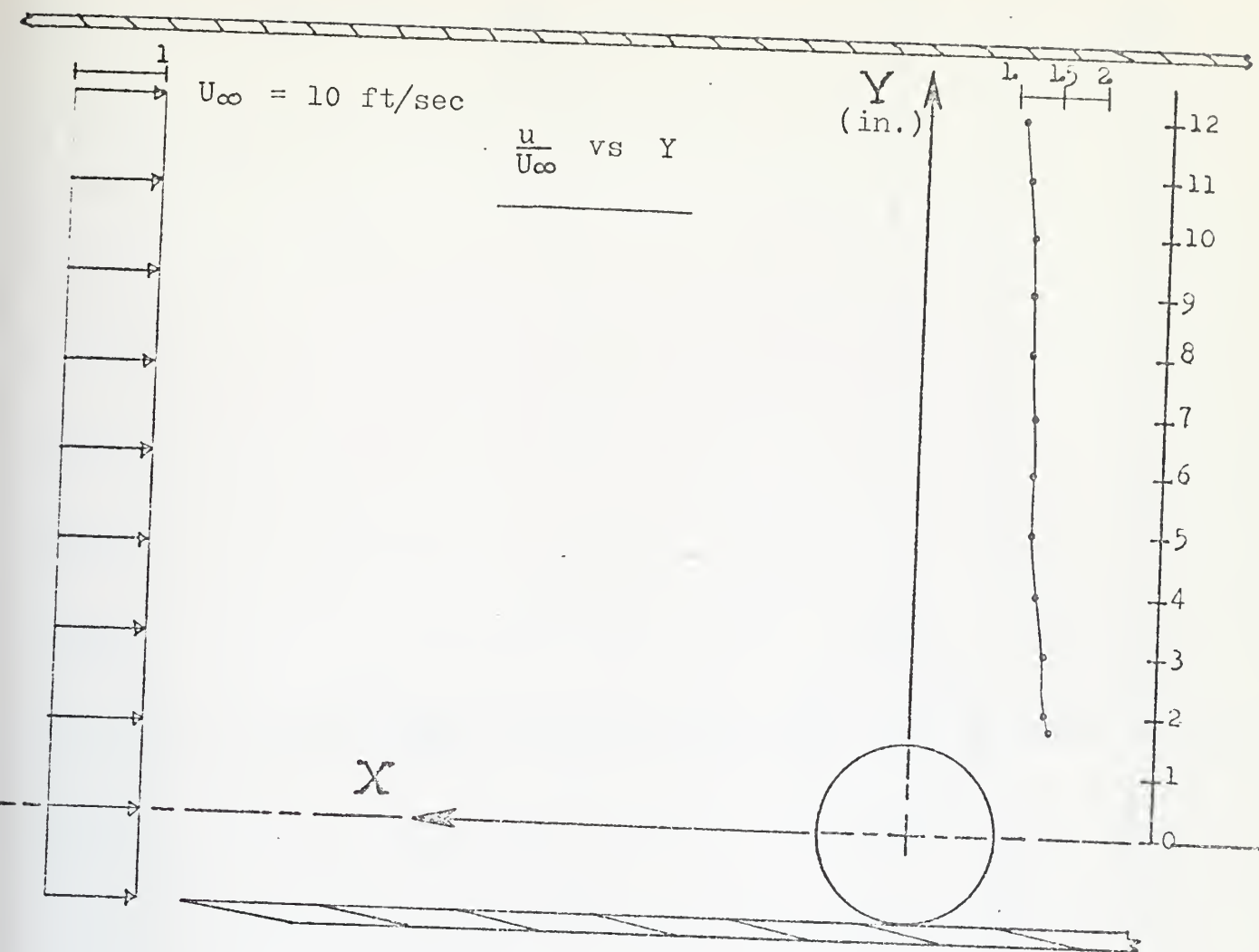
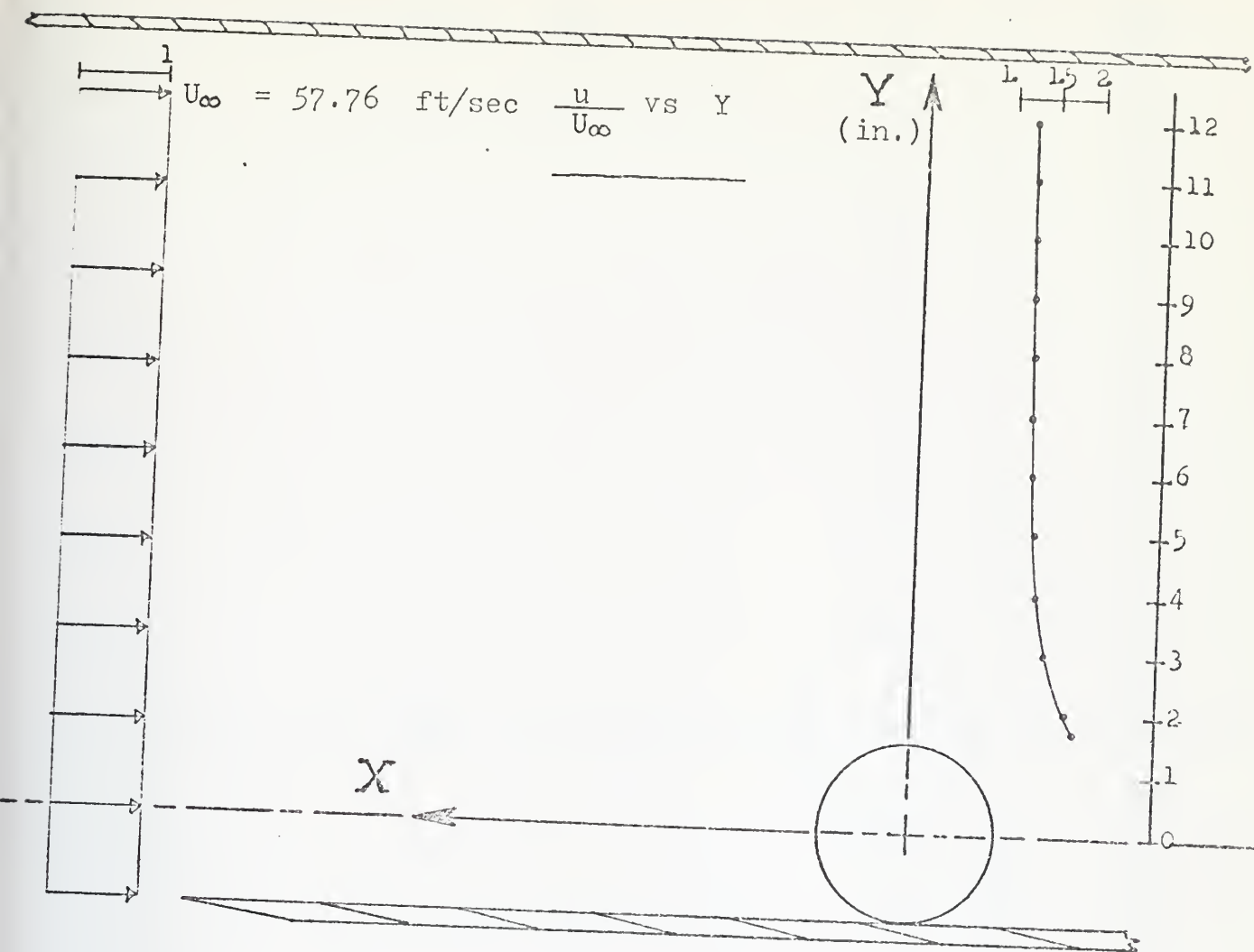


Figure 18. Velocity profile at the top of the cylinder for  $d/r=0.0$ .









SCALE: 1" = 3"

Figure 20. Velocity profile at the top of the cylinder for  $d/r = 0.0$ .



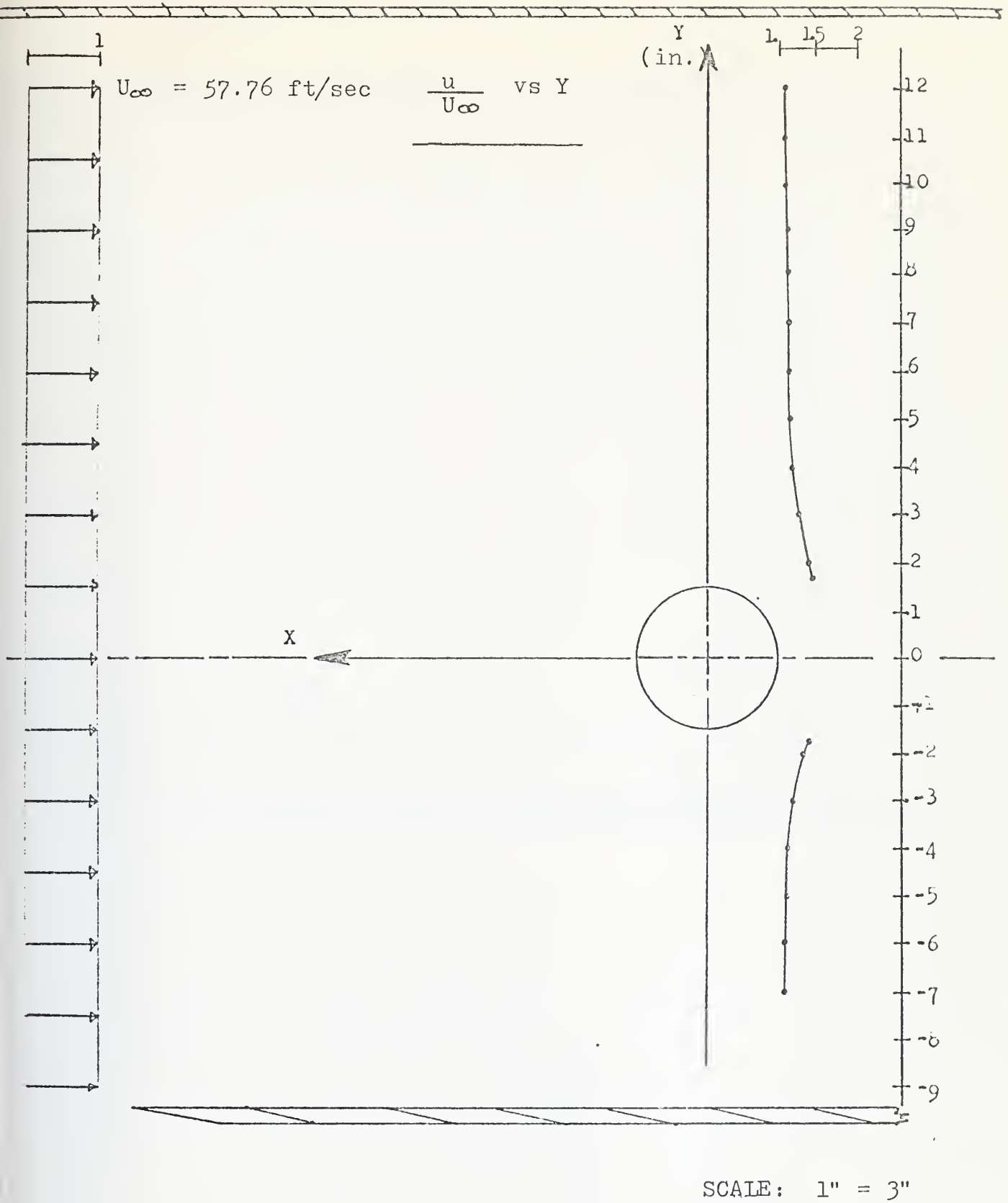
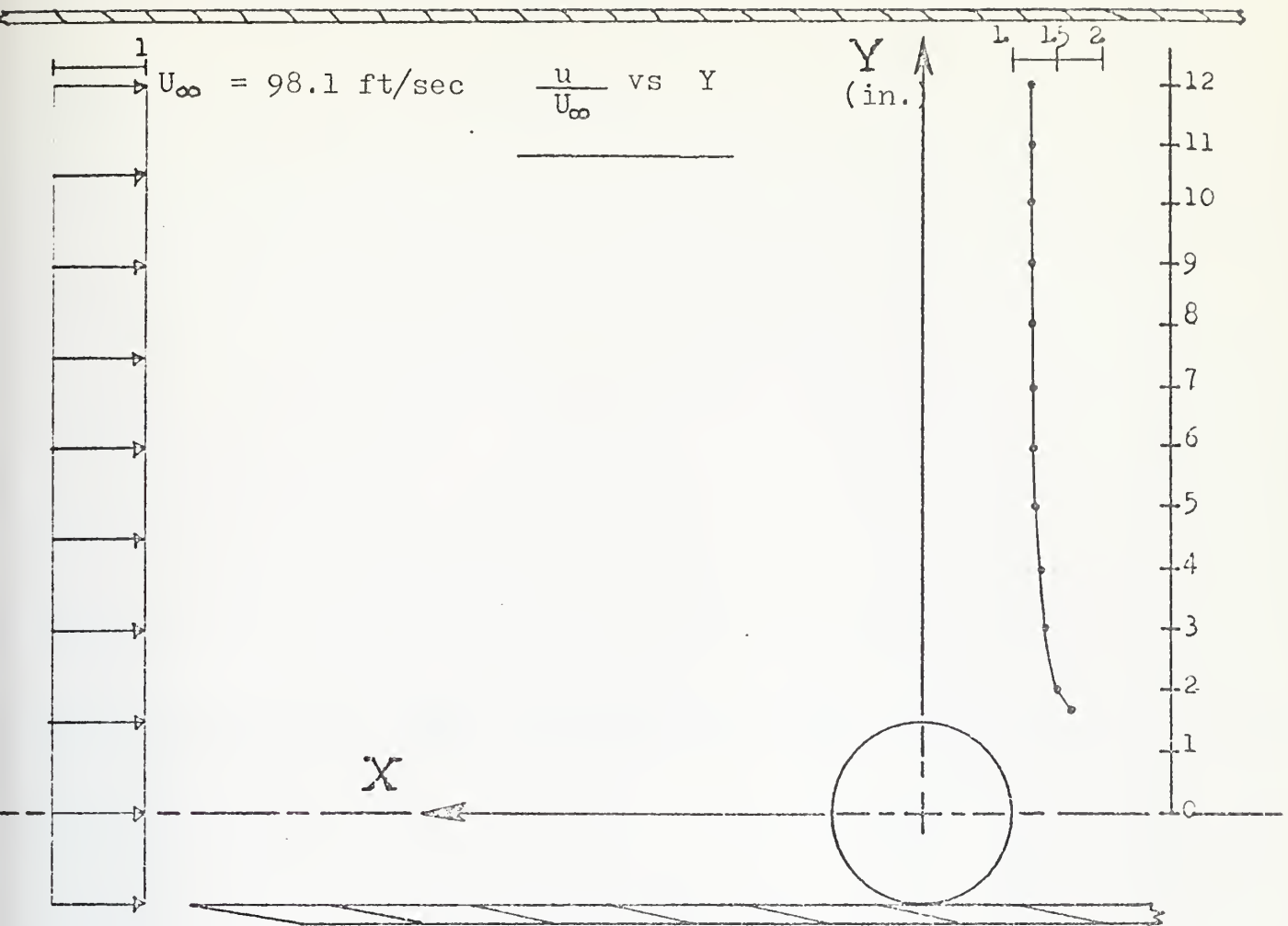


Figure 21. Velocity profiles at the top and bottom of the cylinder for  $d/r = 5.33$ .





SCALE: 1" = 3"

Figure 22. Velocity profile at the top of the cylinder for  $d/r = 0.0$ .



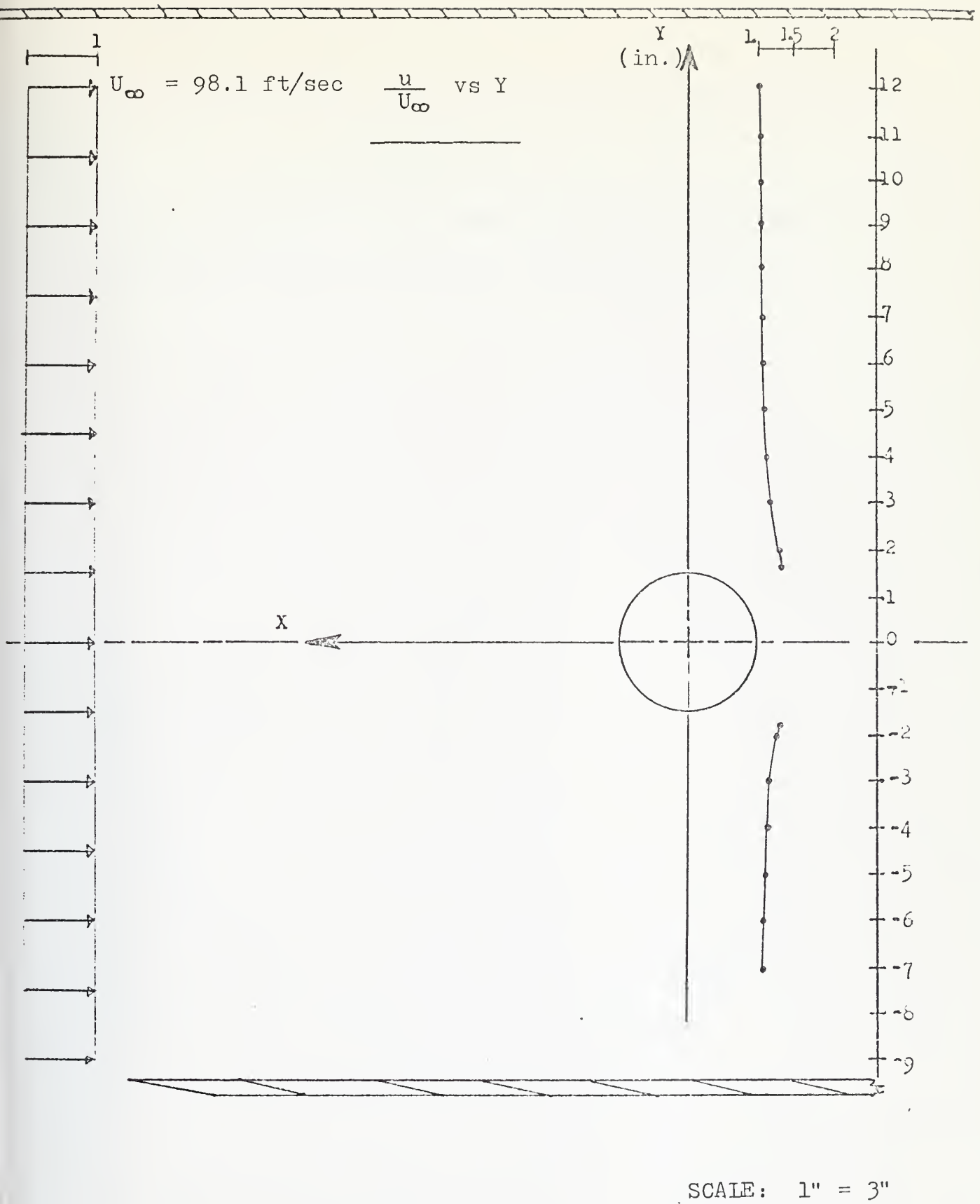


Figure 23. Velocity profiles at the top and bottom of the cylinder for  $d/r = 5.33$ .



## APPENDIX D

Additional plots of the Nusselt number versus gap size for Reynolds numbers of 16,000, 90,000 and 153,000.



Nu .

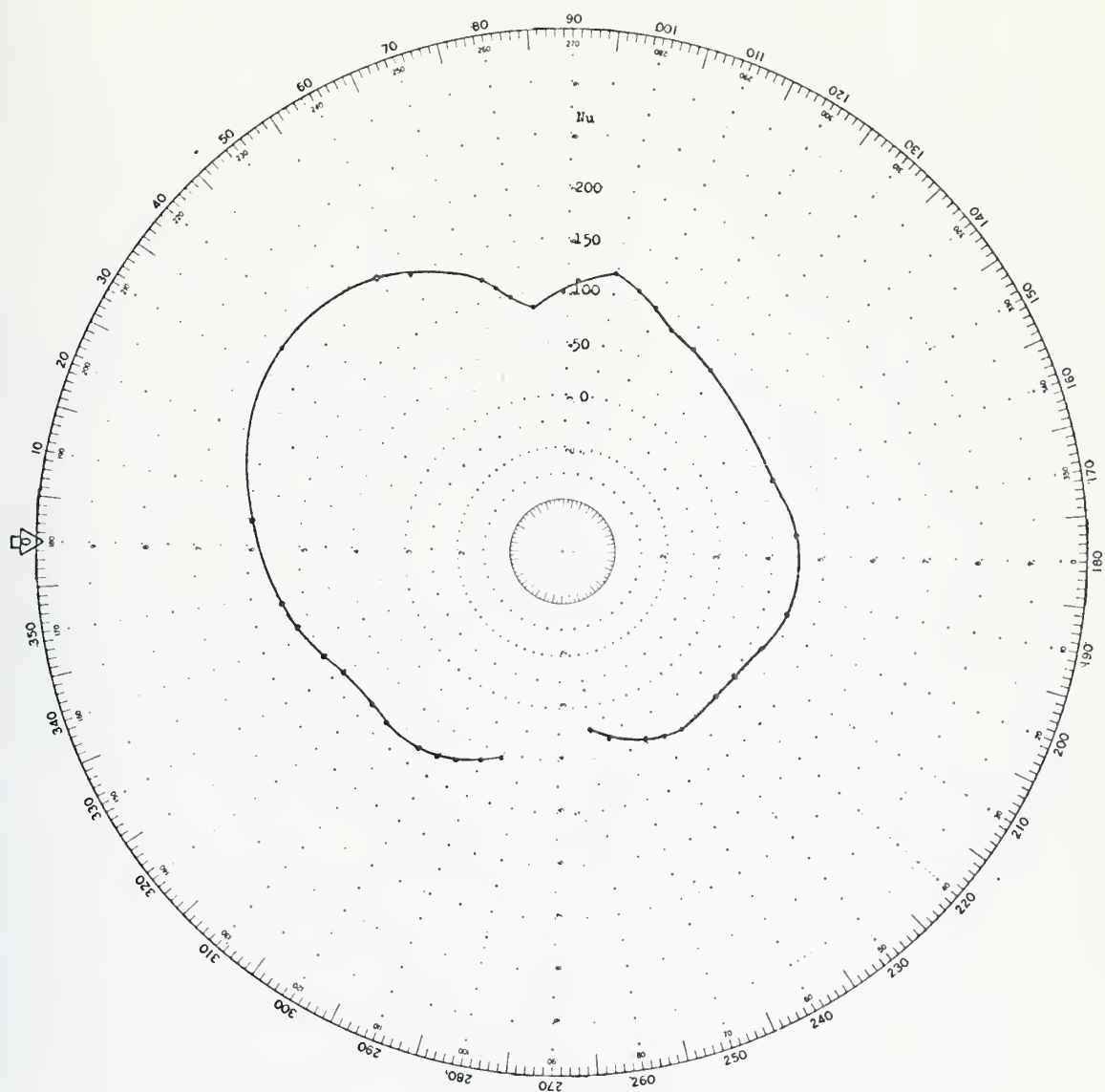


Figure 24. Local Nusselt number on the surface of a cylinder placed near a plane surface for  $Re = 16,000$ ,  $L/D = 4$ ,  $d/r = 0.0$ .



Nu .

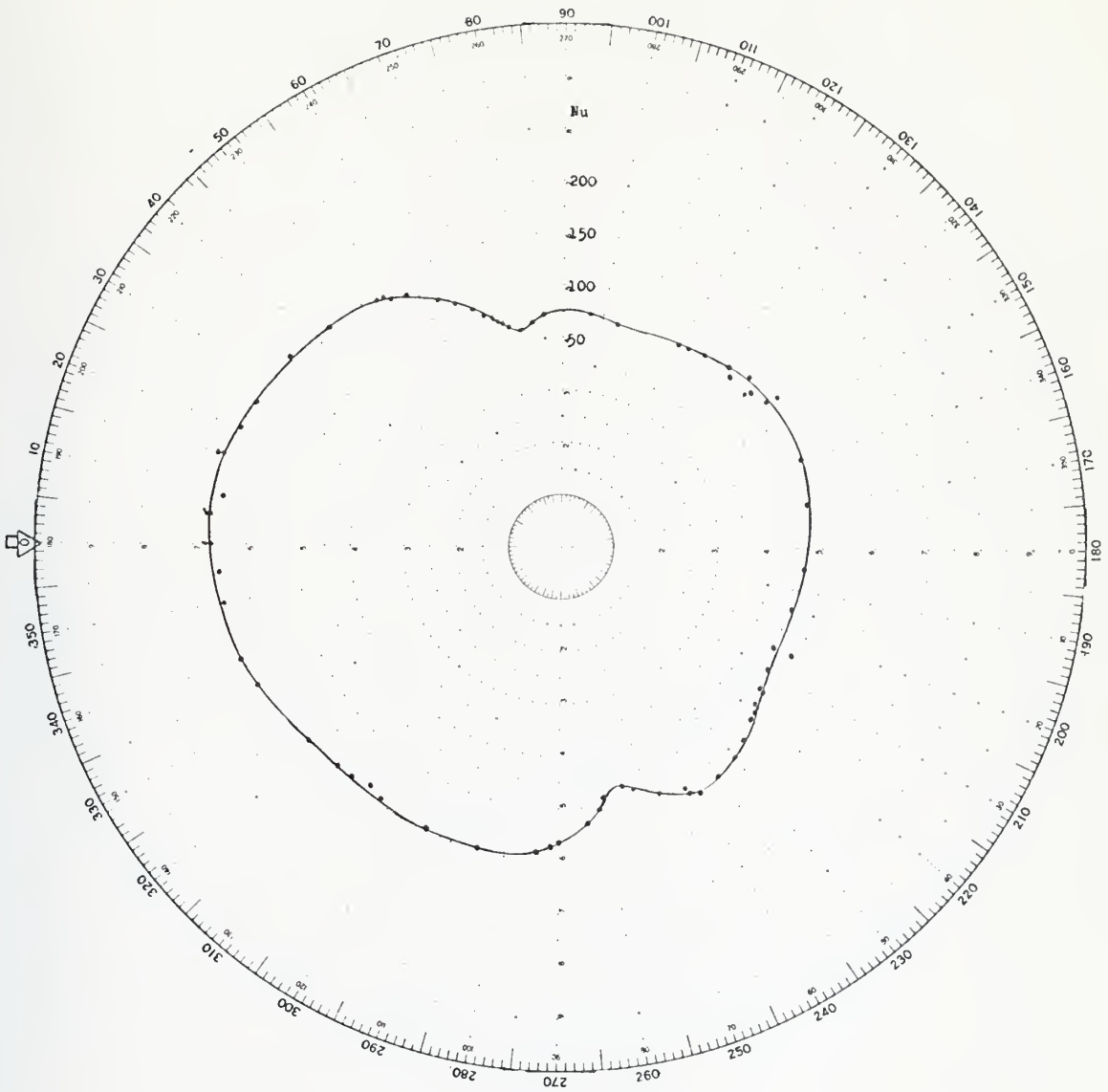


Figure 25. Local Nusselt number on the surface of a cylinder placed near a plane surface for  $Re = 16,000$ ,  $L/D = 4$ ,  $d/r = 0.25$ .



Nu

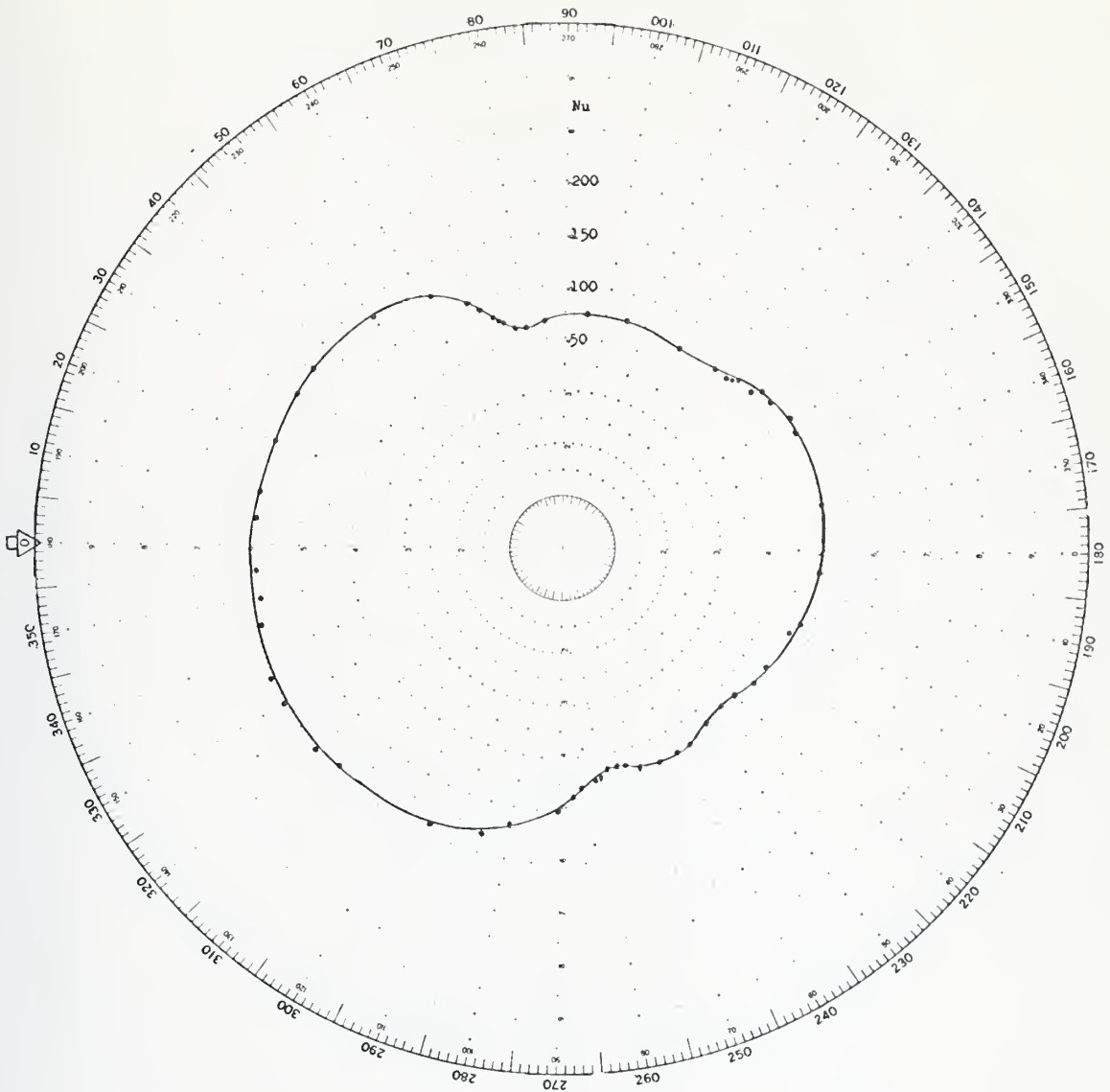


Figure 26. Local Nusselt number on the surface of a cylinder placed near a plane surface for  $Re = 16,000$ ,  $L/D = 4$ ,  $d/r = 0.5$ .



Nu .

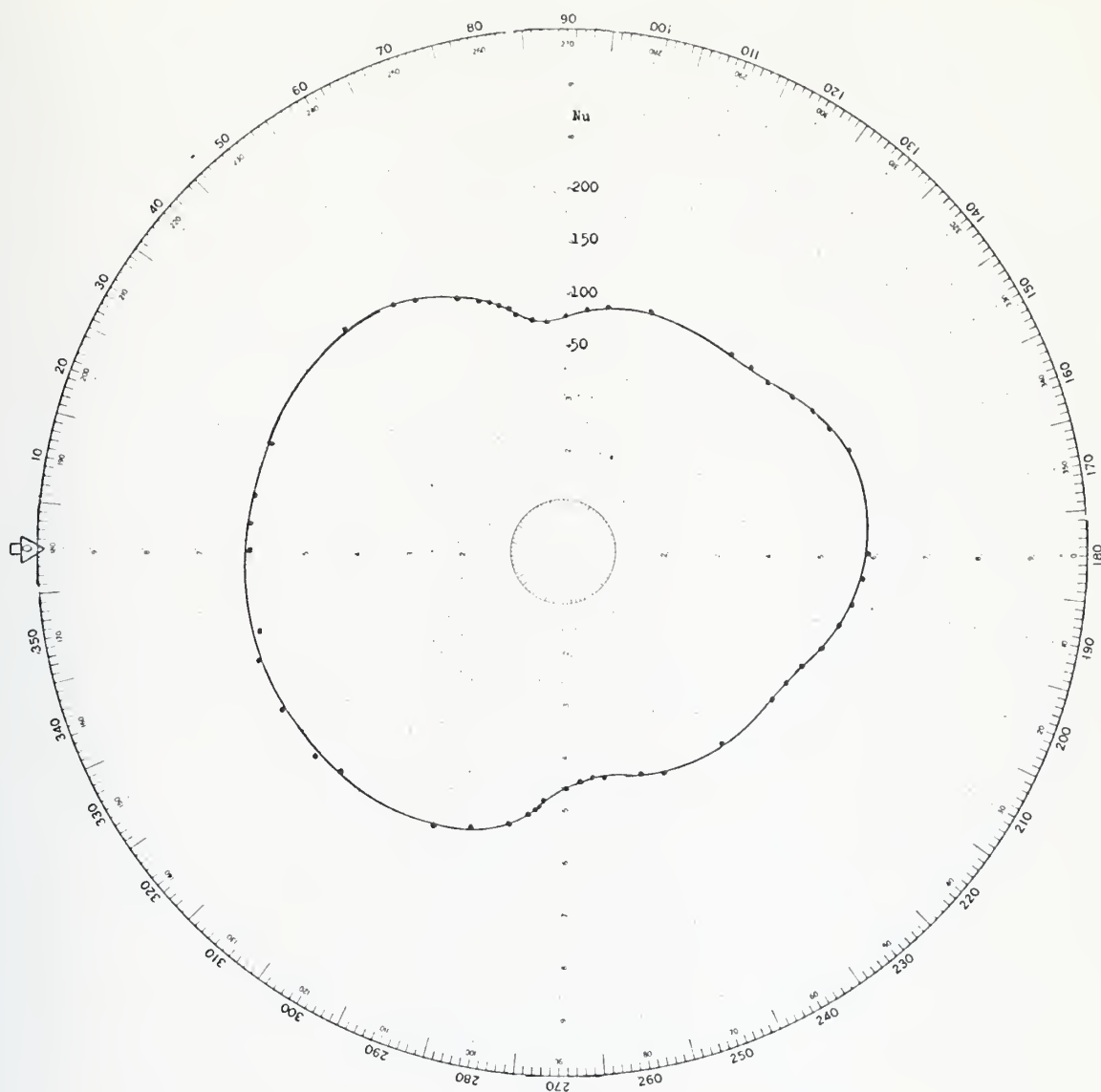


Figure 27. Local Nusselt number on the surface of a cylinder placed near a plane surface for  $Re = 16,000$ ,  $L/D = 4$ ,  $d/r = 1.0$ .



Nu •

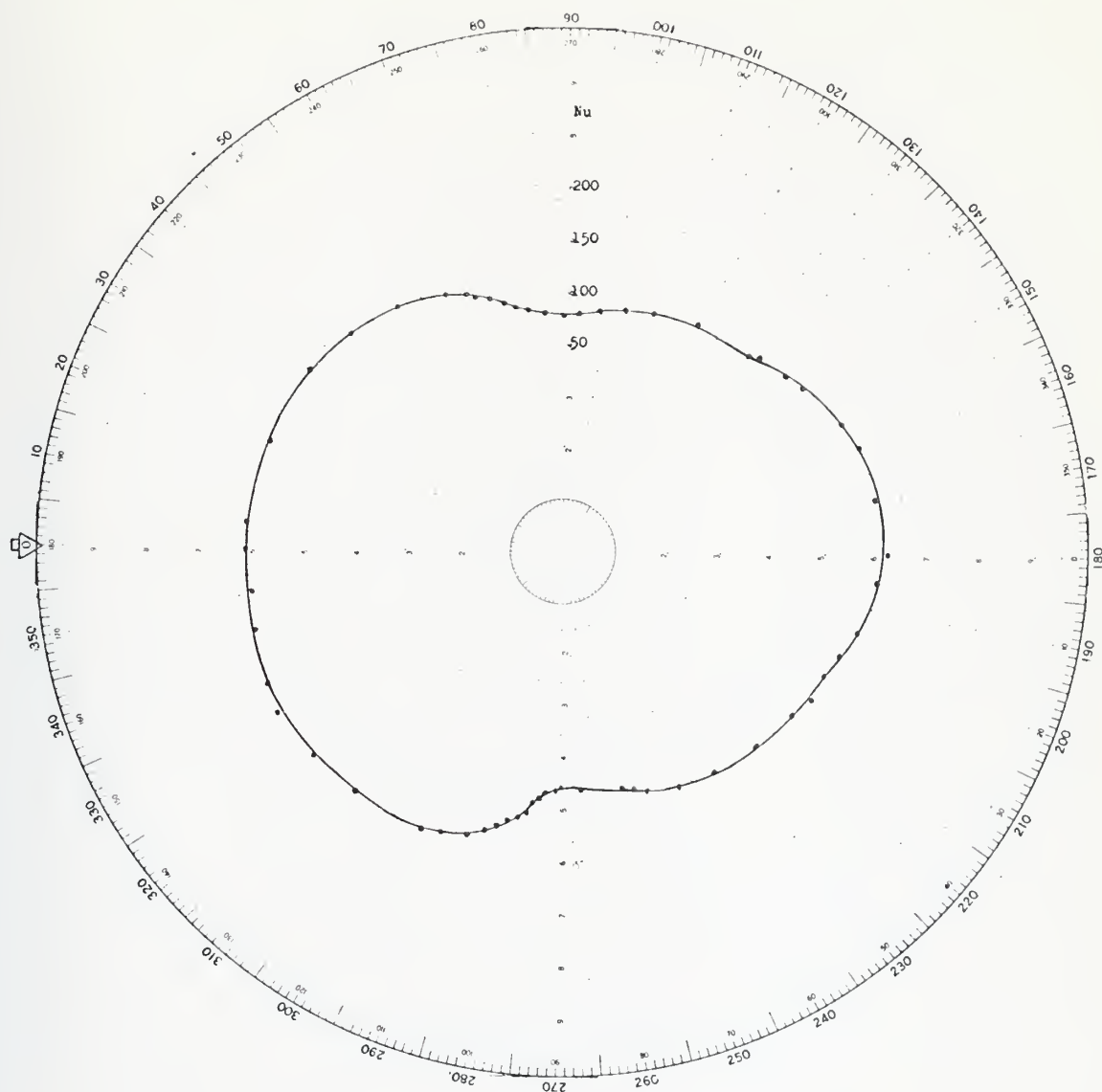


Figure 28. Local Nusselt number on the surface of a cylinder placed near a plane surface for  $Re = 16,000$ ,  $L/D = 4$ ,  $d/r = 2.0$ .



Nu .

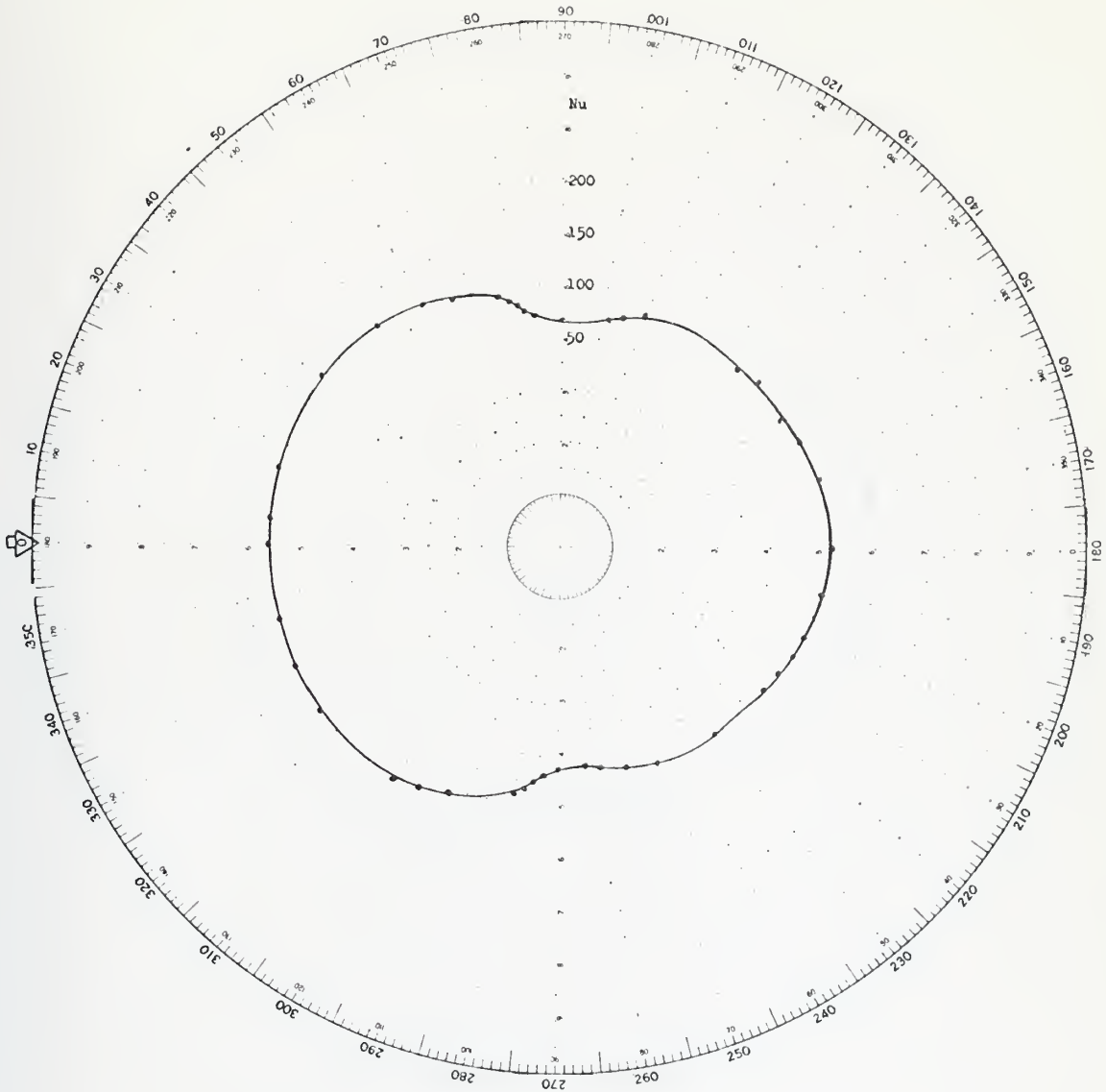


Figure 29. Local Nusselt number on the surface of a cylinder placed near a plane surface for  $Re = 16,000$ ,  $L/D = 4$ ,  $d/r = 3.0$ .



Nu .

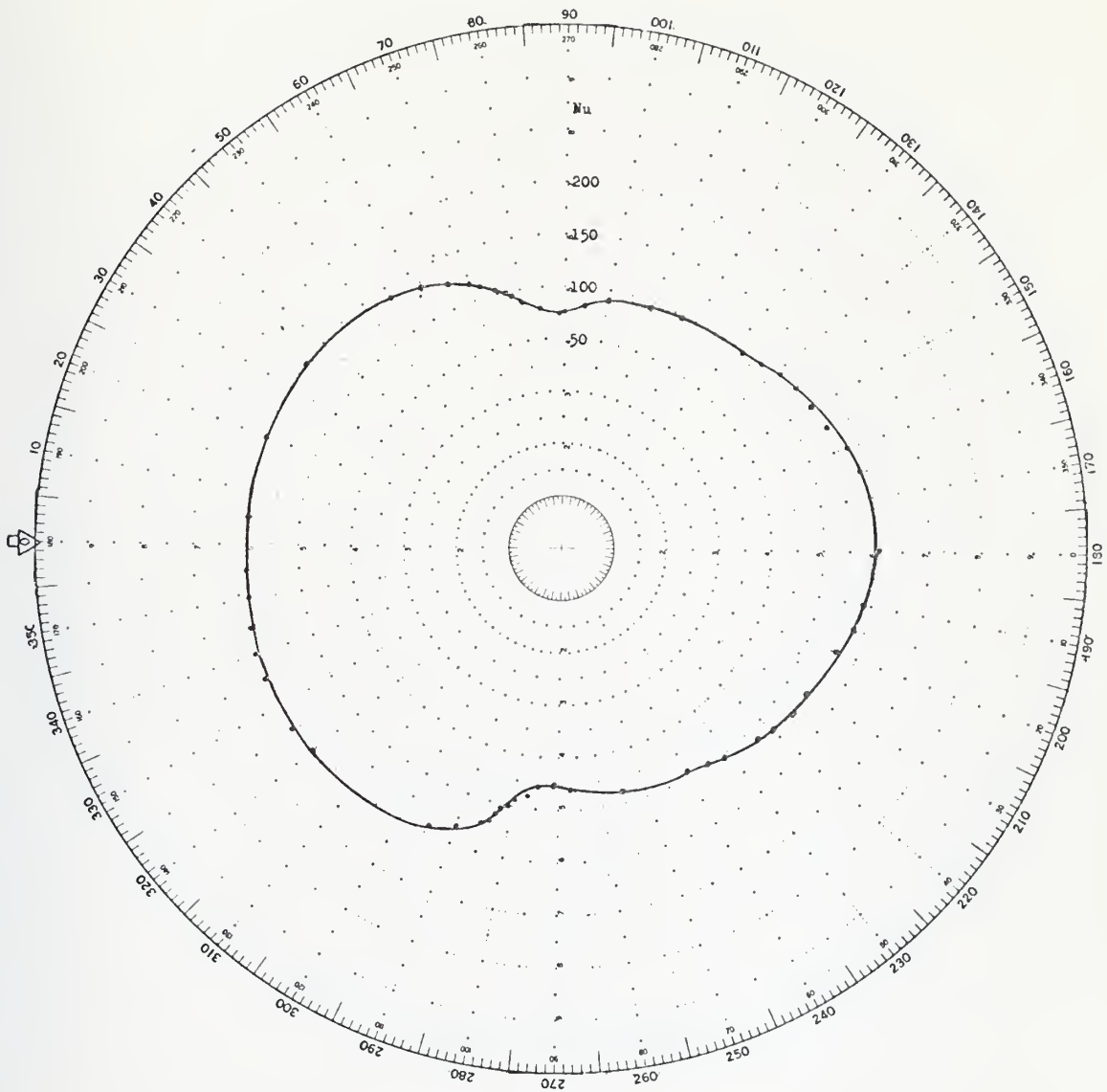


Figure 30. Local Nusselt number on the surface of a cylinder placed near a plane surface for  $Re = 16,000$ ,  $L/D = 4$ ,  $d/r = 4.0$ .



Nu

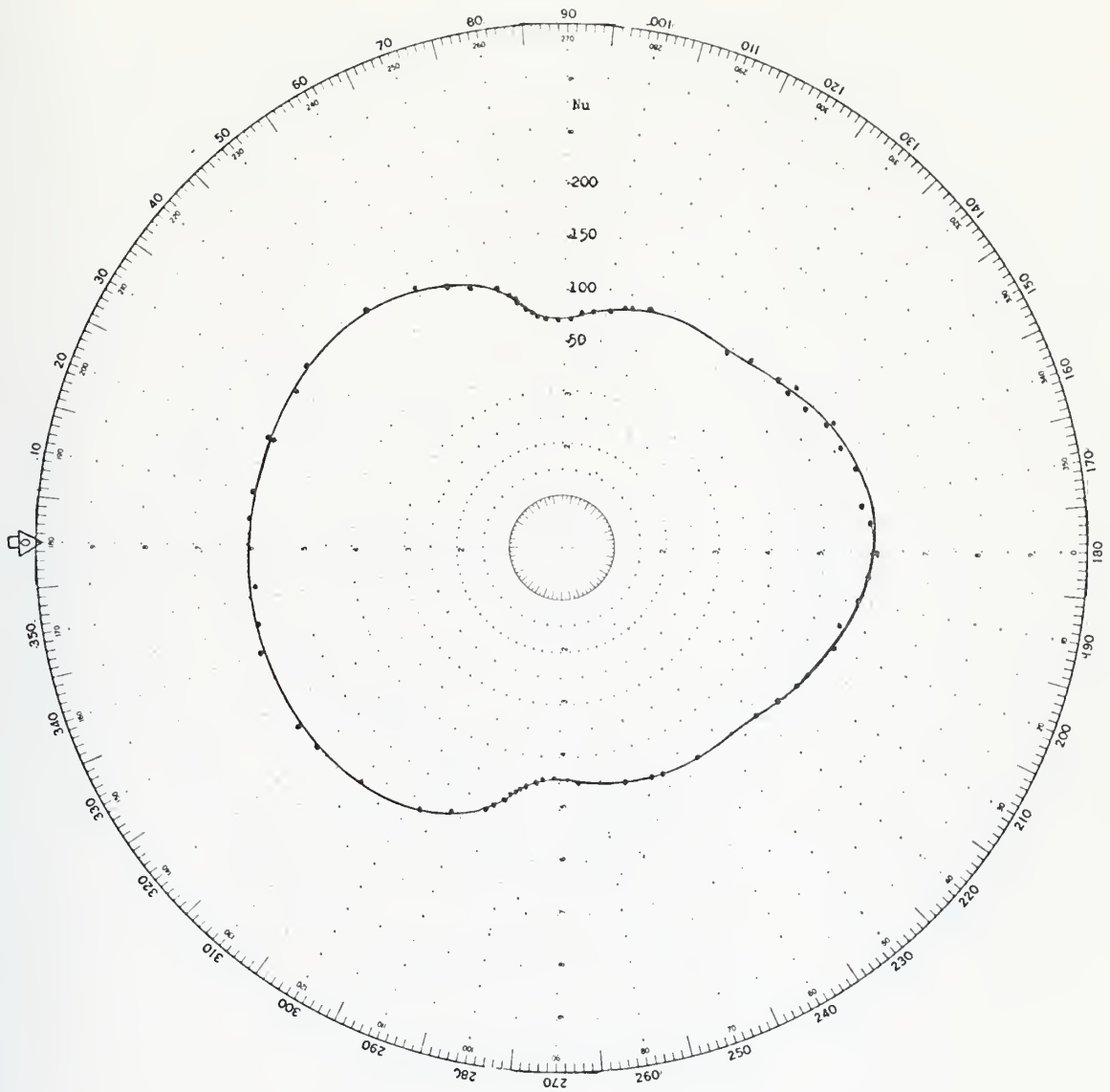


Figure 31. Local Nusselt number on the surface of a cylinder placed near a plane surface for  $Re = 16,000$ ,  $L/D = 4$ ,  $d/r = 5.33$ .



Nu

$C_p$

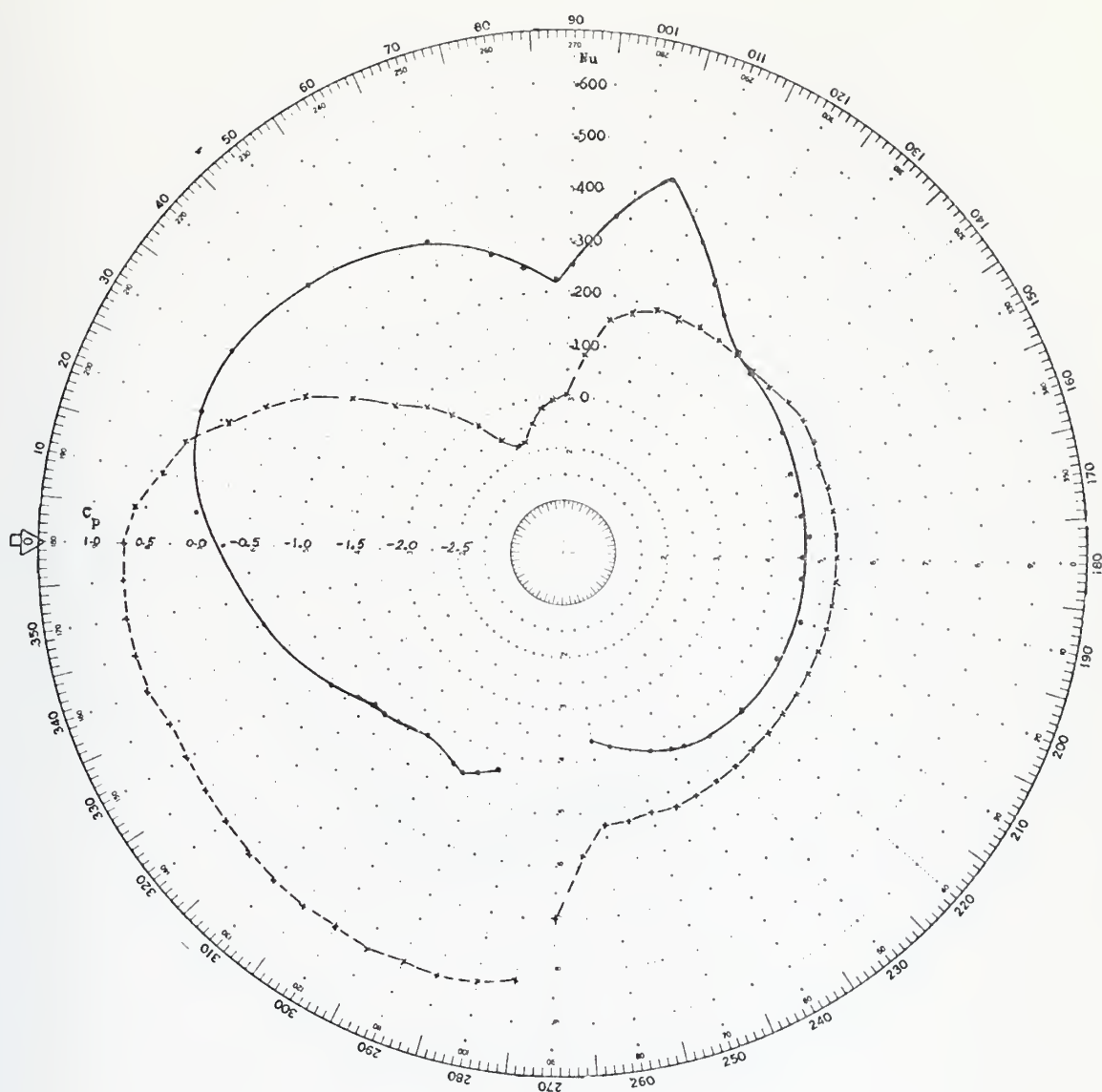


Figure 32. Local Nusselt number and pressure coefficient on the surface of a cylinder placed near a plane surface for  $Re = 90,000$ ,  $L/D = 4$ ,  $d/r = 0.0$ .



$Nu$     •  
 $C_p$     x

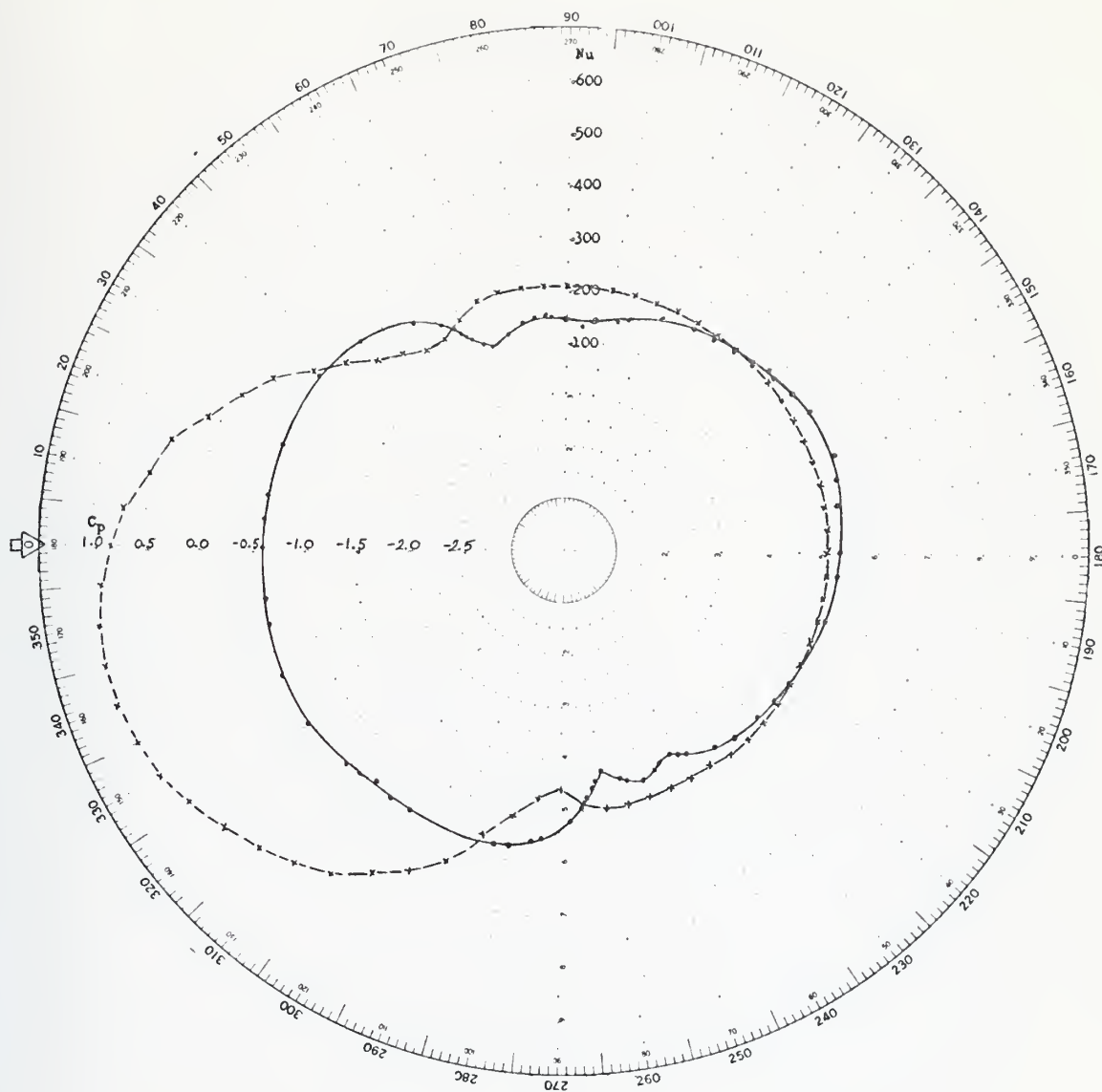


Figure 33. Local Nusselt number and pressure coefficient on the surface of a cylinder placed near a plane surface for  $Re = 90,000$ ,  $L/D = 4$ ,  $d/r = 0.25$ .



Nu    •  
Cp    x

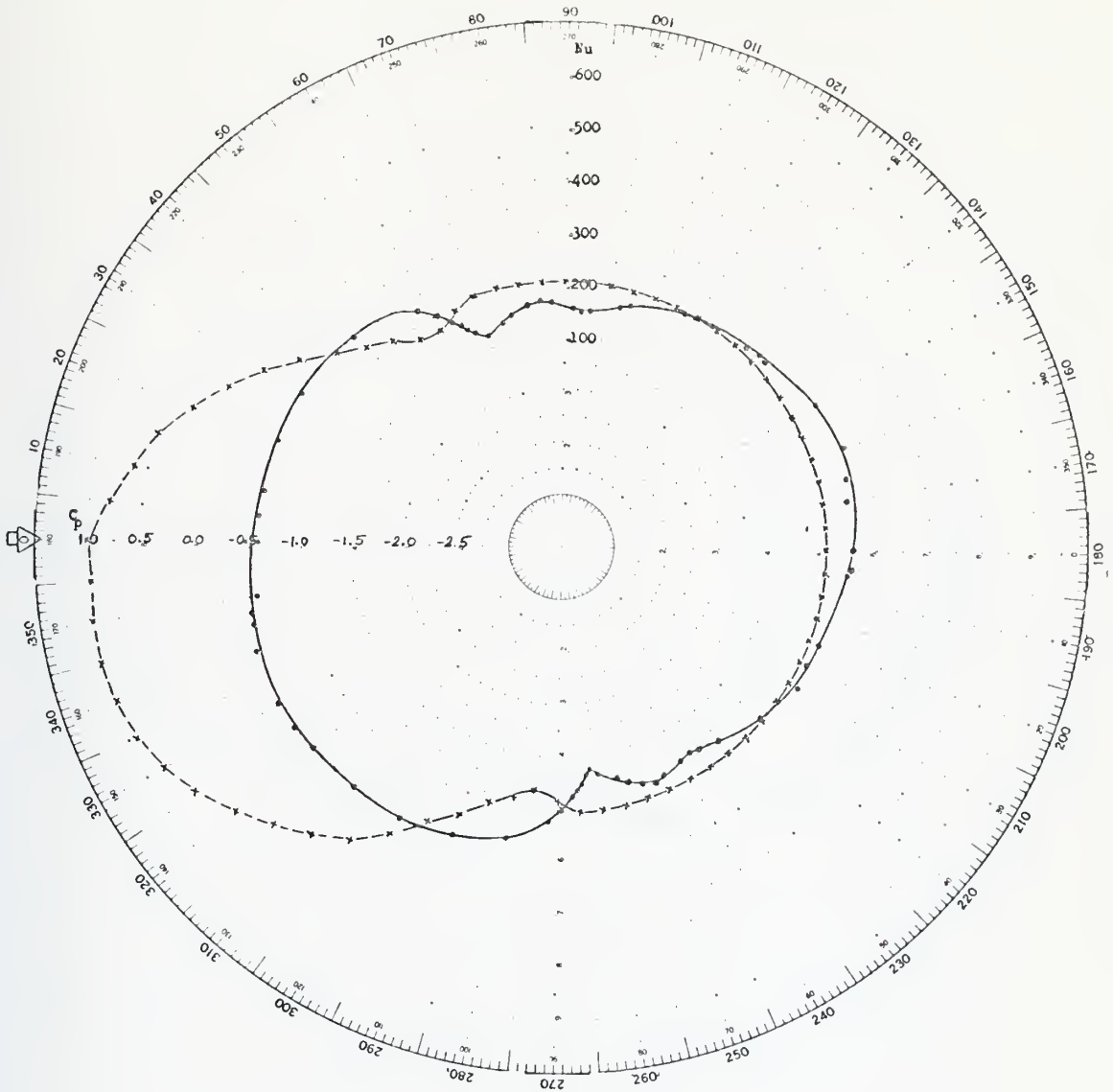


Figure 34. Local Nusselt number and pressure coefficient on the surface of a cylinder placed near a plane surface for  $Re = 90,000$ ,  $L/D = 4$ ,  $d/r = 0.5$ .



Nu    •  
Cp    x

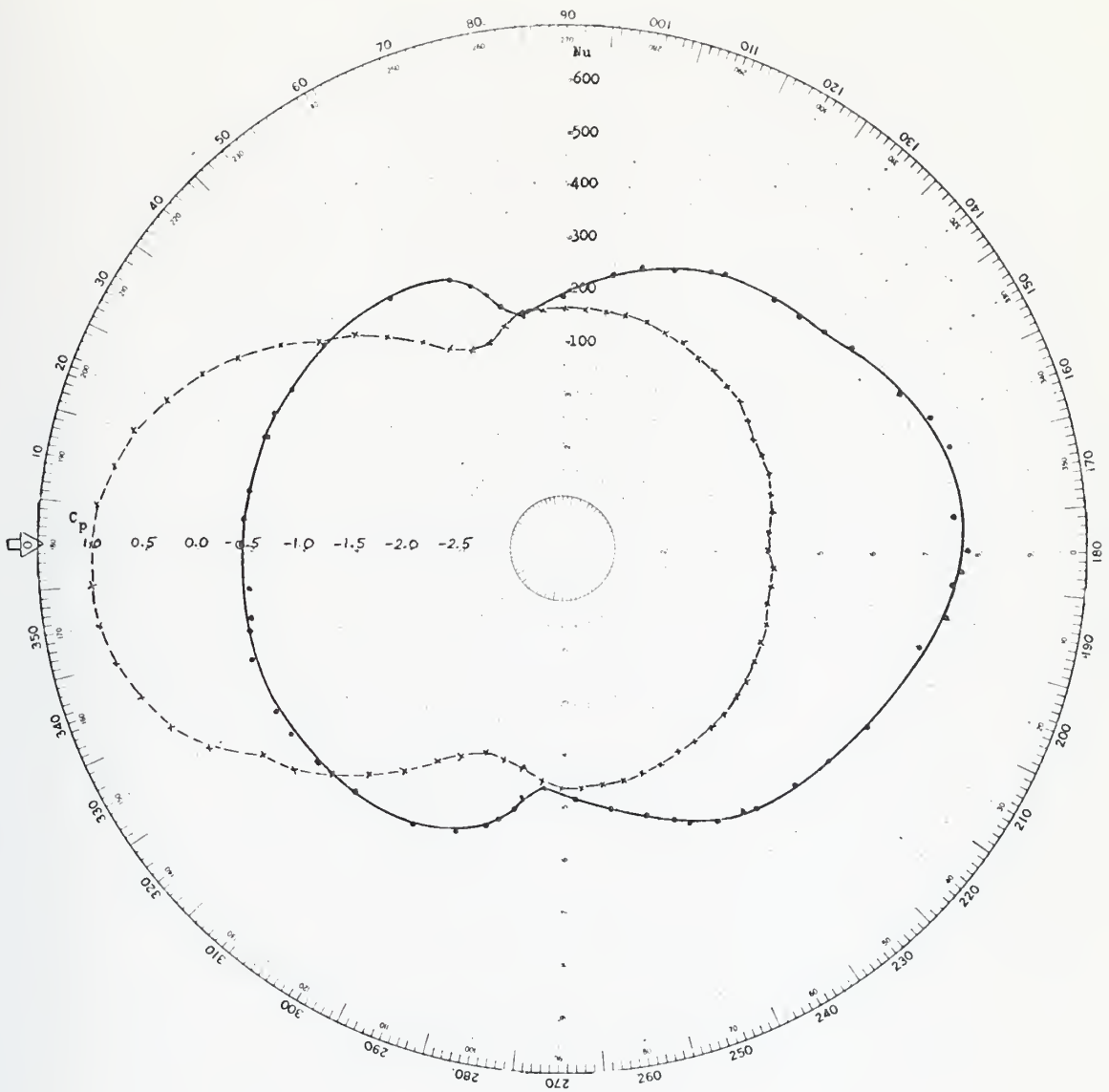


Figure 35. Local Nusselt number and pressure coefficient on the surface of a cylinder placed near a plane surface for  $Re = 90,000$ ,  $L/D = 4$ ,  $d/r = 1.0$ .



Nu    •  
Cp    x

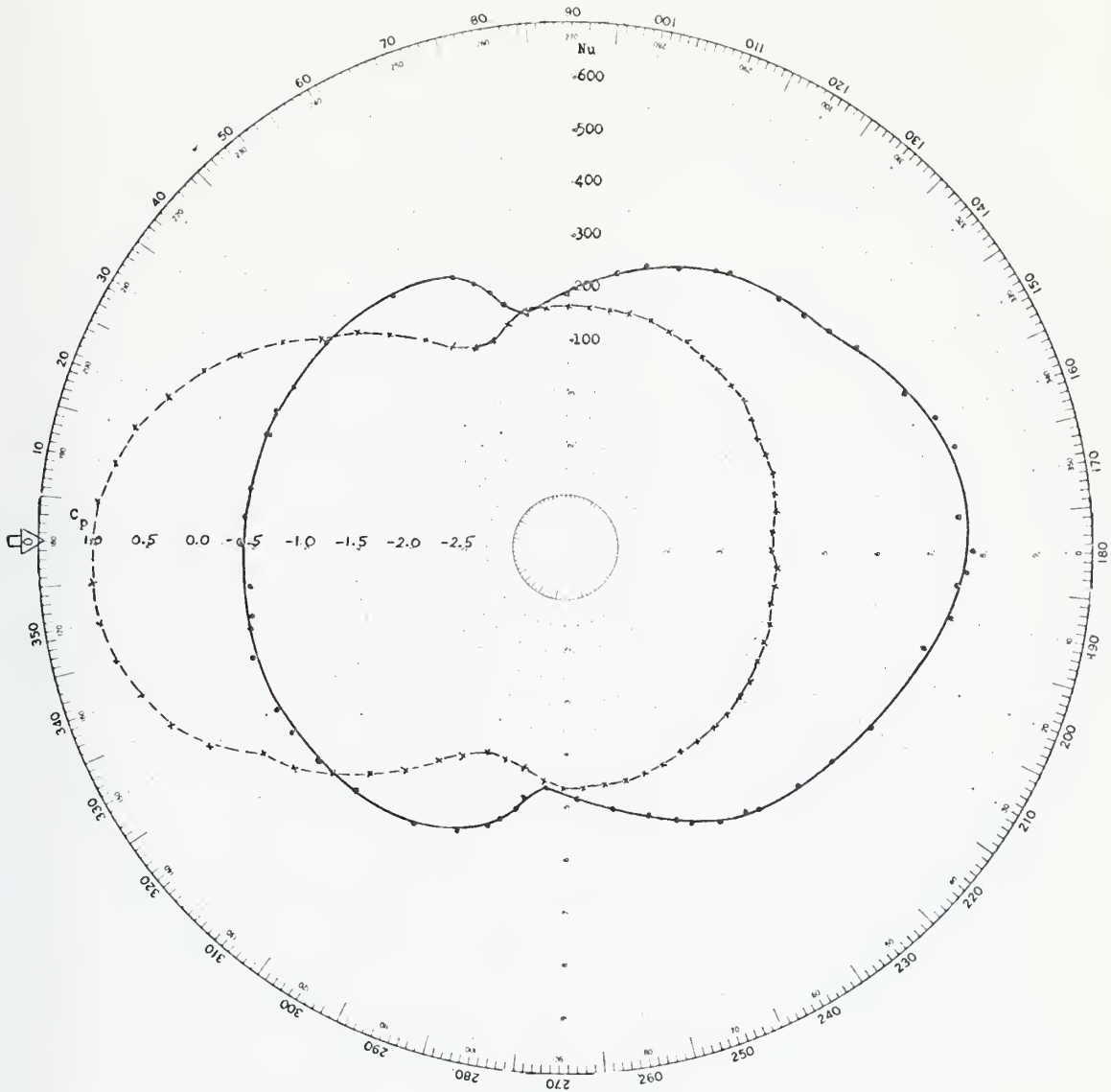


Figure 36. Local Nusselt number and pressure coefficient on the surface of a cylinder placed near a plane surface for  $Re = 90,000$ ,  $L/D = 4$ ,  $d/r = 2.0$ .



Nu    •  
Cp    x

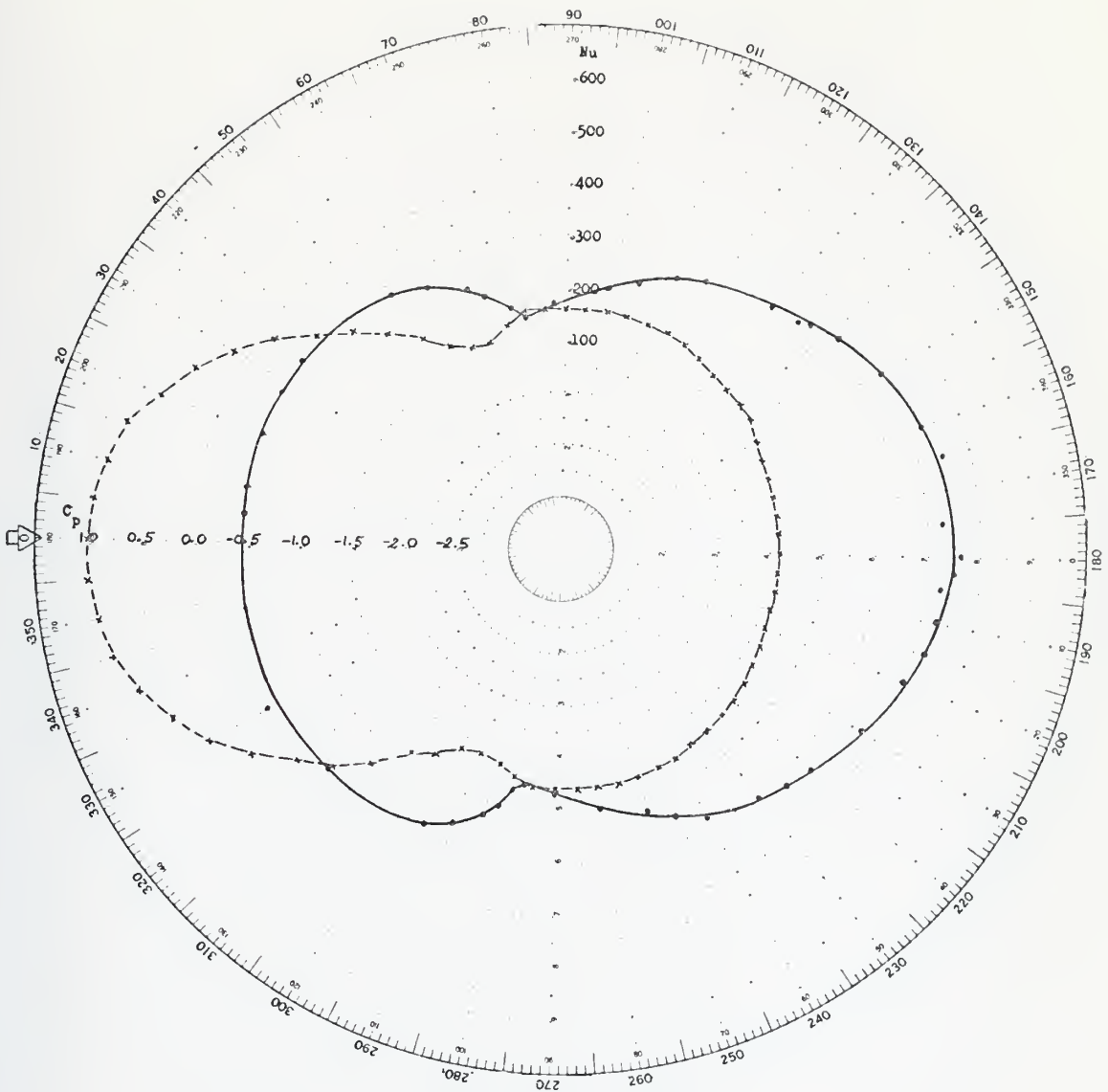


Figure 37. Local Nusselt number and pressure coefficient on the surface of a cylinder placed near a plane surface for  $Re = 90,000$ ,  $L/D = 4$ ,  $d/r = 3.0$ .



Nu    •  
Cp    x

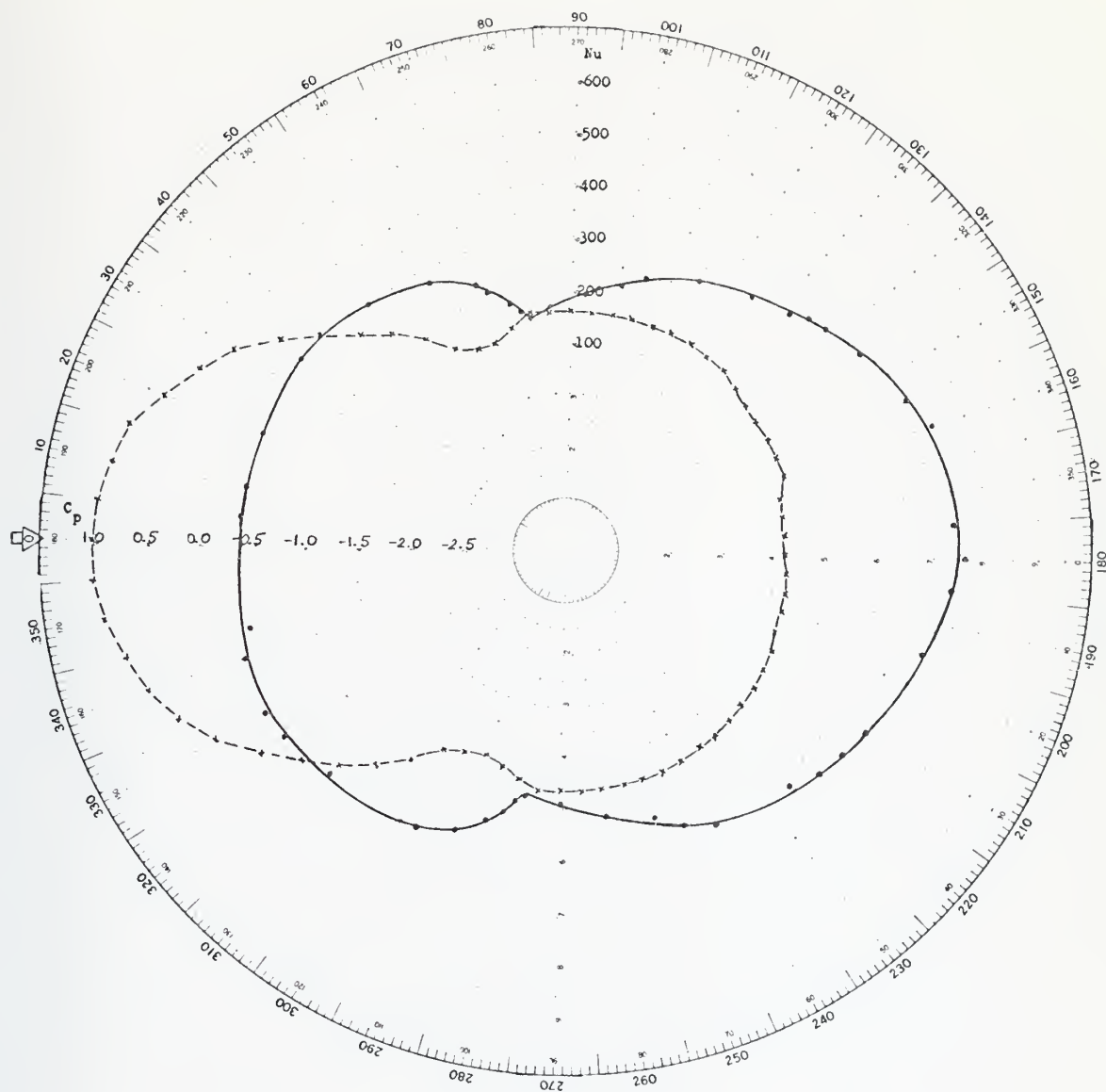


Figure 38. Local Nusselt number and pressure coefficient on the surface of a cylinder placed near a plane surface for  $Re = 90,000$ ,  $L/D = 4$ ,  $d/r = 4.0$ .



$Nu$  .

$C_p$  x

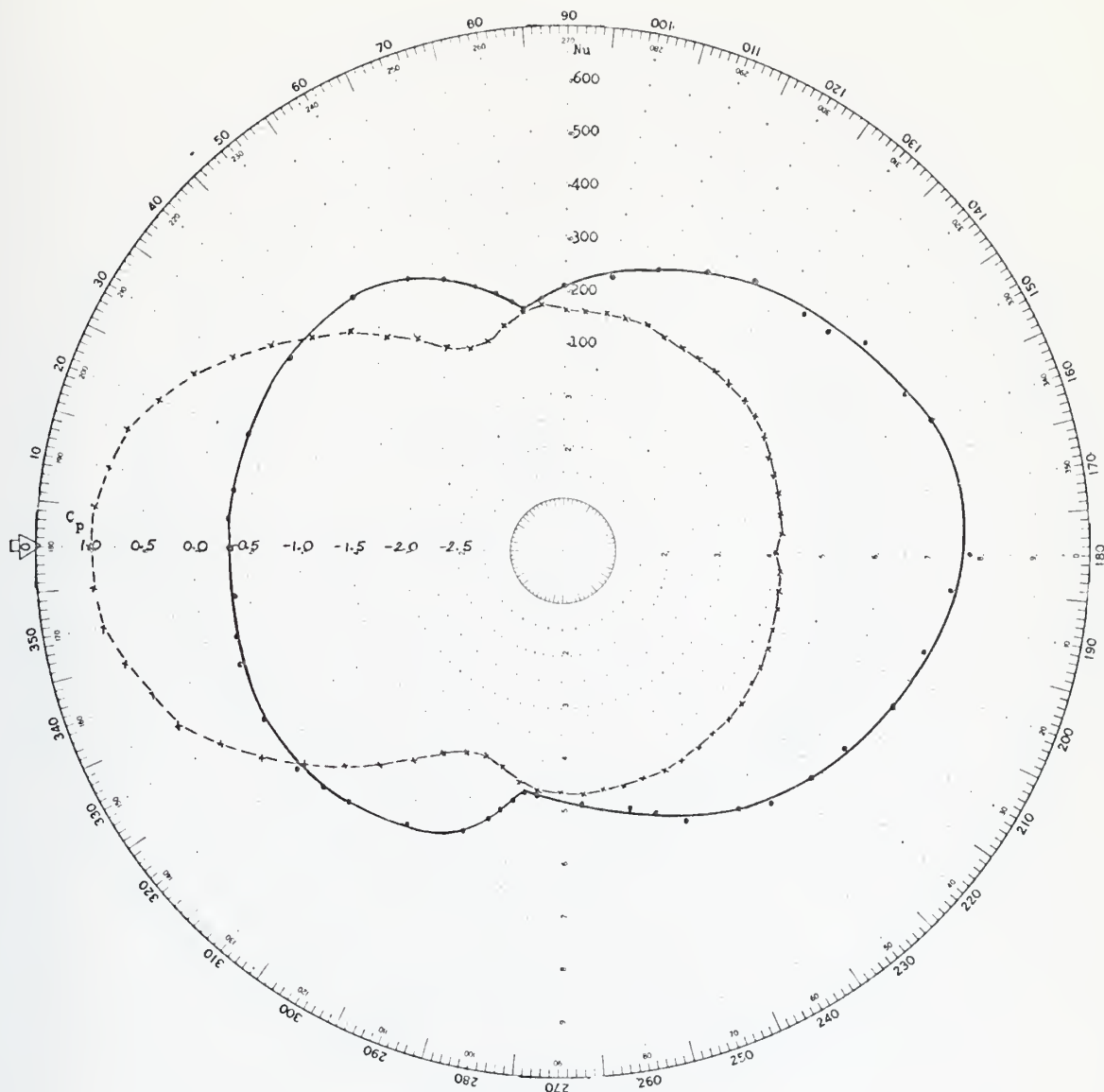


Figure 39. Local Nusselt number and pressure coefficient on the surface of a cylinder placed near a plane surface for  $Re = 90,000$ ,  $L/D = 4$ ,  $d/r = 5.33$ .



Nu    •  
Cp    x

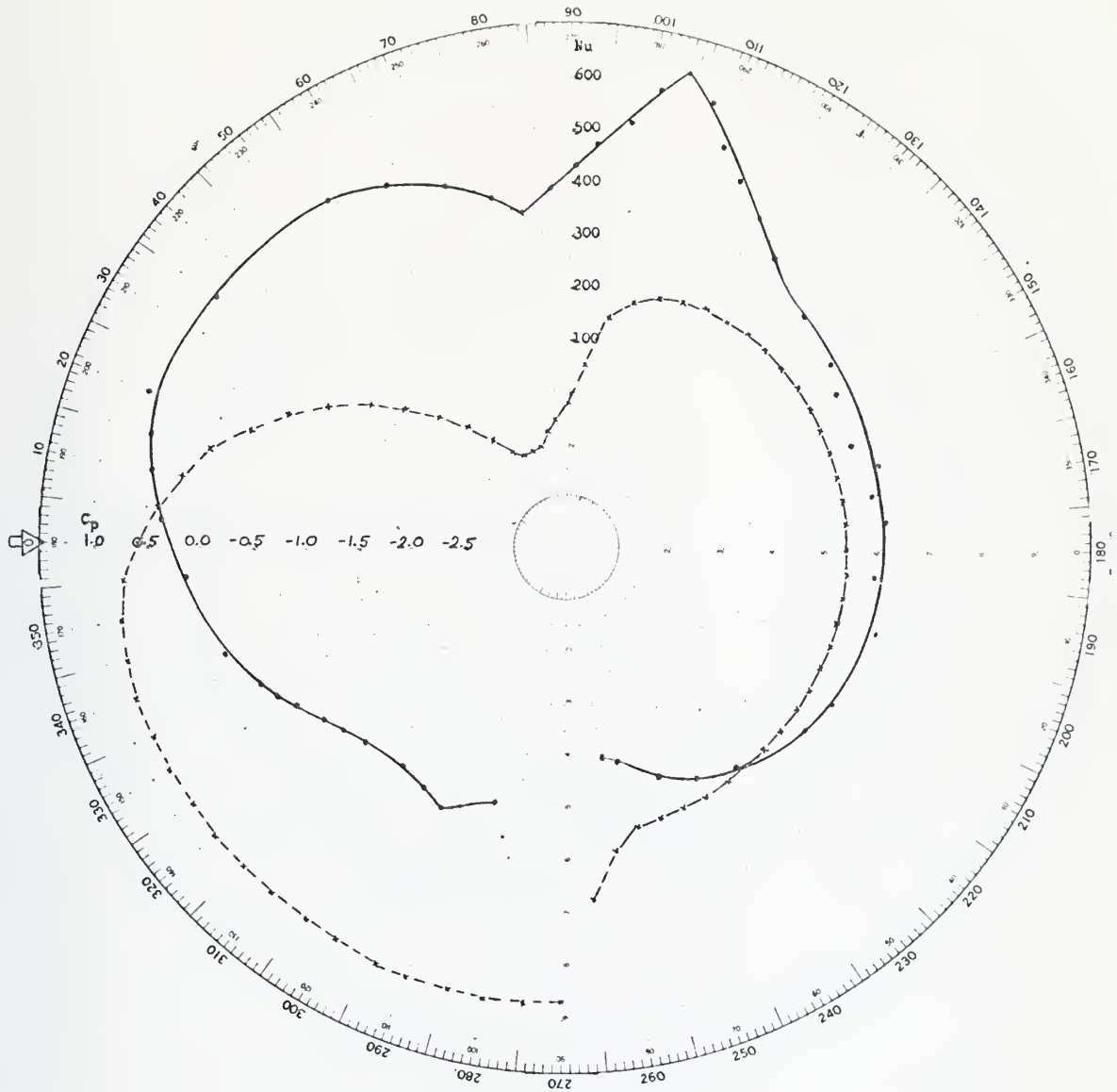


Figure 40. Local Nusselt number and pressure coefficient on the surface of a cylinder placed near a plane surface for  $Re = 153,000$ ,  $L/D = 2$ ,  $d/r = 0.0$ .



Nu ·  
Cp x

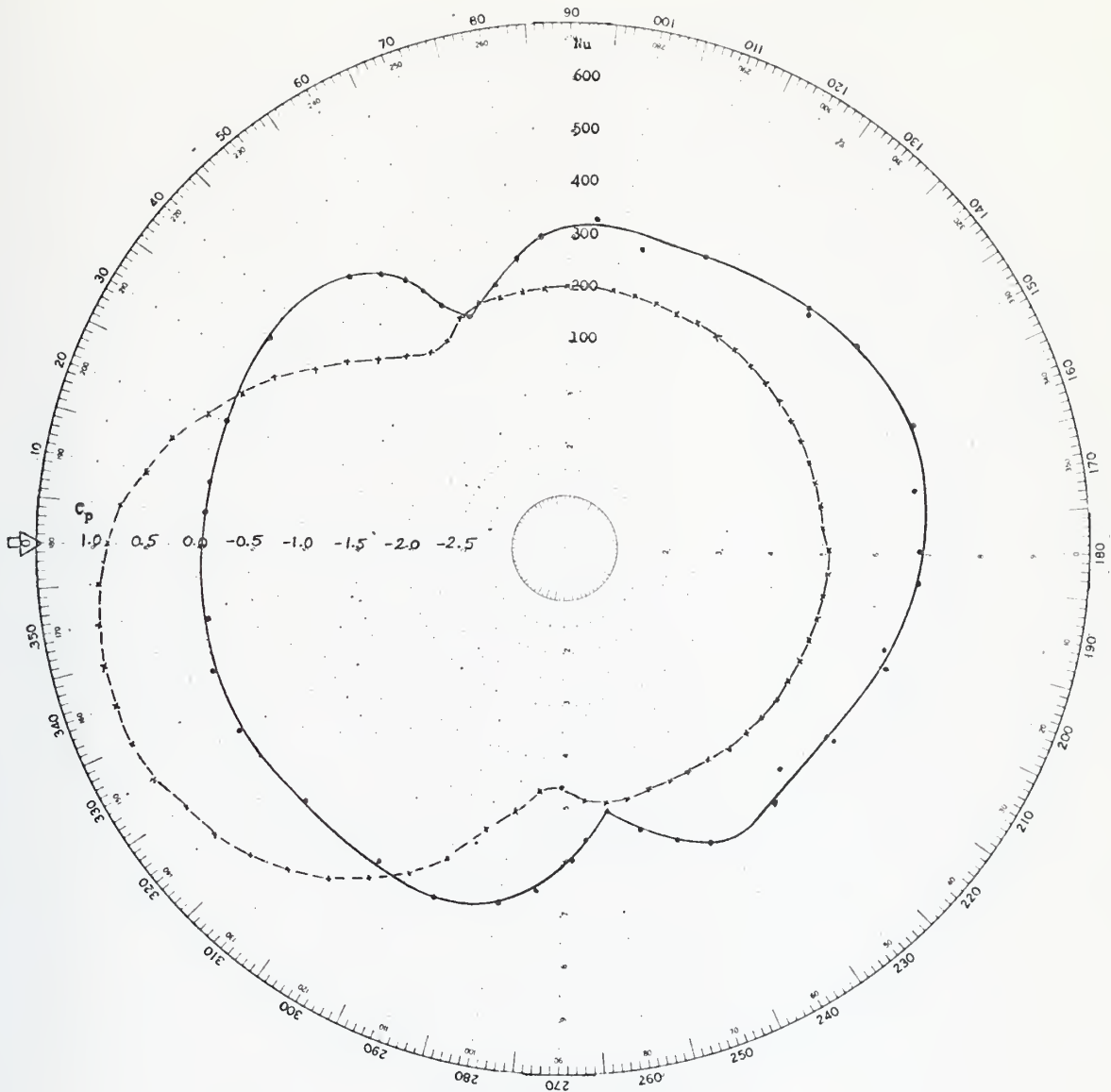


Figure 41. Local Nusselt number and pressure coefficient on the surface of a cylinder placed near a plane surface for  $Re = 153,000$ ,  $L/D = 2$ ,  $d/r = 0.25$ .



Nu    •  
Cp    x

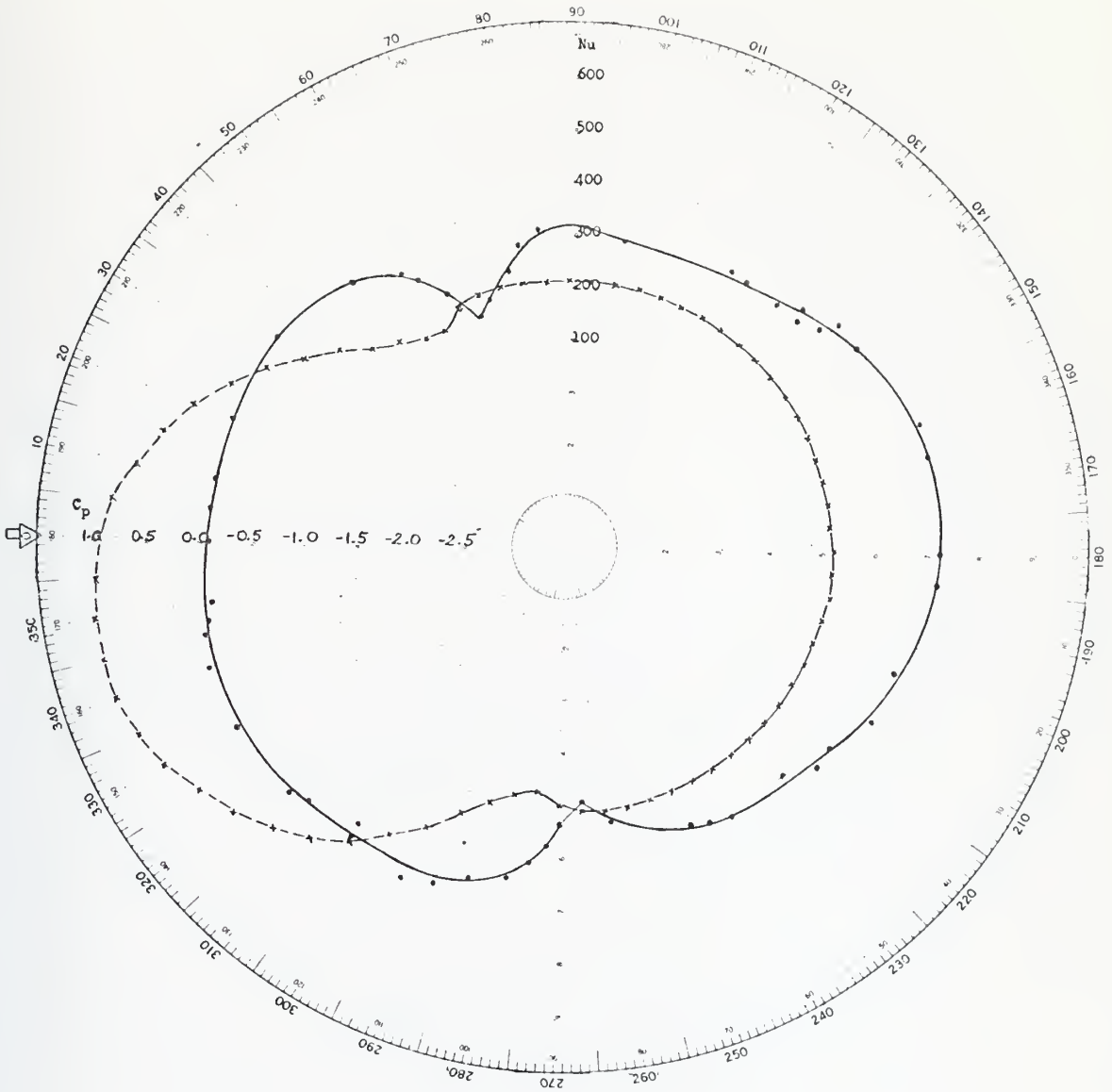


Figure 42. Local Nusselt number and pressure coefficient on the surface of a cylinder placed near a plane surface for  $Re = 153,000$ ,  $L/D = 2$ ,  $d/r = 0.5$ .



Nu .  
Cp x

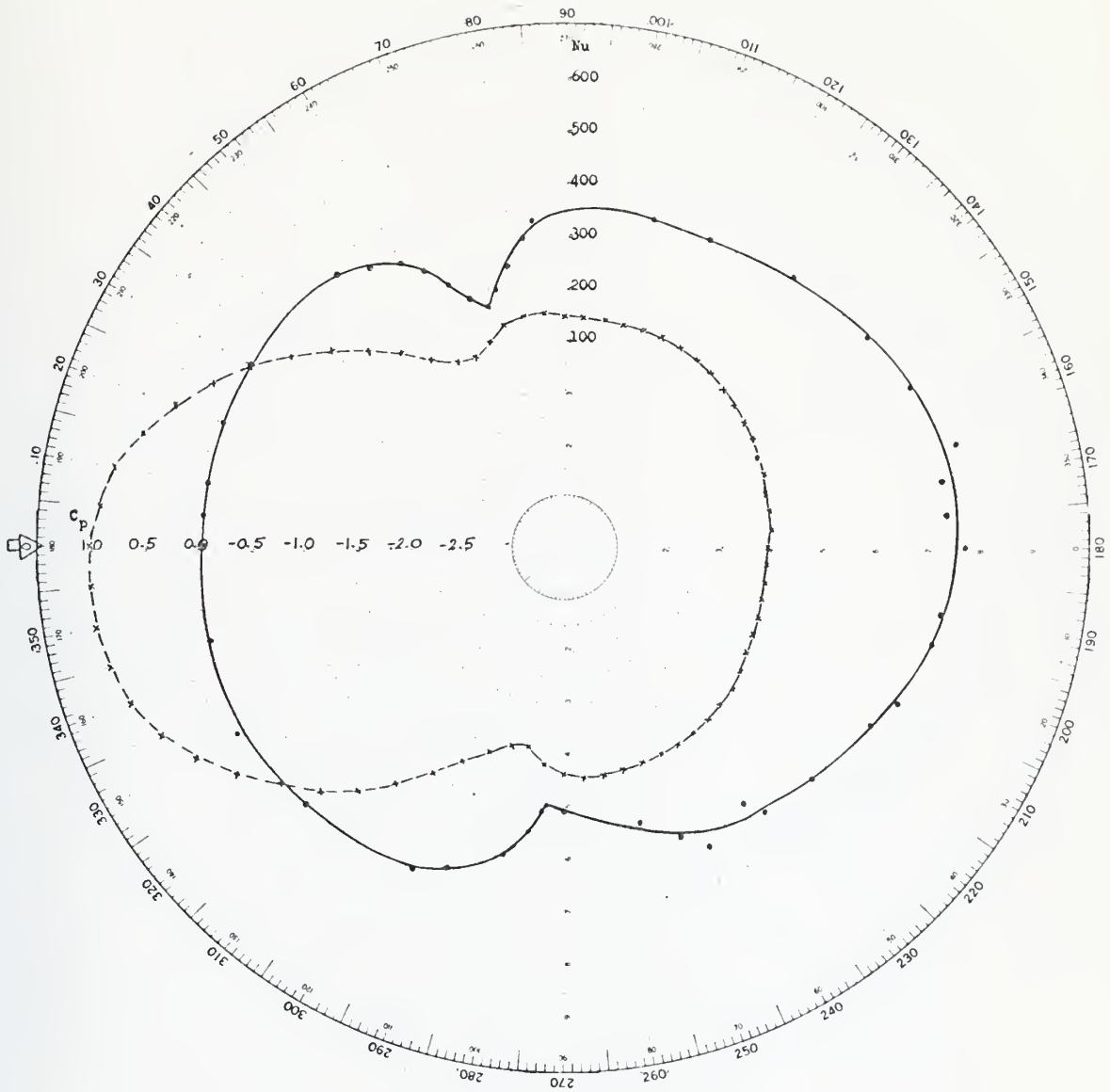


Figure 43. Local Nusselt number and pressure coefficient on the surface of a cylinder placed near a plane surface for  $Re = 153,000$ ,  $L/D = 2$ ,  $d/r = 1.0$ .



Nu    •  
Cp    x

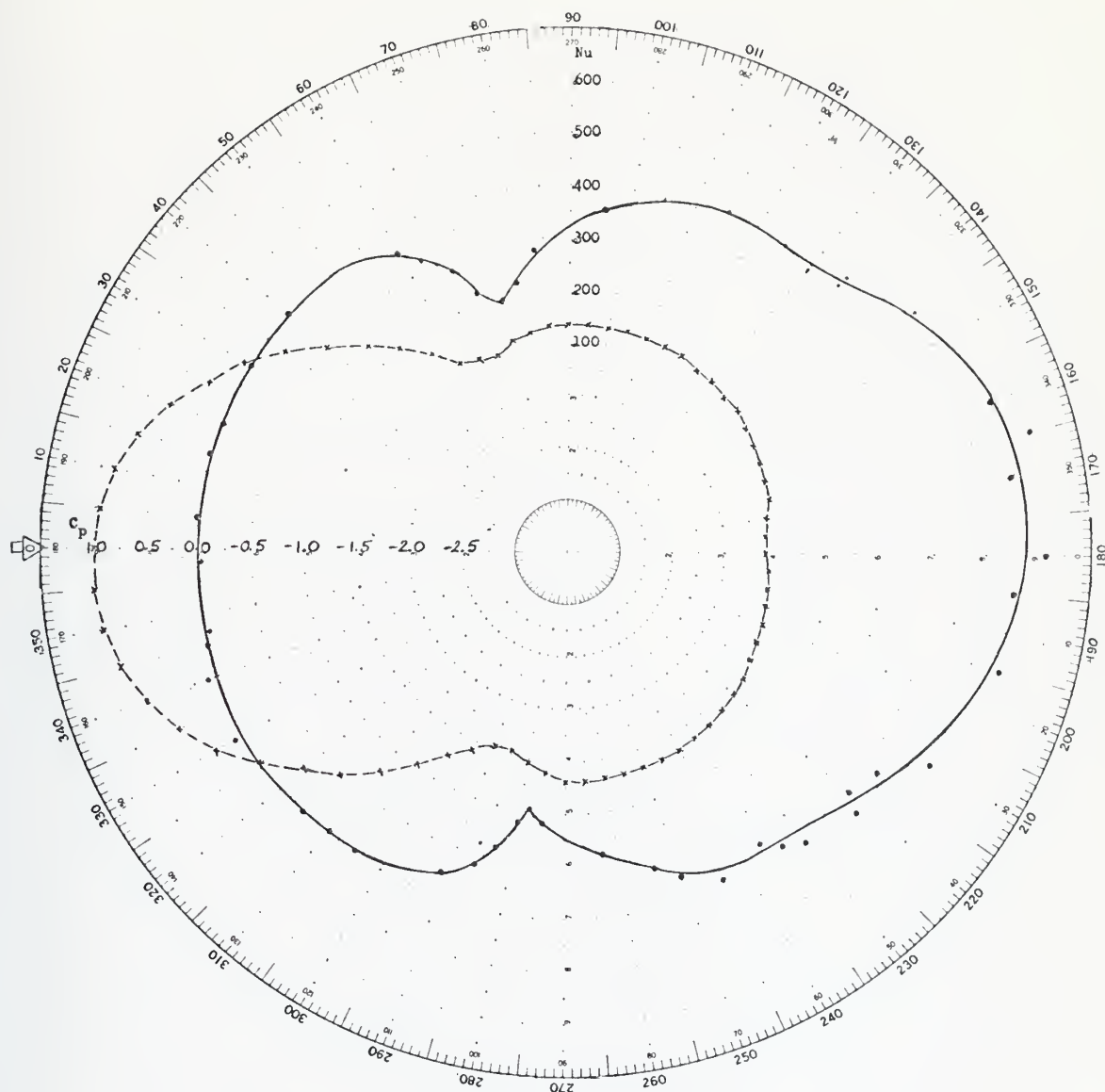


Figure 44. Local Nusselt number and pressure coefficient on the surface of a cylinder placed near a plane surface for  $Re = 153,000$ ,  $L/D = 2$ ,  $d/r = 2.0$ .



Nu    •  
Cp    x

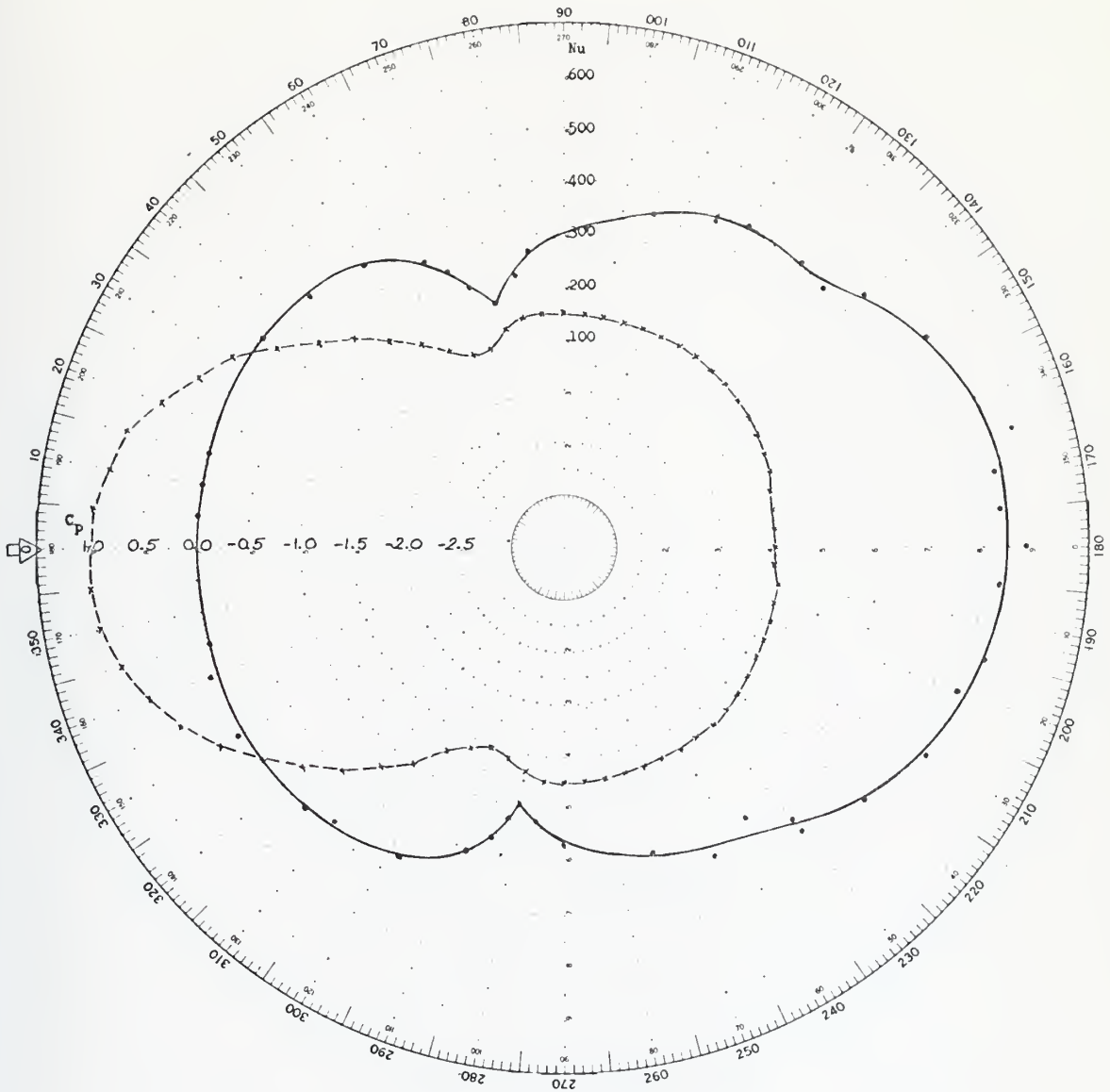


Figure 45. Local Nusselt number and pressure coefficient on the surface of a cylinder placed near a plane surface for  $Re = 153,000$ ,  $L/D = 2$ ,  $d/r = 3.0$ .



Nu    .  
Cp    x

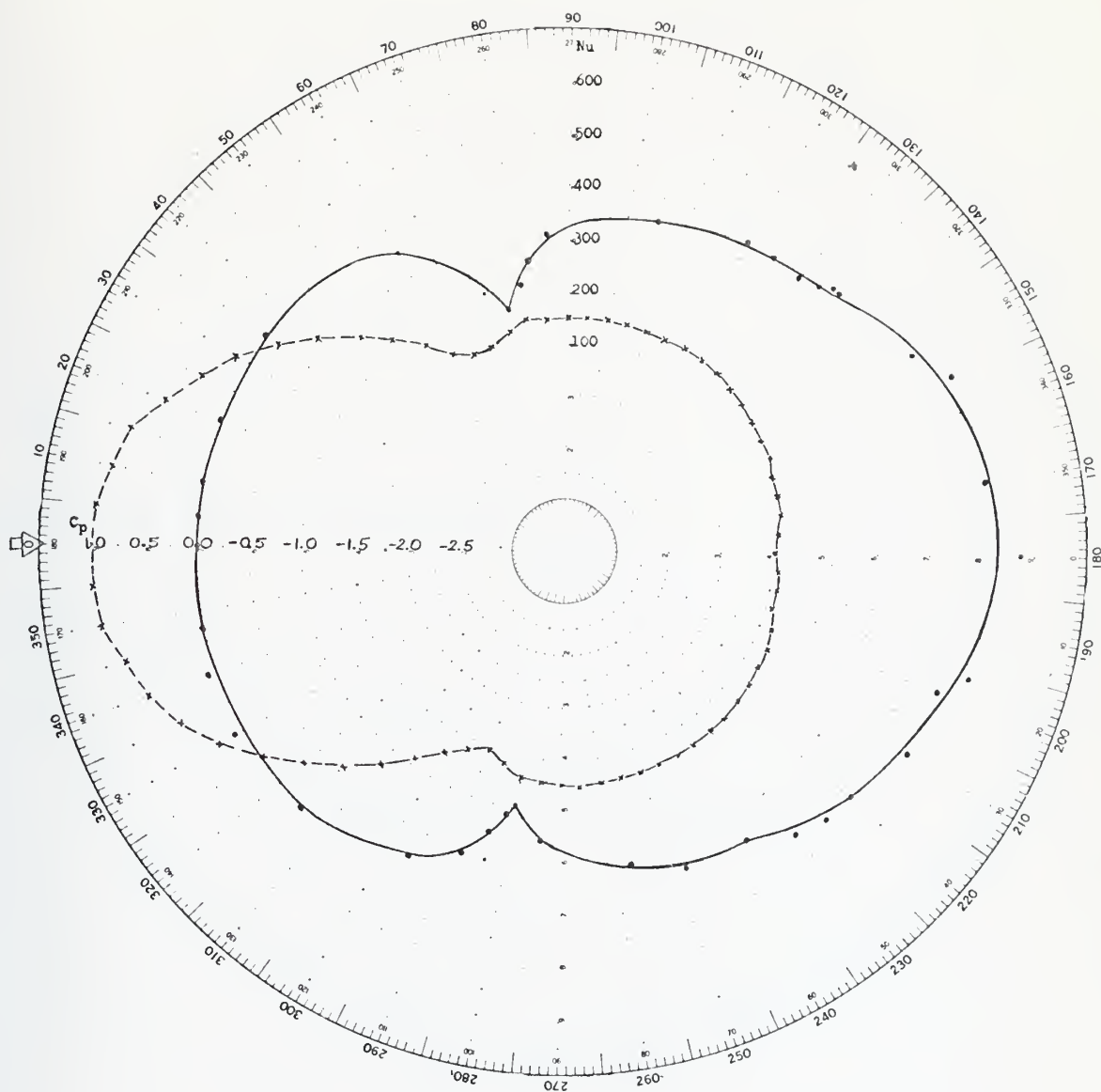


Figure 46. Local Nusselt number and pressure coefficient on the surface of a cylinder placed near a plane surface for  $Re = 153,000$ ,  $L/D = 2$ ,  $d/r = 4.0$ .



Nu .  
Cp x

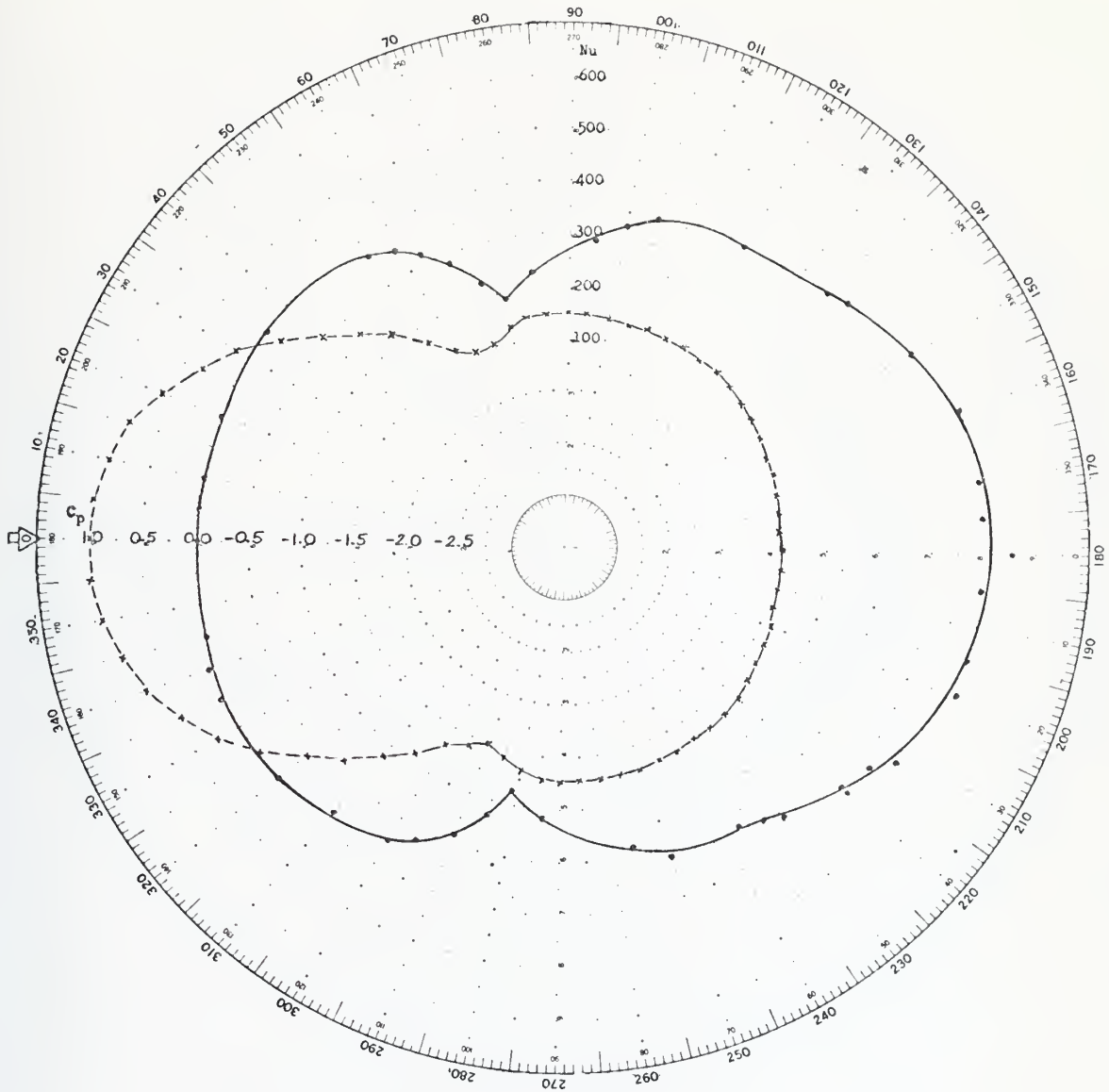


Figure 47. Local Nusselt number and pressure coefficient on the surface of a cylinder placed near a plane surface for  $Re = 153,000$ ,  $L/D = 2$ ,  $d/r = 5.33$ .



Nu .  
Cp x

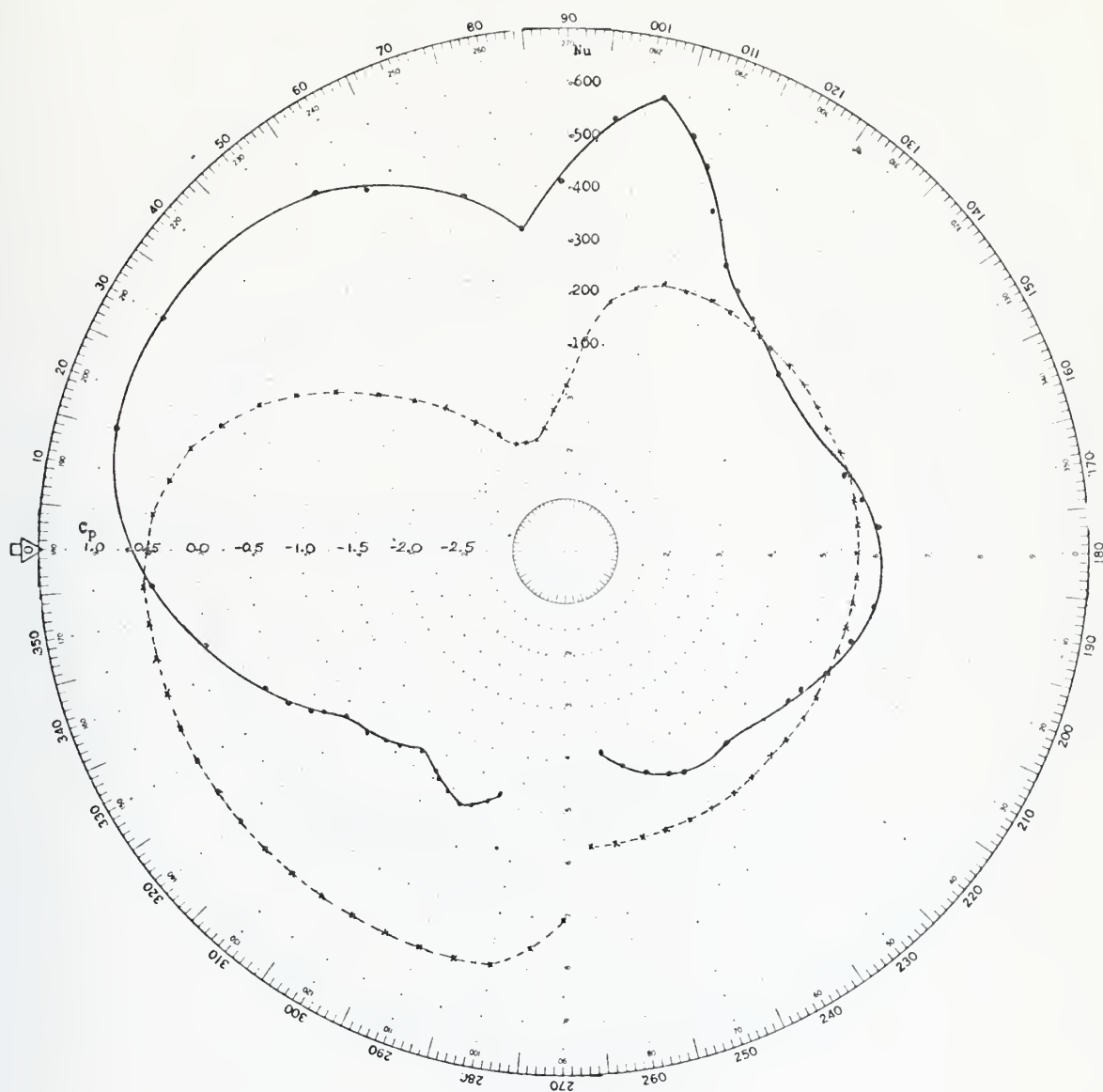


Figure 48. Local Nusselt number and pressure coefficient on the surface of a cylinder placed near a plane surface for  $Re = 153,000$ ,  $L/D = 8$ ,  $d/r = 0.0$ .



Nu    .  
Cp    x

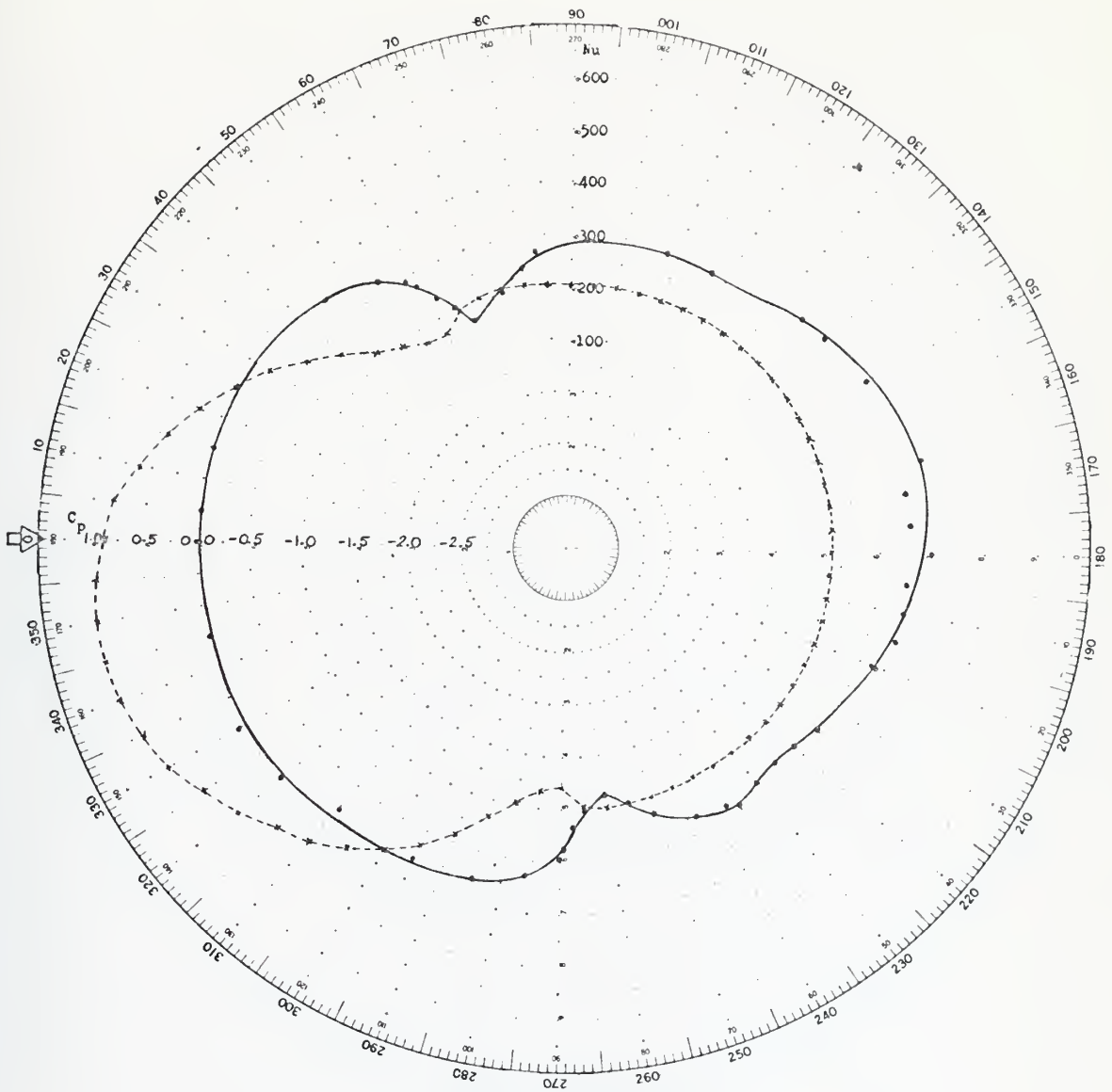


Figure 49. Local Nusselt number and pressure coefficient on the surface of a cylinder placed near a plane surface for  $Re = 153,000$ ,  $L/D = 8$ ,  $d/r = 0.25$ .



Nu ·

Cp x

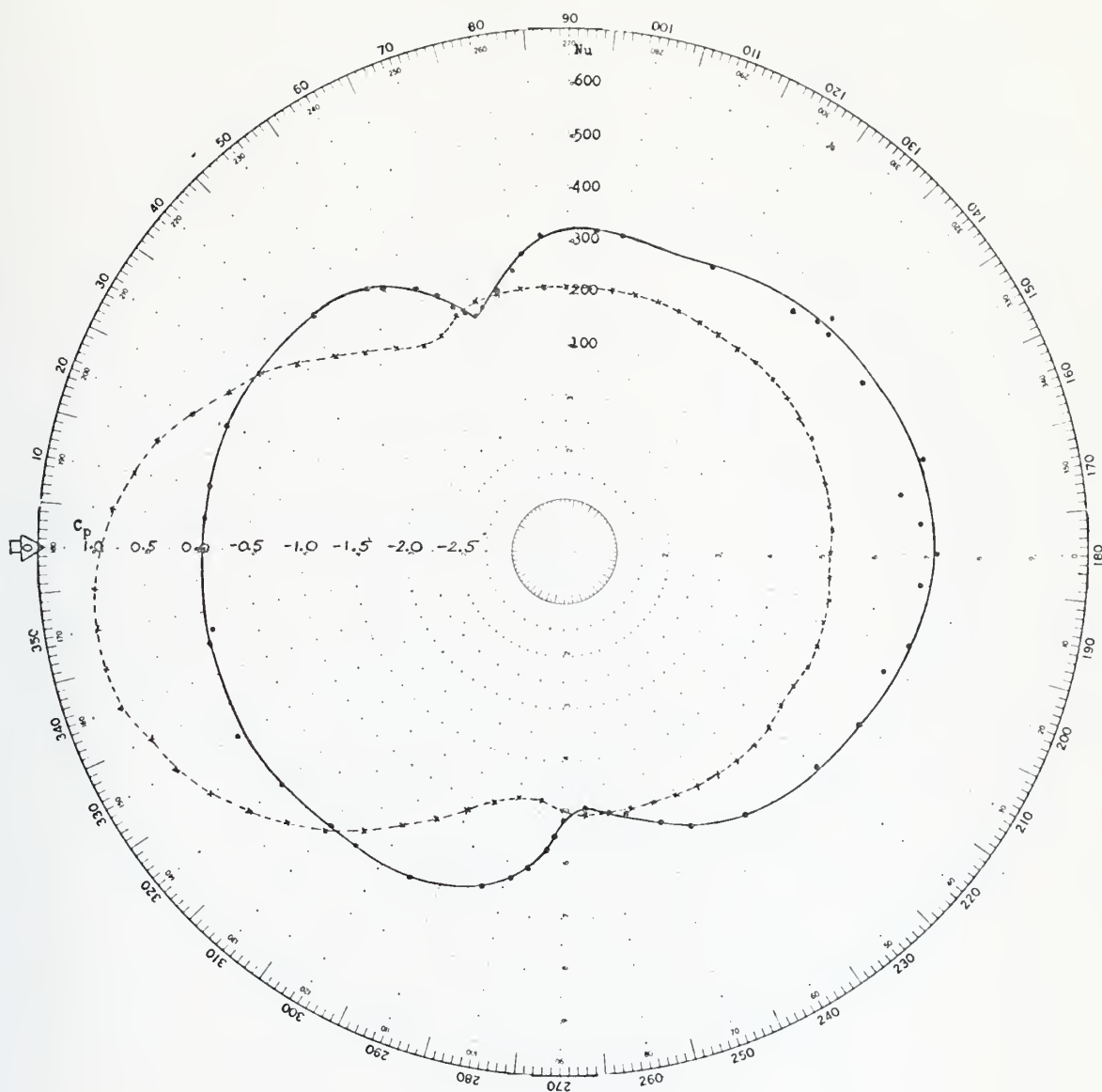


Figure 50. Local Nusselt number and pressure coefficient on the surface of a cylinder placed near a plane surface for  $Re = 153,000$ ,  $L/D = 8$ ,  $d/r = 0.5$ .



Nu .  
Cp x

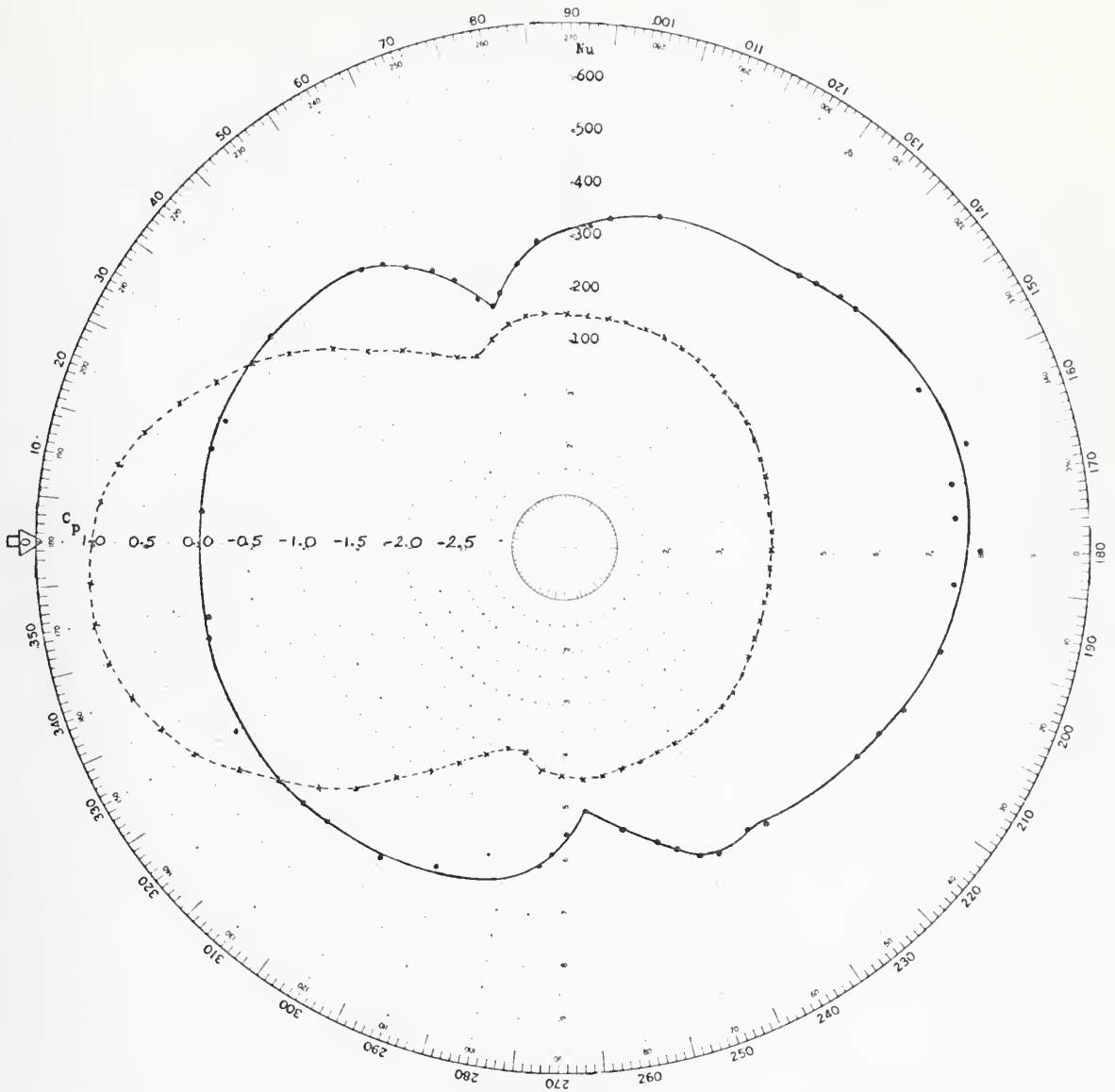


Figure 51. Local Nusselt number and pressure coefficient on the surface of a cylinder placed near a plane surface for  $Re = 153,000$ ,  $L/D = 8$ ,  $d/r = 1.0$ .



$h_u$  .  
 $C_p$  x

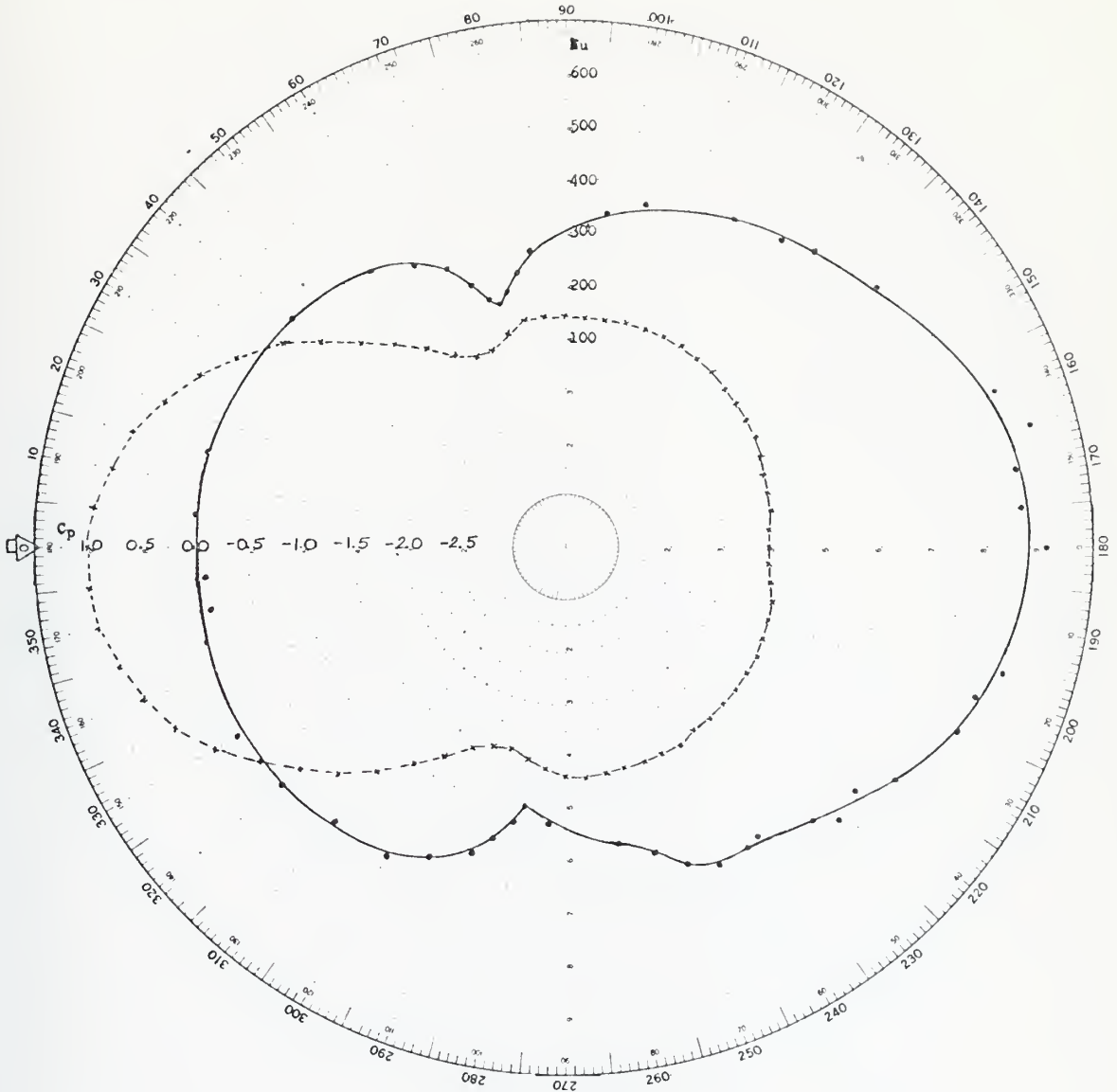


Figure 52. Local Nusselt number and pressure coefficient on the surface of a cylinder placed near a plane surface for  $Re = 153,000$ ,  $L/D = 8$ ,  $d/r = 2.0$ .



Nu .

Cp x

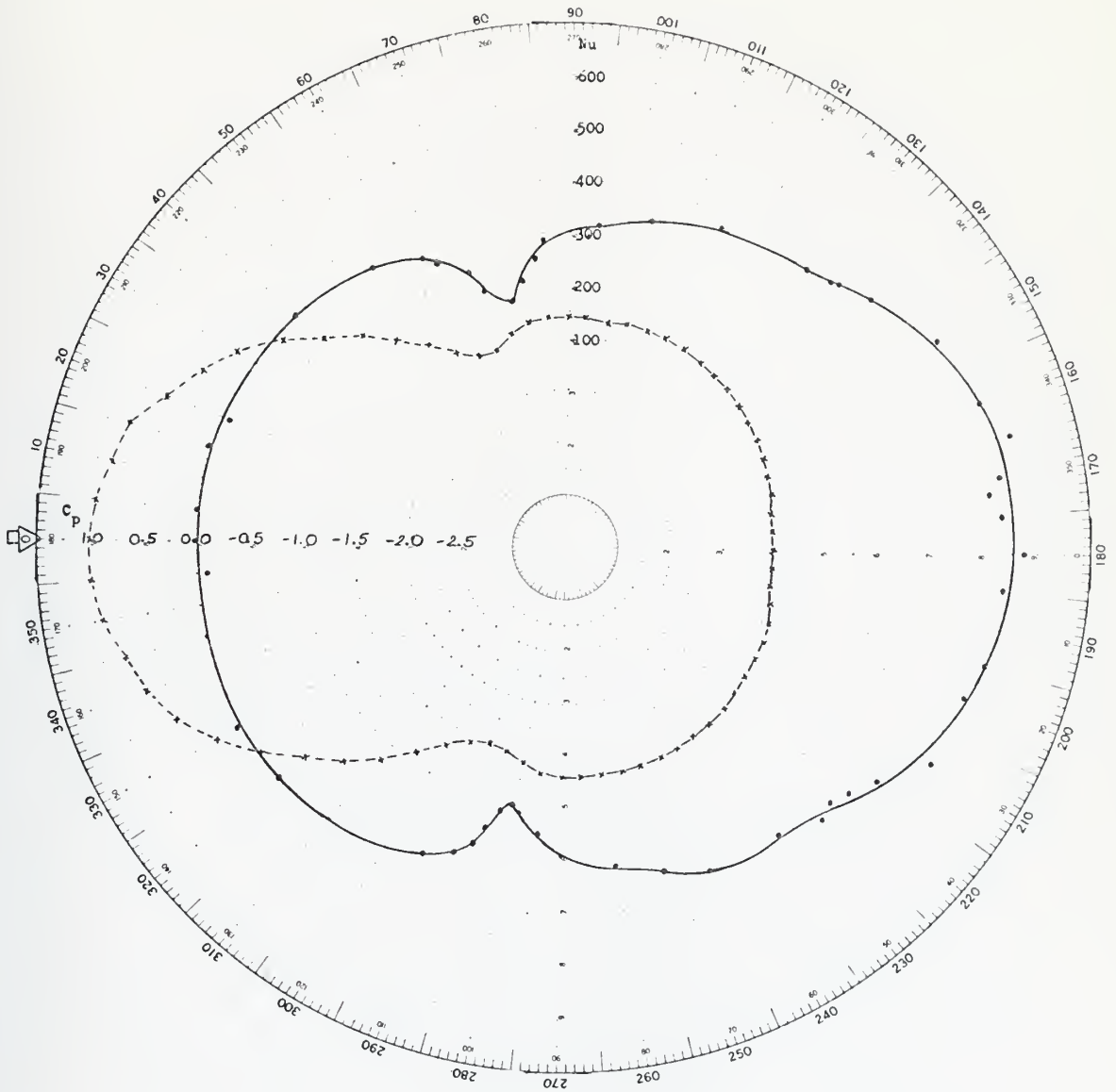


Figure 53. Local Nusselt number and pressure coefficient on the surface of a cylinder placed near a plane surface for  $Re = 153,000$ ,  $L/D = 8$ ,  $d/r = 3.0$ .



Nu .

Cp x

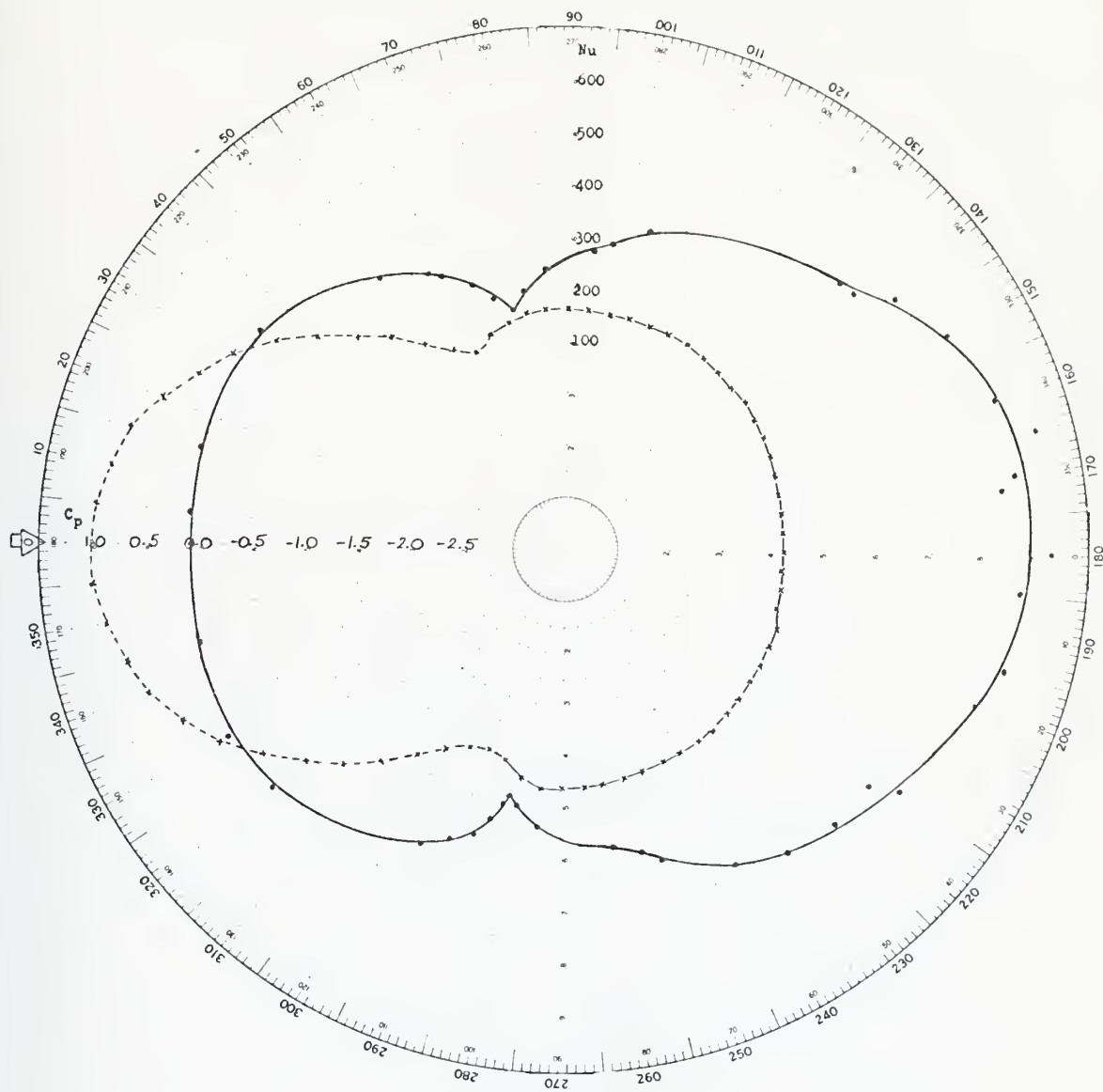


Figure 54. Local Nusselt number and pressure coefficient on the surface of a cylinder placed near a plane surface for  $Re = 153,000$ ,  $L/D = 8$ ,  $d/r = 4.0$ .



Nu ·

$C_p \times$

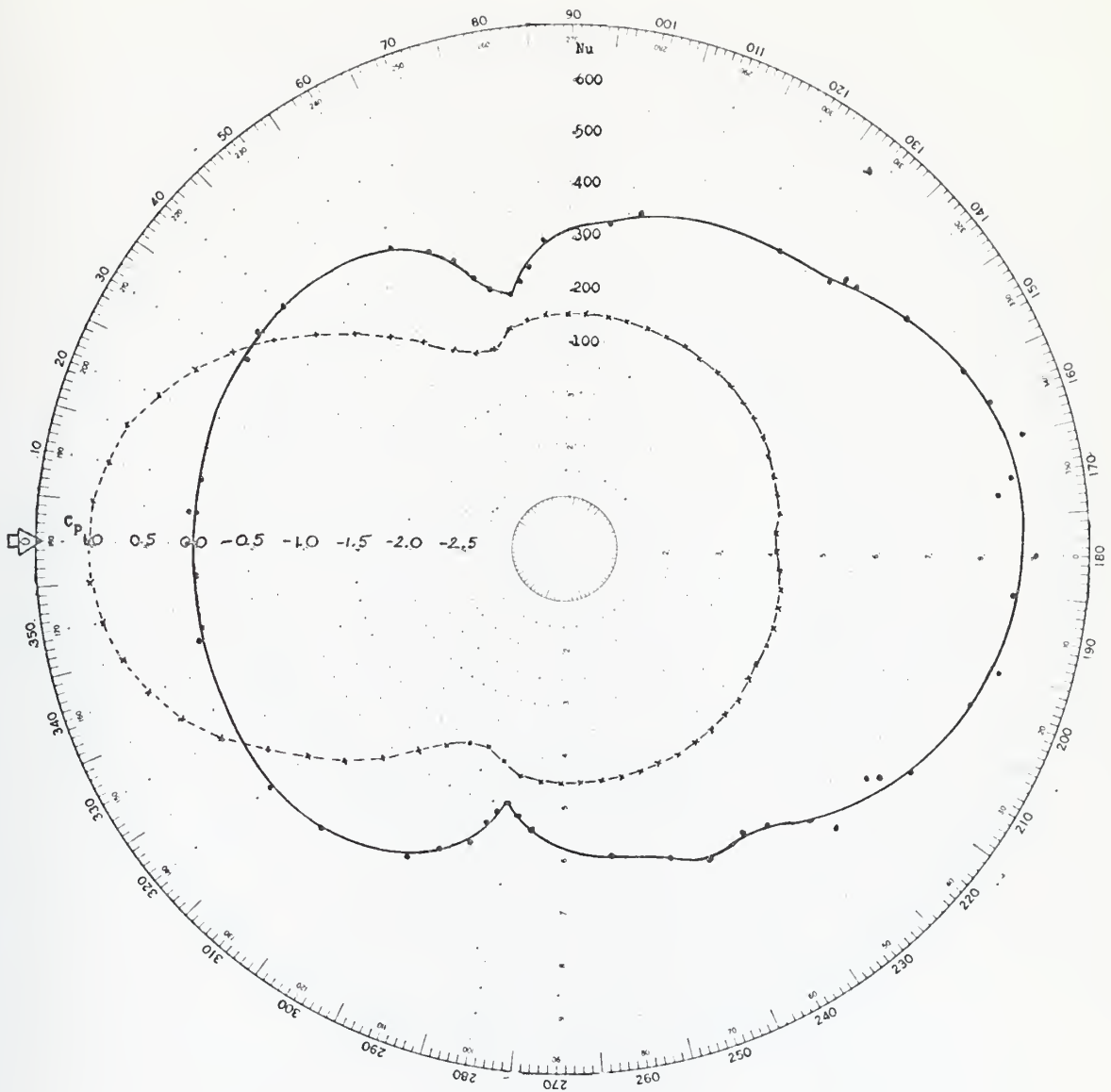


Figure 55. Local Nusselt number and pressure coefficient on the surface of a cylinder placed near a plane surface for  $Re = 153,000$ ,  $L/D = 8$ ,  $d/r = 5.33$ .



Nu .

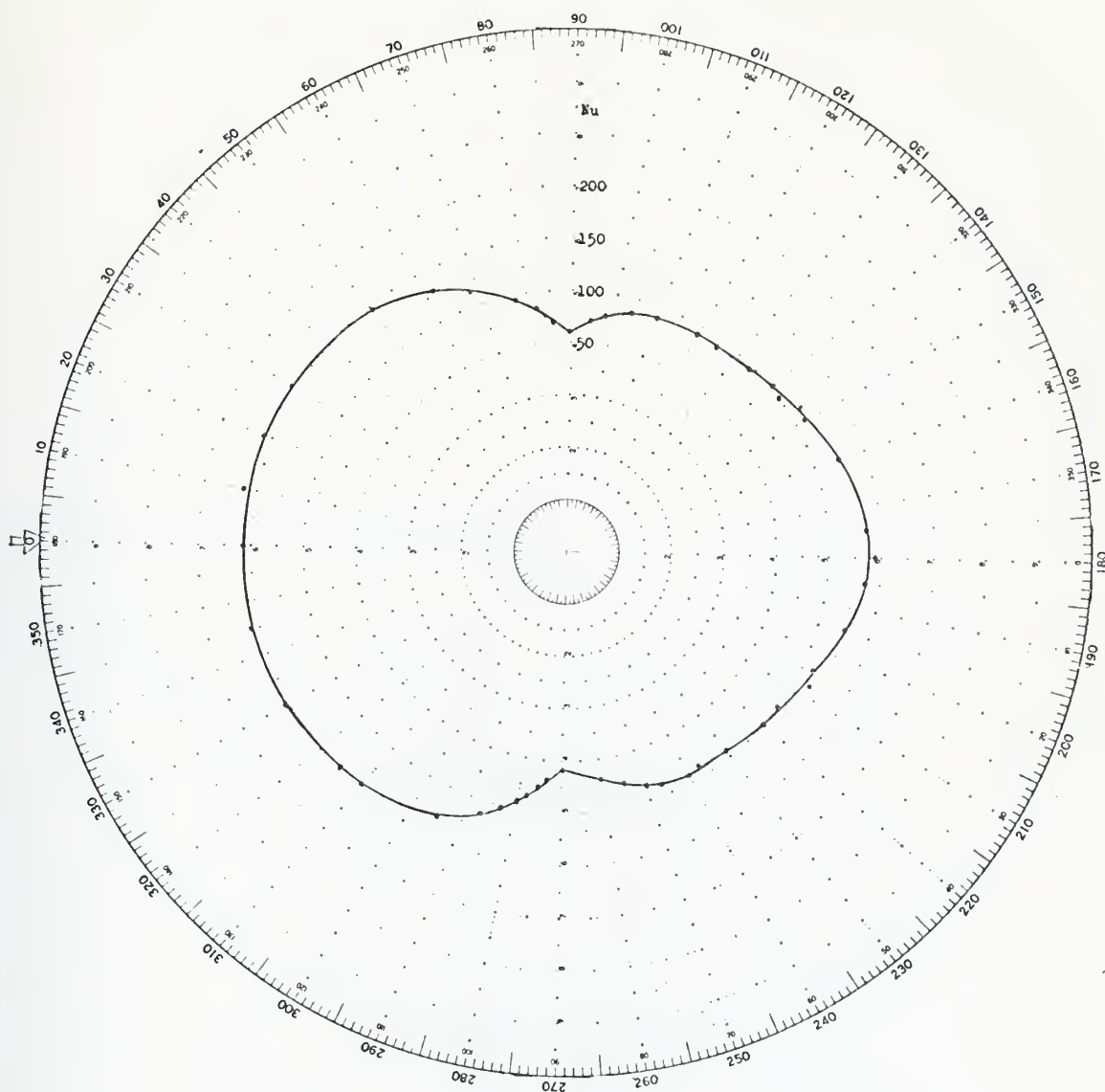


Figure 56. Local Nusselt number on the surface of a free cylinder for  $Re = 16,000$ .



Nu ·

Cp x

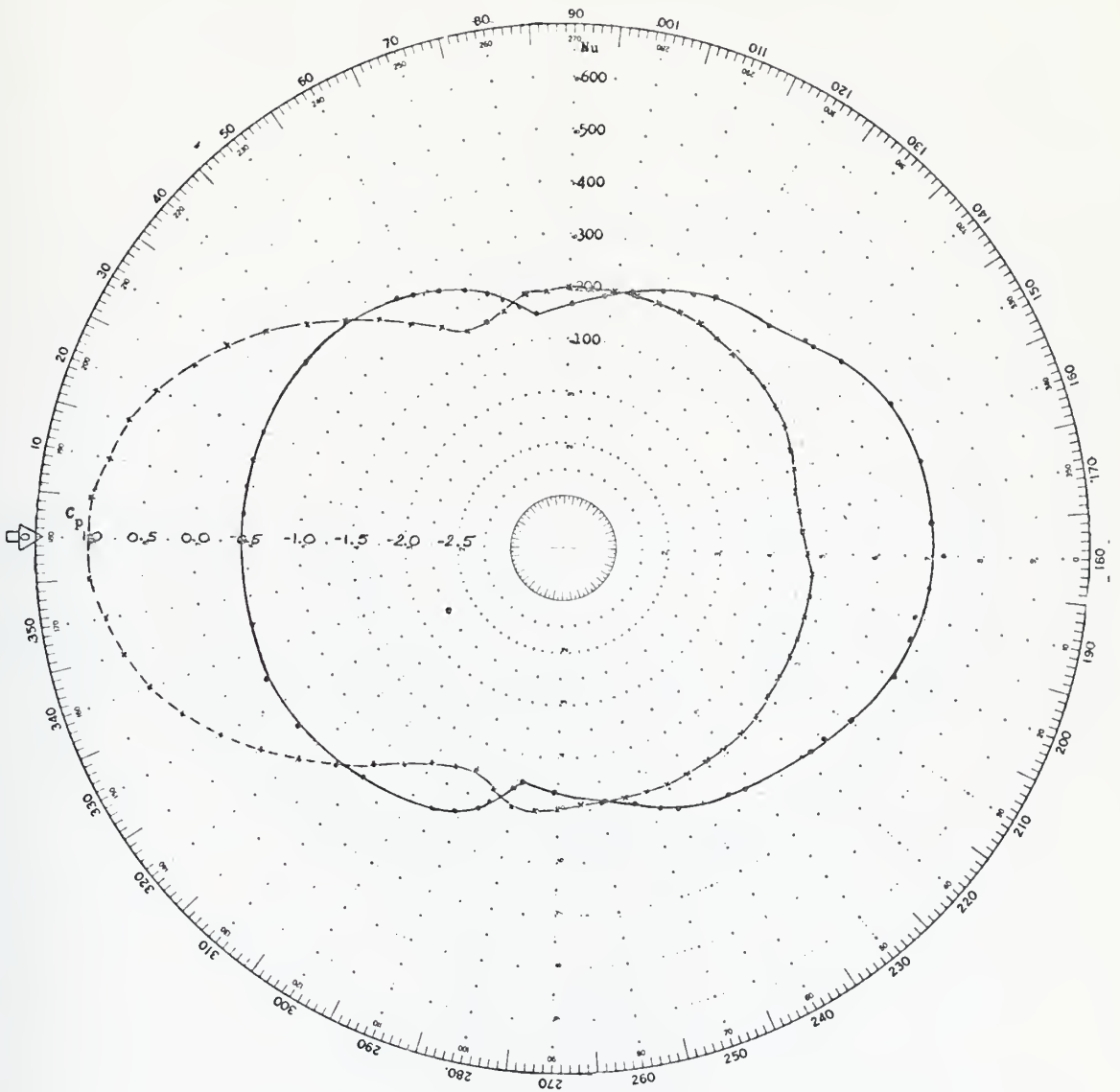


Figure 57. Local Nusselt number and pressure coefficient on the surface of a free cylinder for  $Re = 90,000$ .



$Nu$     •  
 $C_p$     x

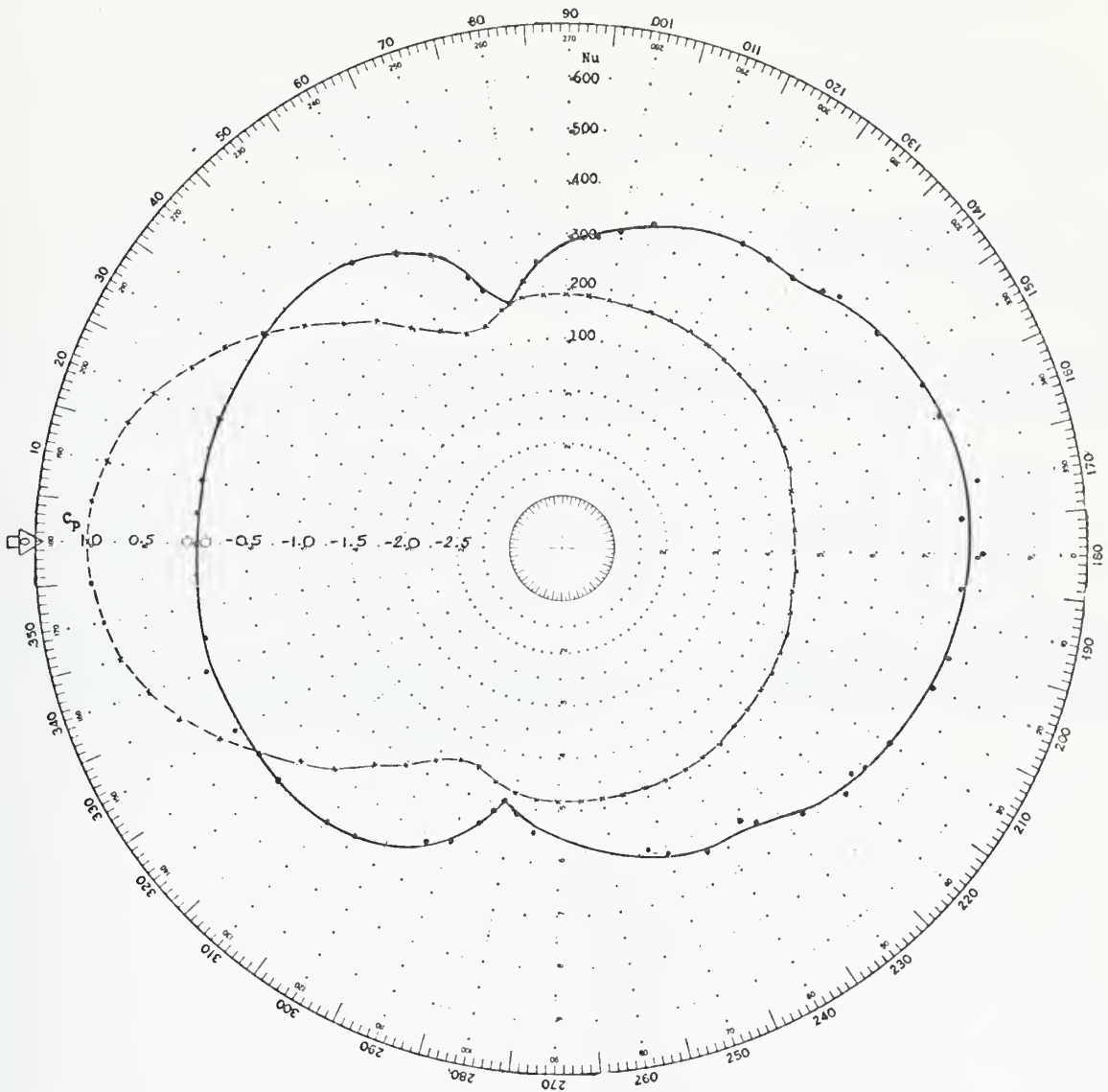


Figure 58. Local Nusselt number and pressure coefficient on the surface of a free cylinder for  $Re = 153,000$ .



## LIST OF REFERENCES

1. McComas, J. P., Experimental Investigation of Ground Effects on a Heated Cylinder in Crossflow, MSME Thesis, Naval Postgraduate School, 1974.
2. Gnerlich, C. H., The Convective Heat Transfer Behavior of a Heated Cylinder Located Near a Plane Surface, MSME Thesis, Naval Postgraduate School, 1975.
3. Achenbach, E. Distribution of Local Pressure and Skin Friction Around a Circular Cylinder in Cross-flow up to  $Re = 5 \times 10^6$ , J. Fluid Mech. (1968), vol. 34, part 4, pp. 625-639.
4. Goktun, S., Drag and Lift Characteristics of a Cylinder Placed Near a Plane Surface, MSME Thesis, Naval Postgraduate School, 1975.
5. Cooper, T. E., Meyer, J. F., and Field, R. J., Liquid Crystal Thermography and its Application to the Study of Convective Heat Transfer, Journal of Heat Transfer, v. 97, pp. 442-450, August 1975.
6. Kline, S. J. and McClintock, F. A., "Describing Uncertainties in Single-Sample Experiments," Mechanical Engineering, v. 75, p. 3-8, January 1953.



# INITIAL DISTRIBUTION LIST

	No. Copies
1. Defense Documentation Center Cameron Station Alexandria, Virginia 22314	2
2. Library, Code 0212 Naval Postgraduate School Monterey, California 93940	2
3. Department Chairman, Code 59 Department of Mechanical Engineering Naval Postgraduate School Monterey, California 93940	1
4. T. E. Cooper, Code 59 Cg Department of Mechanical Engineering Naval Postgraduate School Monterey, California 93940	5
5. Istanbul Teknik Üniversitesi Mk. Fakültesi Taşkışla, Istanbul Turkey	1
6. Lt. Ender Kösemen Kizilelma Ziya Gokalp Sok. No. 18/6 Findikzade, Istanbul, Turkey	1







Thesis  
K826  
c.1

Köseman

Thermal studies of a  
heated cylinder placed  
near a plane surface.

133597

Thesis  
K826  
c.1

Köseman

Thermal studies of a  
heated cylinder placed  
near a plane surface.

133597

thesK826

Thermal studies of a heated cylinder pla



3 2768 002 10498 6

DUDLEY KNOX LIBRARY